Global spatiotemporal dynamics of inland water body storage during the satellite altimetry era

by

Fangfang Yao

B.S., Anhui Normal University, 2012
M.S., University of Chinese Academy of Sciences, 2015

AN ABSTRACT OF A DISSERTATION

submitted in partial fulfillment of the requirements for the degree

DOCTOR OF PHILOSOPHY

Department of Geography and Geospatial Sciences
College of Arts and Sciences

KANSAS STATE UNIVERSITY
Manhattan, Kansas

2020

Abstract

Lakes and reservoirs are essential components of the global hydrological cycle. They function as sentinels of climate change, and provide indispensable water supply, energy generation, aquatic ecosystems for meeting agricultural, industrial, and domestic needs. Despite the importance of lakes and reservoirs to natural systems and human societies, their water storage dynamics are poorly understood on a global scale, especially in remote and harsh environments such as the Tibetan Plateau. The challenge has been even amplified by the currently declining global network of gauging measurements. This knowledge gap prevents a fundamental understanding of the terrestrial water cycle and surface water availability, and thus impedes effective water resource management. Recent regional evidence has suggested that water-abundant regions show increasing trends in surface water extents whereas water-limited regions exhibit decreasing trends. However, whether this divergence also holds true for the storage of open water bodies across the entire land surface remains unknown. A synergy of fine resolution optical imagery and level measurements by satellite altimetry has the potential to accurately deduce lake/reservoir storage variations. However, the existing estimates of lake/reservoir storage changes are mostly limited by the number/size of studied water bodies and the low temporal frequencies in time series, primarily owing to atmospheric contaminations in satellite imagery and inadequate spatiotemporal coverage in altimetry.

This dissertation aims to mitigate the above technical limitations through several remote sensing method advancements, and to leverage multi-mission satellites to investigate the recent lake/reservoir storage dynamics and their implications for the regional and global water cycles. Specifically, this dissertation is orientated to three overarching questions: 1) how has the lake water storage across the landlocked inner Tibetan Plateau changed over the recent decades and

what was the dominant driver? 2) Can we improve the methodology of lake/reservoir area time series mapping in order to better enable a temporarily consistent monitoring of water storage dynamics in the world? 3) Did the recent trends in global open-surface water storage exhibit a divergence between arid and humid regions, and if so, what does this divergence indicate for the global water cycle and water management?

The above questions were addressed in three chapters. Chapter 2 provides a comprehensive and spatially explicit quantification of lake storage changes across the inner Tibetan Plateau since 2002, through a synergy of satellite imagery and freely-available digital elevation models. By further incorporating satellite gravity observations to a water balance model, the dominant driver of this regional lake storage variation was attributed to net precipitation, i.e., precipitation minus evapotranspiration, rather than glacial melting. Chapter 3 introduces a novel method that substantially improves the temporal coverage in lake/reservoir area mapping, by effectively recovering inundation areas from contaminated spectral images with a relative error of 2.2%. Inclusion of recovered water areas from contaminated images improved the monthly coverage for 400+ lakes and reservoirs in the world by an average of 43%. Chapter 4 combines this novel mapping method and a constellation of satellite altimeters to reveal monthly storage changes in 1000+ major lakes/reservoirs worldwide from 1992 to 2018, the entire satellite altimetry era thus far. The finding confirms a multi-decadal divergence in global open-surface water storage between endorheic (arid/semiarid) and exorheic (more humid) regions. This divergence indicates an amplified contrast between fresh and saline water abundance, and was partially induced by the increasing water impoundment behind dams. Due to the divergence, global lakes and reservoirs slowed down the observed sea level rise by only ~1% during the past nearly three decades.

Global spatiotemporal dynamics of inland water body storage during the satellite altimetry era

by

Fangfang Yao

B.S., Anhui Normal University, 2012
M.S., University of Chinese Academy of Sciences, 2015

A DISSERTATION

submitted in partial fulfillment of the requirements for the degree

DOCTOR OF PHILOSOPHY

Department of Geography and Geospatial Sciences
College of Arts and Sciences

KANSAS STATE UNIVERSITY
Manhattan, Kansas

2020

Approved by:

Major Professor
Jida Wang

Copyright

Abstract

Lakes and reservoirs are essential components of the global hydrological cycle. They function as sentinels of climate change, and provide indispensable water supply, energy generation, aquatic ecosystems for meeting agricultural, industrial, and domestic needs. Despite the importance of lakes and reservoirs to natural systems and human societies, their water storage dynamics are poorly understood on a global scale, especially in remote and harsh environments such as the Tibetan Plateau. The challenge has been even amplified by the currently declining global network of gauging measurements. This knowledge gap prevents a fundamental understanding of the terrestrial water cycle and surface water availability, and thus impedes effective water resource management. Recent regional evidence has suggested that water-abundant regions show increasing trends in surface water extents whereas water-limited regions exhibit decreasing trends. However, whether this divergence also holds true for the storage of open water bodies across the entire land surface remains unknown. A synergy of fine resolution optical imagery and level measurements by satellite altimetry has the potential to accurately deduce lake/reservoir storage variations. However, the existing estimates of lake/reservoir storage changes are mostly limited by the number/size of studied water bodies and the low temporal frequencies in time series, primarily owing to atmospheric contaminations in satellite imagery and inadequate spatiotemporal coverage in altimetry.

This dissertation aims to mitigate the above technical limitations through several remote sensing method advancements, and to leverage multi-mission satellites to investigate the recent lake/reservoir storage dynamics and their implications for the regional and global water cycles. Specifically, this dissertation is orientated to three overarching questions: 1) how has the lake water storage across the landlocked inner Tibetan Plateau changed over the recent decades and

what was the dominant driver? 2) Can we improve the methodology of lake/reservoir area time series mapping in order to better enable a temporarily consistent monitoring of water storage dynamics in the world? 3) Did the recent trends in global open-surface water storage exhibit a divergence between arid and humid regions, and if so, what does this divergence indicate for the global water cycle and water management?

The above questions were addressed in three chapters. Chapter 2 provides a comprehensive and spatially explicit quantification of lake storage changes across the inner Tibetan Plateau since 2002, through a synergy of satellite imagery and freely-available digital elevation models. By further incorporating satellite gravity observations to a water balance model, the dominant driver of this regional lake storage variation was attributed to net precipitation, i.e., precipitation minus evapotranspiration, rather than glacial melting. Chapter 3 introduces a novel method that substantially improves the temporal coverage in lake/reservoir area mapping, by effectively recovering inundation areas from contaminated spectral images with a relative error of 2.2%. Inclusion of recovered water areas from contaminated images improved the monthly coverage for 400+ lakes and reservoirs in the world by an average of 43%. Chapter 4 combines this novel mapping method and a constellation of satellite altimeters to reveal monthly storage changes in 1000+ major lakes/reservoirs worldwide from 1992 to 2018, the entire satellite altimetry era thus far. The finding confirms a multi-decadal divergence in global open-surface water storage between endorheic (arid/semiarid) and exorheic (more humid) regions. This divergence indicates an amplified contrast between fresh and saline water abundance, and was partially induced by the increasing water impoundment behind dams. Due to the divergence, global lakes and reservoirs slowed down the observed sea level rise by only ~1% during the past nearly three decades.

Table of Contents

List of Figures

List of Tables

Acknowledgements

Pursuing a doctorate degree in Geography at Kansas State University over the past four years has been a wonderful experience in my life. Doing research in such a tranquil and small town and exchanging ideas with many great scientists and colleagues were so enjoyable. I want to take the opportunity to express my gratitude to all those who helped and supported me during my Ph.D. life.

First of all, I would like to thank my advisor Dr. Jida Wang. Dr. Wang is a great person and mentor. He helped me a lot with both life and research. He is so kind and generous to provide whatever I needed. I can clearly recall his warm welcome when I first arrived at K-State. He spent two whole days on helping me settle down here. His kind and warm support cannot be overstated. Although being very busy as an Assistant Professor, Dr. Wang was easily reachable to me and his other students even at nights or weekends. Our routine meetings were very helpful. Over the past four years, Dr. Wang advised me on formulating science questions, conducting thorough literature reviews, writing proposals, and revising manuscripts. Without his tremendous support and guidance, this Ph.D. dissertation would have been hardly achieved. I am grateful to Dr. Wang for providing collaboration opportunities with him and other scientists in his network. Through these collaborations, I contributed myself to additional publications and further extended my research network. I also owe much to Dr. Wang's peer-review invitations. These peer-review experience helped me become a critical scholar. Dr. Wang is an excellent example to follow. He showed me a clear path towards tenure. He is always devoted to conducting high-quality research and advising students. His rigorous science attitude, strong enthusiasm, and endless patients inspired all of us in his group.

I would like to extend my thanks to other committee members, Dr. Charles Martin and Dr. Arnaud Temme from K-State, Dr. Jean-François Crétaux from Centre national d'études spatiales (CNES), France, and Dr. Yoshihide Wada from the International Institute of Applied Systems Analysis (IIASA), Austria. Dr. Martin enhanced my knowledge of human-environment interactions and advised me on writing through detailed comments and edits. Taking his course of Human Impacts on the Environment was very beneficial. He motivated me to think deeply on human impacts on water resources. Dr. Temme's office is close to mine and his door was always open to me. He treated me as a colleague rather than a student. Discussing research with him was enjoyable. He helped me with statistical methods and enriched my knowledge of lake formation. My sincere gratitude also goes to the two external committee members, Dr. Crétaux and Dr. Wada, who helped my academic development by not only providing valuable scientific advice, but also increasing my research accountability and broadening my academic network. I worked closely with Dr. Crétaux. He was always interested in any updates of my Ph.D. work and provided many constructive comments and suggestions every time. Particularly, he has been extremely supportive to provide me with the altimetry data from his lab. To promote my research visibility, he invited me to deliver a talk about Tibetan lake dynamics and climate change (Chapter 2 of this dissertation) in the "25 Years of Progress in Radar Altimetry" Symposium in Portugal. I also owe my gratitude to the insight and support of Dr. Wada. His many papers on global hydrology have inspired me tremendously. Annual meetings with Dr. Wada during the recent few AGU conferences were particularly fruitful and unforgettable, where he provided timely comments on my presentations and valuable advice for my career development. While being my external committee, Dr. Wada always provided immediate responses to my questions. His comments and suggestions on my Ph.D. research are insightful and constructive, particularly

from the aspects of how to construct significant and potentially high-profile research. I learnt a lot through collaborations with him.

All committee members were incredibly supportive for my future career development. For example, their strong endorsements contributed to my success in winning the competitive postdoc fellowship from the Cooperative Institute for Research in Environmental Sciences (CIRES) at the University of Colorado Boulder. I also appreciate the support of other K-State faculty members, to name a few, Drs. John Harrington, Douglas Goodin, Shawn Hutchinson, Kendra McLauchlan, Abigail Langston, Katherine Nelson, Stacy Hutchinson, and Aleksey Sheshukov.

I am grateful to many friends at K-State and beyond, including Blake Walter, Meng Ding, Aote Xin, Abu Maroof, Takuto Urano, Colin Bailey, Gabriel Granco, Subarna Chatterjee, Avantika Ramekar, Thomas Larsen, Abbey Marcotte, Kathy Su, Ray Luo, Jordan McAlister, Justin Wright, Di Dong and Chao Wang. Their help and company are highly appreciated, especially those from Blake and Chao. I overlapped with Blake during the first two years of my Ph.D. Daily conversations with him were fruitful. I was adapted to the new American life much faster owing to his generous help. His continued support on improving my writing were deeply appreciated. Chao has been my close friend for twelve years. Our collaborations have started since we were undergraduate and became more extensive during my Ph.D. period. When I told him my initial ideas for Chapter 3, he was even more excited than I was. His assistance in coding substantially improved my working efficiency. His encouragement inspired me a lot to accomplish this Ph.D. work. He was very generous with his time and ideas to help.

I am deeply indebted to my girlfriend Kehan for her support, encouragement, company, and sacrifice over the past six years. Her endless encouragement was my primary motivation to

overcome many challenges, particularly completing this Ph.D. I greatly appreciate her constant company which has brought me so many wonderful moments and so much happiness during my graduate student life. I owe her many holidays and several birthdays during the pursuit of my Ph.D. I will return my love much more in the coming years.

Finally, I would like to thank my family: my parents. My father taught me to be nice and patient and my mother inspired me to be tough and diligent. They are incredibly supportive for my decisions although I have been going farther and farther from home. I sincerely wish they stay happy and healthy, and I hope to visit them soon.

Dedication

This dissertation is dedicated to my mother.

Publications and Presentations

PUBLICATIONS

JOURNAL ARTICLES

Google Scholar Profile: https://scholar.google.com/citations?user=1T2Z0FYAAAAJ

2019 **F. Yao**, J. Wang, C. Wang, and J.-F. Crétaux. Constructing long-term high-frequency time series of global lake and reservoir areas using Landsat imagery. *Remote Sensing of Environment*, 232 (2019): 111210, doi:10.1016/j.rse.2019.111210.

2018 J. Wang, C. Song, J.T. Reager, **F. Yao**, J.S. Famiglietti, Y. Sheng, G.M. MacDonald, F. Brun, H. Müller Schmied, R.A. Marston, and Y. Wada. 2018. Recent global decline in endorheic basin water storages. *Nature Geoscience*, 11: 926-932, doi:10.1038/s41561-018-0265-7.

2018 **F. Yao**, J. Wang, K. Yang, C. Wang, B.A. Walter, and J.-F. Crétaux. 2018. Lake storage variation on the endorheic Tibetan Plateau and its attribution to climate change since the new millennium. *Environmental Research Letters*, 13: 064011, doi:10.1088/1748-9326/aab5d3.

2017 K. Yang, **F. Yao**, J. Wang, J. Luo, Z. Shen, C. Wang and C. Song. 2017. Recent dynamics of alpine lakes on the endorheic Changtang Plateau from multi-mission satellite data. *Journal of Hydrology*, 552, 633-45, doi.org/10.1016/j.jhydrol.2017.07.024.

2015 **F. Yao**, C. Wang, D. Dong, J. Luo, Z. Shen, and K. Yang. 2015. High-resolution mapping of urban surface water using ZY-3 multi-spectral imagery. *Remote Sensing*, 7(9), 12336-12355, doi.org/10.3390/rs70912336.

SCIENTIFIC DATASETS

2018 **F. Yao**, J. Wang, K. Yang, C. Wang, B.A. Walter, and J.-F. Crétaux. 2018. High resolution data set of annual lake areas and water storage across the Inner Tibet, 2002-2015. PANGAEA, doi.org/10.1594/PANGAEA.888706.

2018 J. Wang, C. Song, J.T. Reager, **F. Yao**, J.S. Famiglietti, Y. Sheng, G.M. MacDonald, F. Brun, H. Müller Schmied, R.A. Marston, and Y. Wada. 2018. Terrestrial water storage changes in global endorheic regions, 2002-2016. PANGAEA, doi.org/10.1594/PANGAEA.895895.

CONFERENCE PRESENTATIONS

* ORAL ** INVITED

2019 **F. Yao**, J. Wang, C. Wang, and J.-F. Crétaux (2019, December). Towards time-continuous long-term monitoring of global lakes and reservoirs: a novel algorithm for improving temporal frequency of lake area time series. 2019 American Geophysical Union Fall Meeting. San Francisco, CA.

2019* J. Wang, C. Song, J.T. Reager, **F. Yao**, J.S. Famiglietti, Y. Sheng, G.M. MacDonald, F. Brun, H. Müller Schmied, R.A. Marston, and Y. Wada (2019, December). Recent global decline in endorheic basin water storage and its implications for the water cycle. 2019 American Geophysical Union Fall Meeting. San Francisco, CA.

2019 C. Wang, M. Yu, Q. Gao, and **F. Yao** (2019, December). The impacts of solar photovoltaic farms on land surface temperature in the continental United States. 2019 American Geophysical Union Fall Meeting. San Francisco, CA.

2019 B.A. Walter, J. Wang, and **F. Yao** (2019, July). An enhanced inventory of global dams and reservoirs and their contribution to sea level. 2019 NASA Water Resources Science Team Meeting. Portland, OR.

2018* **F. Yao**, J. Wang, C. Wang, and J.-F. Crétaux (2018, December). Constructing high-frequency time series of global lake and reservoir storage changes using Landsat imagery and radar altimetry. 2018 American Geophysical Union Fall Meeting. Washington, D.C.

2018* **F. Yao**, J. Wang, K. Yang, C. Wang, B. Walter, and J.-F. Crétaux (2018, October). Recent volumetric variability in alpine lakes on the endorheic Tibet and its link to climate change. 2018 Regional AAG. Manhattan, KS.

2018 J. Wang, B.A. Walter, and **F. Yao** (2018, October). Where are dams and reservoirs, and how do they affect surface water budget? 2018 Regional AAG. Manhattan, KS.

2018** **F. Yao**, J. Wang, K. Yang, C. Wang, B.A. Walter, and J.-F. Crétaux (2018, September). Lake storage variation on the endorheic Tibetan Plateau and its attribution to climate change since the new millennium. 2018 Ocean Surface Topography Science Team (OSTST) meeting. Ponta Delgada, São Miguel Island Azores Archipelago, Portugal.

2018 B.A. Walter, J. Wang, and **F. Yao** (2018, April). An Enhanced Inventory of Global Dams and Reservoirs And Their Contribution to Sea Level 2018 *American Association of Geographers Annual Meeting*. New Orleans, LA

2017* **F. Yao**, J. Wang, K. Yang, C. Wang, B.A. Walter, and J.-F. Crétaux (2017, December). Recent volumetric variability in alpine lakes on the endorheic Tibet and its link to climate change. 2017 *American Geophysical Union Fall Meeting.* New Orleans, LA.

2017* **F. Yao**, J. Wang, C. Song, and T. Urano (2017, April). Recent dynamics of global lake water storage revealed by remote sensing. 2017 *American Association of Geographers Annual Meeting*. Boston, MA.

2017* J. Wang, C. Song, Y. Wada, Y. Sheng, **F. Yao**, B.A. Walter, T. Urano, M. Ding, and C. Bailey (2017, April). Global surface water storage in the new Millennium: dynamics, implications, and challenges. 2017 *American Association of Geographers Annual Meeting*. Boston, MA.

2016 K. Yang, **F. Yao**, J. Luo, Z. Shen, C. Wang (2016, December). Combined Landsat Satellite and HJ Satellite for Monitoring Large Alpine Lakes on the Changtang Plateau over 2009-2014. 2016 *American Geophysical Union Fall Meeting*. San Francisco, CA.

Chapter 1 - Introduction

1.1 Overview

Lakes are depressions on land surface that hold standing or slowly flowing water permanently, seasonally or ephemerally (Hutchinson 1957; Williamson et al. 2009). Covering ~3% of global land area (Figure 1.1), lakes are important components of the hydrological and biogeochemical cycles (Bastviken et al. 2011; Müller Schmied et al. 2014; Oki and Kanae 2006). They store the largest proportion of liquid water on Earth's land surface and constitute millions of unique aquatic ecosystems worldwide (Messager et al. 2016). Due to their physical abundance and easy (open-surface) accessibility, lakes and reservoirs serve as one of the major water supplies (along with river discharge and groundwater) globally (Alsdorf et al. 2007). In addition to water supply, they provide ecological, economic and sociological benefits, including the cycling of carbon, pollutants and nutrients (Adrian et al. 2009; Bastviken et al. 2011; Williamson et al. 2009), waterbird habitats (Jia et al. 2018; Wurtsbaugh et al. 2017), inland fishery and shrimp production (McIntyre et al. 2016), sand and mineral extraction (Bioeconomics 2012; Lai et al. 2014), energy generation (Conway et al. 2017), and many recreational services (e.g., swimming, boating, birdwatching, and ice skating) (Brammer et al. 2015; Polunin 2008).

Lakes are sentinels of climate change (Schindler 2009; Sheng and Yao 2009; Williamson et al. 2009). Several variables of lakes have been identified as essential climate variables (ECVs), including lake level, water extent, lake surface water temperature, lake ice thickness, lake ice cover, and lake color (WMO 2016). Some of the variables (e.g., surface water temperature, lake ice, and lake color) are sensitive to changes in air temperature, while others (e.g., lake level and water extent) are closely linked to natural variability and shifts (e.g., wetter or drier) of hydroclimate (Williamson et al. 2009). Existing studies have revealed that warming

has resulted in increasing lake surface temperatures, expanding lake phytoplankton blooms, decreasing ice covers, and changing mixing regimes (Ho et al. 2019; O'Reilly et al. 2015; Sharma et al. 2019; Woolway and Merchant 2019), posing significant stresses on water quality. As warming has induced more climate extremes (flooding and droughts) (Allen and Ingram 2002), the precipitation and river discharge that feed lakes and reservoirs are being increasingly variable (Rodell et al. 2018; Syed et al. 2010). Regional evidence has shown dramatic changes in water quantity (e.g., area and storage) in lakes and reservoirs, particularly in regions that are the most vulnerable to climate change, such as arctic, alpine, and arid/semiarid regions (Crétaux et al. 2016; Smith et al. 2005; Song et al. 2014b; Wang et al. 2018; Yang et al. 2017).

Climate change is not the only source that threatens lakes and reservoirs; increasing anthropogenic stress on these aquatic systems is also evident. The human water use has doubled over the past 50 years (Wada et al. 2011). To meet the ever-growing water demand, two-thirds of the global rivers are regulated by dams (Grill et al. 2019), but four billion people are still suffering water shortage for one month or more annually (Mekonnen and Hoekstra 2016). Global population is projected to increase by another 40% in 2050, requiring 11% more water from reservoirs (Bruinsma 2009; Lehner et al. 2011). Unsustainable water withdrawal and recent long-term droughts have resulted in the desiccation of many large saline lakes and the declines of water levels in many reservoirs in arid and semiarid regions (Hassanzadeh et al. 2012; Hoerling et al. 2014; Wang et al. 2018; Wurtsbaugh et al. 2017), which caused environmental degradation, human health problems (e.g., dust storm owing to exposed saline lakebed), food and energy shortages. By contrast, precipitation extremes have triggered dozens of dam failures per year (Vahedifard et al. 2017), threatening human life and property and flooding croplands downstream. Therefore, an improved understanding of the changing water storage in global lakes

and reservoirs is crucial for predicting regional food yields, hydropower production, and human and ecosystem health (Conway et al. 2017; Gernaat et al. 2017; Griffin and Kellogg 2004; Hassanzadeh et al. 2012; Micklin 1988; Wurtsbaugh et al. 2017). An improved monitoring of lake/reservoir storage dynamics also serves as a fundamental basis for formulating sustainable water managements and migrating climate impacts on surface water (Crétaux et al. 2015; Gao et al. 2012; Ho et al. 2017).

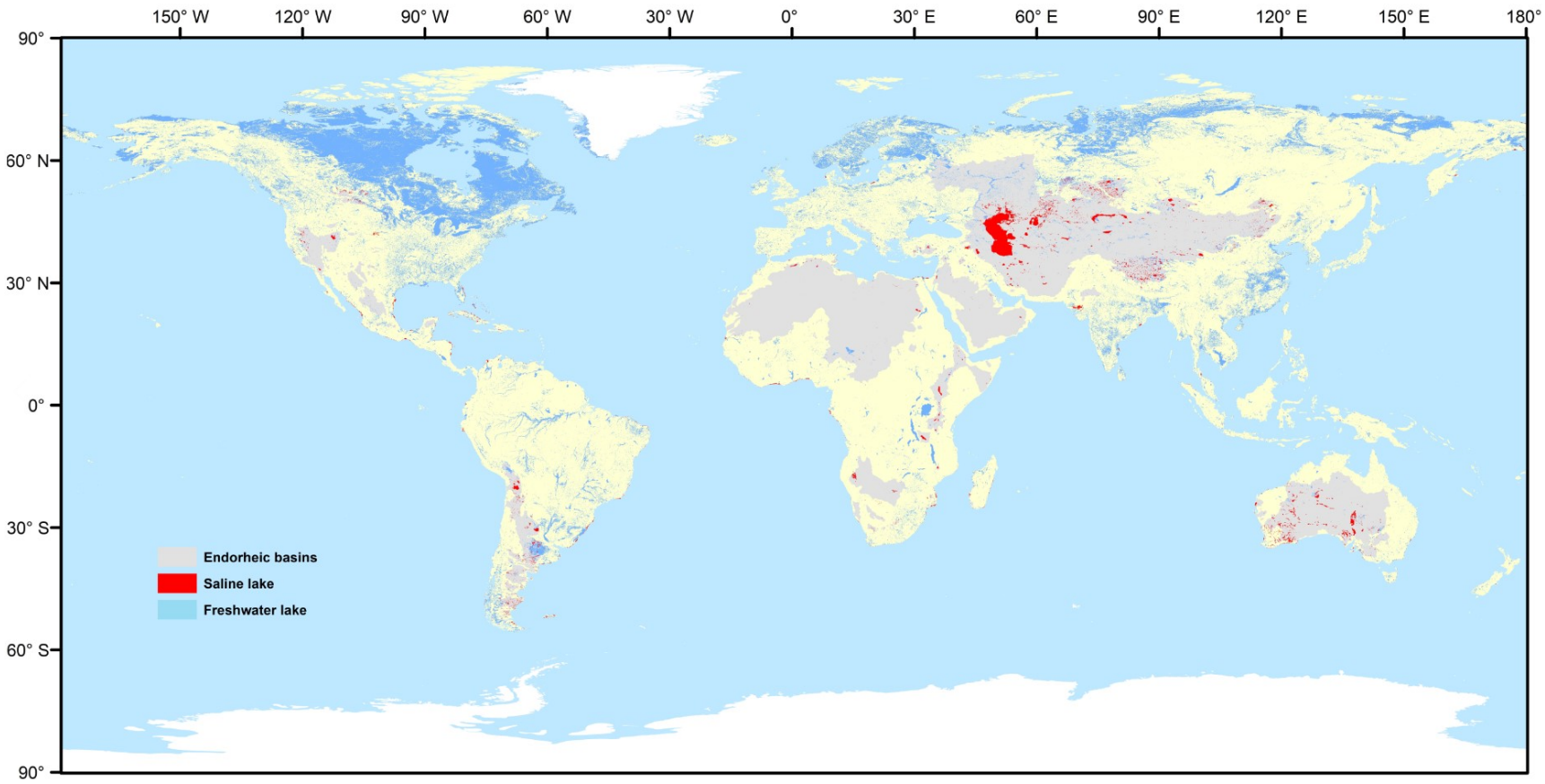

Figure 1.1 Global distribution of lakes and reservoirs in circa 2000 (source: Meng 2019; Wang et al. 2015). Lakes and reservoir shown here include perennial water bodies larger than 0.4 ha (excluding river channels), mapped from circa-2000 Landsat images (Sheng et al. 2016).

1.2 Motivation and statement of the problem

Although lakes and reservoirs provide a large portion of the terrestrial water supply and manifold benefits (ecologically, economically, and sociologically), their water storage is poorly monitored at large geographical scales, especially in remote regions (e.g., Tibetan Plateau), due to limited gauging networks (Calmant et al. 2008). Consequently, spatial and temporal variations of lake/reservoir water storage and their implications for regional and global water cycles remain less understood (Biancamaria et al. 2016). Nevertheless, satellite remote sensing provides new opportunities for measuring lake water storage changes. Changes in lake water storage can be deduced from area changes observed by satellite imagery and level changes measured by satellite altimetry (Zhu et al. 2013). Since the 1990s, radar altimetry has been used to measure inland water levels with repeatability varying from 10 to 35 days (Crétaux et al. 2011). These radar altimeters provided level measurements from space with decimeter accuracy, making accurate assessments of storage variations possible (Gao et al. 2012). Owing to the coarse footprints (typically 10 km or so) and large inter-track distance (>70 km), only large water bodies (e.g., >10-50 km^2) could be effectively observed by the past and current satellite radar altimeters. The lidar/laser altimeters ICESat (Ice, Cloud, and land Elevation Satellite) provide elevation measurements at a finer footprint (70m). Thus, it can be applied to measure water level for smaller water bodies (Song et al. 2013; Zhang et al. 2017). However, its short duration (2003-2009) and long revisit time (~90 days) may introduce large uncertainty for the estimation of long-term water level trends (Crétaux et al. 2016). Due to similar limitations, the follow-up generation ICESat-2, launched in 2018, has not been able to substantially benefit long-term water level monitoring. Therefore, long-term water level records have been mainly derived from radar altimeters. Several databases, including Hydroweb (Crétaux et al. 2011), Global Reservoir

and Lake Monitor (G-REALM) (Birkett et al. 2011), and the Database for Hydrological Time Series of Inland Waters (DAHITI) (Schwatke et al. 2015), provide level variations for about six hundred large lakes and reservoirs globally, processed from the constellation of existing satellite radar altimeters. Although these databases combined consecutive altimeter missions (since 1992), their level records have inconsistent temporal coverages that vary from one to two and half decades (Birkett et al. 2011; Crétaux et al. 2011; Schwatke et al. 2015).

Table 1.1 Summary of major existing lake storage studies on the Tibetan Plateau

Study	Number of studied lakes	Monitoring Methods	Duration	Temporal/spatial resolutions	Main conclusions	Main limitations
(Zhang et al. 2011)	1 (Nam Co)	Landsat, CBERS, HJ-1A/1B, and bathymetric survey	1976-2009	Monthly to a few years / 30-64m	Lake water storage increased. Increased precipitation and runoff from glacier retreat contributed to lake expansion.	Limited number of studied lakes
(Lei et al. 2013)	6	Landsat and In Situ Measurements	1976-2010	1-15 years / 30m	Storage in six major lakes in the central Tibetan Plateau increased, which was caused by increased precipitation and runoff and decreased evaporation.	Limited number of studied lakes; low temporal resolution
(Song et al. 2013)	30	ICESat and Landsat	1970s-2011	1-2 decades / 30m	Lake water storage increased by 92 Gt from 1970s to 2011.	Limited number of studied lakes; low temporal resolution; lacking examination of the driving mechanisms
(Yang et al. 2016)	114	Digital elevation model (SRTM DEM) and LANDSAT	1976-2013	5-15 years / 30m	Lake water storage increased by 103 Gt during 1976-2013.	Limited number of studied lakes; low temporal resolution; lacking examination of the driving mechanism
(Zhang et al. 2017)	68	ICESat and Landsat	1970s–2015	1-15 years / 30m	Lake water storage increased. The net precipitation dominated the lake storage variations.	Limited number of studied lakes

Table 1.2 Summary of major global studies on lake/reservoir storage changes

Study	Number of studied water bodies	Monitoring methods	Duration	Temporal/Spatial resolutions	Main conclusions	Main limitations
(Gao et al. 2012)	34	MODIS and radar altimetry	1992-2010	16-day / 250m	Reservoir storage changes can be estimated using satellites alone; Mean absolute error is about 4%	Limited number of studied lakes; lacking scientific investigations at global or continental scales
(Crétaux et al. 2016)	~100	Landsat, MODIS, and radar altimetry	1992-now	Sub-monthly to several years / 30-250m	Lakes show different responses to climate change; understanding climate impacts on lake water budgets requires long-term monitoring of lake volume.	Limited number of studied lakes; low temporal resolution; lacking scientific investigations at global or continental scales
(Wang et al. 2018)	144	Landsat, MODIS, and radar altimetry	2002-2016	Monthly to inter-annual / 30-250m	Widespread lake storage decline in endorheic regions.	Limited number of studied lakes; short studied period; low temporal resolution for most studied lakes.
(Schwatke et al. 2019)	32	Landsat, Sentinel-2, and radar altimetry	1984-now	Sub-monthly to several years / 10-30m	A new automated method for constructing time-variable water areas using two satellite missions and a data gap filling technique.	Limited number of studied lakes; lacking scientific investigations at global or continental scales
(Busker et al. 2019)	137	Landsat-based inundation areas, radar altimetry	1984-now	Sub-monthly to several years / 30m	42% of studied lakes have strong area-level correlations. Validated by 18 lakes with in-situ measurements, the mean relative error is 7.42%	Limited number of studied lakes; low temporal resolution; lacking scientific investigations at global or continental scales

To provide a temporally consecutive monitoring of storage changes, previous work has combined inconsistent altimetry level records with consecutive lake areas observed from high temporal (i.e., 1 day) Moderate Resolution Imaging Spectroradiometer (MODIS) imagery (Gao et al. 2012; Tong et al. 2016). However, many lakes and reservoirs (even for large ones) have minor changes around their shores, which may not be discernible owing to the coarse resolution of MODIS imagery (250-500 m in visual and near-infrared bands). Compared with MODIS, Landsat imagery have a much finer spatial resolution (i.e., 30 m) and a nominal temporal resolution of 16 days (or finer if multiple sensors, e.g., from Landsat 5 and 7, are combined). But due to frequent cloud covers (Rossow and Schiffer 1999), recent Landsat-based estimates of lake areas are limited at best to a monthly temporal resolution or, for large water bodies with frequent cloud covers, up to once per a few years (Donchyts et al. 2016; Pekel et al. 2016; Yao et al. 2018). The tradeoff between spatial and temporal resolutions has been identified as a major challenge for monitoring inundation extents, especially in lakes with large seasonal fluctuations (Huang et al. 2018). Compared with large water bodies, monitoring smaller lakes is even more challenging due to lacking water level data (Biancamaria et al. 2016; Song et al. 2014a).

Owing to the above challenges, existing knowledge of recent lake water storage changes is rather limited at large geographic scales, particularly in remote and harsh regions such as the Tibetan Plateau (Table 1.1). The Tibetan Plateau is home to more than one thousand alpine lakes larger than 1 km^2 (Messager et al. 2016; Zhang et al. 2014), but existing approaches for estimating volume variations across the Tibetan Plateau are restricted to a limited number of lakes or multi-year to decadal temporal frequencies (Table 1.1) (Crétaux et al. 2016; Lei et al. 2013; Song et al. 2013; Yang et al. 2016; Zhang et al. 2017). For example, Yang et al. (2016) estimated volume variations in 114 lakes at 5 to 14-year intervals during 1976-2013, but

included only three discreet years (2000, 2005 and 2013) after 2000. Lake dynamics vary across the Tibetan Plateau and exhibit different changing rates during different periods (Crétaux et al. 2016). Particularly, in the past few years (e.g., 2013-2015), expansions of many Tibetan lakes have been decelerated or partially reversed (Yang et al. 2017; Zhang et al. 2017), which suggests the necessity of a continuous, long-term monitoring of their volume variations. Globally, storage in lakes and reservoirs is poorly monitored (Table 1.2), even only for the ~400 largest lakes and reservoirs greater than 500 km^2 (Messager et al. 2016; Walter 2018). Gao et al. (2012) used radar altimetry and MOIDS data to estimate storage variations in only dozens of large reservoirs worldwide in a 16-day interval from 1992 to 2010. Crétaux et al. (2016) provided storage variations for about one hundred lakes by combining satellite imagery and radar altimetry, but the generated storage time series have inconsistent durations that vary from a few years to more than two decades. More recently, Busker et al. (2019) combined historical water extents delineated from Landsat imagery by Pekel et al. (2016) with radar altimetry to construct storage time series during 1984 to 2015 for 137 lakes. However, temporal frequencies of the produced area time series are still limited by the availability of cloud-free images. These limitations prevent these studies from revealing scientific findings on the global scale. Therefore, advanced algorithms are needed to leverage information acquired by different satellite missions to accurately assess storage changes at fine spatial and temporal scales (Crétaux et al. 2016).

The existing assessments of recent changes in surface water area show notable patterns (Donchyts et al. 2016; Pekel et al. 2016; Zou et al. 2018). At the contiguous United States, for example, humid regions (e.g., the Southeast and the North Great Plains) show increasing trends in surface water areas whereas arid and semiarid regions (e.g., the West and the southern Pacific region) experienced a decline in inundation areas during the past three decades (Zou et al. 2018).

Globally, water area losses are more concentrated than area gains, and are mainly located in the world's arid and semiarid regions (Donchyts et al. 2016; Pekel et al. 2016). This contrast seems to reflect a hypothesized divergence in hydroclimate, the so-called "wet-get-wetter, dry-get-drier" pattern (Held and Soden 2006). Divergent trends in total water areas do not necessarily lead to a synchronous divergence in total water storage because different water bodies have different bathymetries (Messager et al. 2016). Whether there is a divergence in surface water storage trends between arid and humid regions, however, has not been examined on a global scale.

1.3 Science questions and objectives

The overarching goal of this dissertation is to advance the understanding of recent lake and reservoir storage dynamics on regional and global scales by leveraging multi-mission satellite data. This goal is approached by addressing three science questions:

Science question 1: how has the lake water storage across the inner Tibetan Plateau changed over the recent decades and what was the dominant driver (e.g., warming or wetting)?

Science question 2: how can we improve the methodology of water area time series mapping using existing remote sensing images, in order to better enable a temporarily consistent monitoring of water storage dynamics in the world?

Science question 3: did the recent global open-surface water storage changes exhibit a divergence between endorheic (arid) and exorheic (humid) regions, and if so, what does this divergence indicate for the global water cycle and water resource management?

To answer these questions, four specific objectives are pursued. Each objective is associated with one hypothesis, as detailed below:

Objective 1: To understand regional lake water storage changes and the link to climate change: a case study in the inner Tibetan Plateau.

The inner Tibetan Plateau experienced widespread lake area expansion since 2000 (Song et al. 2014b), although the lake expansion decelerated over the recent years (e.g., 2013-2015) (Yang et al. 2017; Zhang et al. 2017). However, the driving mechanism of recent lake dynamics remains unclear. Over the recent decades, the unprecedented warming has caused significant glacier retreat (Lei et al. 2012; Xu et al. 2008). Influenced by strengthened westerlies through advection of moisture, the inner Tibetan Plateau also experienced increasing net precipitation (surplus between precipitation and evapotranspiration) (Gao et al. 2015). Both increasing net precipitation and warming-induced increasing runoff from glacier retreat contribute to lake expansion. However, whether the lake expansion was mainly due to warming or wetting remains unknown.

Hypothesis 1: The recent lake storage changes in the inner Tibetan Plateau are dominated by changes in net precipitation (i.e., precipitation minus evapotranspiration) rather than warming-induced glacial melting and permafrost degradation.

Objective 2: To improve the temporal frequency of water area time series for global lake area mapping.

Given inconsistent altimetry level records, consecutive lake area time series are essential for a consecutive monitoring of storage changes. However, cloud contamination often poses a major challenge for producing temporally continuous area time series. The temporal monitoring frequency could be potentially improved by using contaminated images (i.e., those affected by

cloud or observation gaps). However, how to accurately estimate lake areas from the poor-quality contaminated images remains a big challenge.

Hypothesis 2: Contaminated images can be used to increase the temporal frequency of water area time series without sacrificing the accuracy.

Objective 3: To compare lake water storage changes between endorheic (arid) and exorheic (humid) basins.

Whether the "wet-get-wetter-dry-get-drier" pattern holds over the entire land surface is highly debated (Byrne and O'Gorman 2015; Greve et al. 2014; Rodell et al. 2018; Zou et al. 2018). Although global surface water area changes show a general divergence between dry and wet regions (Donchyts et al. 2016; Pekel et al. 2016), whether there is a divergence in surface water storage trends between dry and wet regions remains unknown. Divergent trends in total water area do not necessarily lead to a synchronous divergence in total water storage because different water bodies have different bathymetries (Messager et al. 2016). Examples could be found in the shrinking Great Salt Lake (Utah, USA) and the expanding Lake Seling (Tibet, China) over the past two decades. The area decrease in the Great Salt Lake is much larger than the area increase in Lake Seling, leading to a net loss (~1000 km^2) in the total area of these two lakes (Crétaux et al. 2011; Wurtsbaugh et al. 2017). However, their combined storage increased by 20 Gt due to a greater level increase (a steeper bathymetry) in Lake Seling (Crétaux et al. 2011; Wurtsbaugh et al. 2017). Therefore, a comprehensive assessment of lake and reservoir storage changes is required to confidently test the possible divergence in open surface water storage trends.

Hypothesis 3: The trends in open surface water storage show a divergence in direction between endorheic and exorheic basins. In other words, humid exorheic regions show an increasing trend while arid endorheic regions exhibit a decreasing trend.

Objective 4: To compare storage changes among saline lakes, freshwater lakes, and artificial reservoirs.

Saline lakes are mostly found in arid regions while humid regions are dominated by freshwater lakes and reservoirs. According to some of the finest global lake inventories (Meng 2019; Messager et al. 2016), saline lakes account for 44% of the total lake volume, which is slightly exceeded by freshwater lakes and reservoirs representing the majority 56%. If the hypothesized divergence in open surface water storage between arid and humid regions is true, it probably also leads to an amplified contrast between surface fresh and saline water abundance. Continued dam building in the developing world may result in an increase in global reservoir storage (Grill et al. 2019; Lehner et al. 2011; Walter 2018; Walter et al. 2019). Most of the existing studies estimated global reservoir storage changes using reported/registered reservoir maximum capacities and commission years (Chao et al. 2008; Wada et al. 2016). Since water storages in reservoirs (especially large ones) fluctuate as a result of human water regulations and climate variability, the static maximum capacities may not reflect an accurate estimate of the actual reservoir storage variations. In contrast, regional evidence of saline water storage decline has been seen in the desiccation of many large saline lakes (Chen et al. 2017; Hassanzadeh et al. 2012; Wang et al. 2018; Wurtsbaugh et al. 2017), suggesting a possible net loss of global saline lake storage. If this decline is proved to be true, the water storage loss in saline lakes would signify a positive contribution to the sea level rise. This positive contribution may partially offset

the negative contribution from reservoir impoundments. However, to my best knowledge, no previous studies have provided a comparison of water storage changes among saline lakes, freshwater lakes and reservoirs on the global scale.

Hypothesis 4: The contrast between fresh and saline water abundance was amplified over the recent decades with a decreasing saline water storage and an increasing freshwater storage. Increasing freshwater storage was mainly attributed to recently filled reservoirs. The decreasing saline water storage largely offset the negative contribution from reservoir impoundments on sea level rise.

1.4 Dissertation structure

Following this Introduction Chapter, Chapter 2 focuses on a regional study that investigates the recent lake storage dynamics on the inner Tibetan Plateau and the link to climate change (Objective 1 and Science Question 1). Chapter 3 addresses the challenge in water area time series mapping in order to better assist the monitoring of temporarily consistent/continuous water storage changes (Objective 2 and Science Question 2). Chapter 4 reveals global patterns of lake and reservoir storage changes and their implications for the global water cycle and water resource management (Objective 3 & 4, and Science Question 3).

The objective of Chapter 2 is to understand regional lake water storage changes and the link to climate change on the inner Tibetan Plateau. In this chapter, I integrated optical imagery and digital elevation models (DEMs) to uncover the fine spatial details of lake water storage (LWS) changes across the inner Tibetan Plateau at an annual timescale after the start of the current millennium (from 2002 to 2015). The lake storage trends estimated from DEM-derived hypsometry were validated by hypsometric information based on long-term altimetry

measurements. In an endorheic (hydrologically landlocked) environment such as the inner Tibetan Plateau, net precipitation, i.e., the residual of precipitation after evaporative loss, equals the changes in the terrestrial water storage, which was quantified using the gravity observations of the Gravity Recovery and Climate Experiment (GRACE) satellites. Integrating these observations into a mass balance model, the contribution of net precipitation was examined to test whether the recent lake water storage on the inner Tibetan Plateau was primarily driven by wetting or warming-induced melting runoff from the feeding glaciers. The presented research in this chapter has been published in *Environmental Research Letters* (Yao et al., 2018)

The objective of Chapter 3 is to improve the temporal frequency of water area time series for global lake area mapping. This chapter introduces a novel mapping method that can produce temporally continuous long-term water area time series at a fine spatial resolution for lakes and reservoirs worldwide. Cloud contamination often poses a major challenge for the production of temporally continuous time series. To overcome this challenge, a novel method was developed to improve the temporal frequency of usable Landsat observations for mapping lakes and reservoirs, by effectively recovering inundation areas from contaminated images. This method automated three primary steps on the cloud-based platform Google Earth Engine. It first leveraged multiple spectral indices to optimize water mapping from archival Landsat images acquired since 1992. Errors induced by minor contaminations were next corrected by the topology of isobaths extracted from nearly cloud-free images. The isobaths were then used to recover water areas under major contaminations through an efficient vector-based interpolation. This method was validated on 428 lakes/reservoirs worldwide that range from ~2 km^2 to ~82,000 km^2 with time-variable levels measured by satellite altimeters. The robustness of this method was further verified under five challenging mapping scenarios, including fluvial lakes in humid

basins, reservoirs with complex geometries, saline lakes with high mineral concentrations, lakes/reservoirs in mountainous regions, and pan-Arctic lakes with frequent snow/ice covers. Potential applications on other optical and SAR sensors (e.g., Sentinel-2 and the Surface Water and Ocean Topography (SWOT) mission) were also discussed in this chapter. The presented research in this chapter has been published in *Remote Sensing of Environments* (Yao et al., 2019)

The objectives of Chapter 4 are 1) to compare lake water storage changes between endorheic (arid) and exorheic (humid) basins; 2) to reveal implications of open-surface water storage changes for the global water cycle and water resource management. By leveraging the novel water mapping method (as introduced in Chapter 3) and satellite altimetry, this chapter provides a comprehensive assessment of recent storage changes in major lakes and reservoirs worldwide. Monthly storage anomalies were estimated for more than one thousand major water bodies from 1992 to 2018 (i.e., the existing satellite altimetry era). The quantified lake storage changes were then used to test the hypothesized divergence between 1) arid and humid regions and 2) saline lakes and freshwater bodies. Although this dissertation does not aim to decouple the influences of human forces and climate change on lake storage dynamics, storage changes in recently filled reservoirs were isolated to facilitate the discussion of possible impacts of human water impoundments on the changes in freshwater abundance. Finally, given this comprehensive monitoring of global lake/reservoir storage dynamics, I was able to calculate a more definite impact of open surface water bodies on the recent sea level change.

1.5 References

Allen, M.R., & Ingram, W.J. (2002). Constraints on future changes in climate and the hydrologic cycle. *Nature, 419*, 224, doi:10.1038/nature01092.

Alsdorf, D.E., Rodriguez, E., & Lettenmaier, D.P. (2007). Measuring surface water from space. *Reviews of Geophysics*, 45, RG2002, doi:10.1029/2006RG000197.

Bastviken, D., Tranvik, L.J., Downing, J.A., Crill, P.M., & Enrich-Prast, A. (2011). Freshwater methane emissions offset the continental carbon sink. *science, 331*, 50-50, doi:10.1126/science.1196808.

Biancamaria, S., Lettenmaier, D.P., & Pavelsky, T.M. (2016). The SWOT mission and its capabilities for land hydrology. *Surveys in Geophysics*, 37, 307-337, doi:10.1007/s10712-015-9346-y.

Bruinsma, J. (2009). The resource outlook to 2050: by how much do land, water and crop yields need to increase by 2050. In, *Expert meeting on how to feed the world in* (pp. 24-26)

Busker, T., Roo, A.d., Gelati, E., Schwatke, C., Adamovic, M., Bisselink, B., Pekel, J.-F., & Cottam, A. (2019). A global lake and reservoir volume analysis using a surface water dataset and satellite altimetry. *Hydrology and Earth System Sciences*, 23, 669-690, doi:10.5194/hess-23-669-2019.

Byrne, M.P., & O'Gorman, P.A. (2015). The response of precipitation minus evapotranspiration to climate warming: Why the "wet-get-wetter, dry-get-drier" scaling does not hold over land. *Journal of Climate, 28*, 8078-8092, doi:10.1175/JCLI-D-15-0369.1.

Calmant, S., Seyler, F., & Cretaux, J.F. (2008). Monitoring continental surface waters by satellite altimetry. *Surveys in Geophysics*, 29, 247-269, doi:10.1007/s10712-008-9051-1.

Chao, B.F., Wu, Y., & Li, Y. (2008). Impact of artificial reservoir water impoundment on global sea level. *science, 320*, 212-214, doi:10.1126/science.1154580.

Chen, J., Pekker, T., Wilson, C., Tapley, B., Kostianoy, A., Cretaux, J.F., & Safarov, E. (2017). Long‐term Caspian Sea level change. *Geophysical research letters, 44*, 6993-7001, doi:10.1002/2017GL073958.

Conway, D., Dalin, C., Landman, W.A., & Osborn, T.J. (2017). Hydropower plans in eastern and southern Africa increase risk of concurrent climate-related electricity supply disruption. *Nature Energy, 2*, 946-953, doi:10.1038/s41560-017-0037-4.

Crétaux, J.-F., Abarca-del-Río, R., Berge-Nguyen, M., Arsen, A., Drolon, V., Clos, G., & Maisongrande, P. (2016). Lake volume monitoring from space. *Surveys in Geophysics*, 37, 269-305, doi:10.1007/s10712-016-9362-6.

Crétaux, J.-F., Biancamaria, S., Arsen, A., Bergé-Nguyen, M., & Becker, M. (2015). Global surveys of reservoirs and lakes from satellites and regional application to the Syrdarya river basin. *Environmental Research Letters*, 10, 015002, doi:10.1088/1748-9326/10/1/015002.

Crétaux, J.-F., Jelinski, W., Calmant, S., Kouraev, A., Vuglinski, V., Bergé-Nguyen, M., Gennero, M.-C., Nino, F., Del Rio, R.A., & Cazenave, A. (2011). SOLS: A lake database to monitor in the Near Real Time water level and storage variations from remote sensing data. *Advances in space research*, 47, 1497-1507, doi:10.1016/j.asr.2011.01.004.

Donchyts, G., Baart, F., Winsemius, H., Gorelick, N., Kwadijk, J., & van de Giesen, N. (2016). Earth's surface water change over the past 30 years. *Nature Climate Change*, 6, 810-813, doi:10.1038/nclimate3111.

Gao, H., Birkett, C., & Lettenmaier, D.P. (2012). Global monitoring of large reservoir storage from satellite remote sensing. *Water Resources Research*, 48, W09504, doi:10.1029/2012WR012063.

Gao, Y., Li, X., Leung, L.R., Chen, D., & Xu, J. (2015). Aridity changes in the Tibetan Plateau in a warming climate. *Environmental Research Letters, 10*, 034013, doi:10.1088/1748-9326/10/3/034013.

Gernaat, D.E., Bogaart, P.W., van Vuuren, D.P., Biemans, H., & Niessink, R. (2017). High-resolution assessment of global technical and economic hydropower potential. *Nature Energy, 2*, 821-828, doi:10.1038/s41560-017-0006-y.

Greve, P., Orlowsky, B., Mueller, B., Sheffield, J., Reichstein, M., & Seneviratne, S.I. (2014). Global assessment of trends in wetting and drying over land. *Nature Geoscience, 7*, 716, doi:10.1038/ngeo2247.

Griffin, D.W., & Kellogg, C.A. (2004). Dust storms and their impact on ocean and human health: dust in Earth's atmosphere. *EcoHealth, 1*, 284-295, doi:10.1007/s10393-004-0120-8.

Grill, G., Lehner, B., Thieme, M., Geenen, B., Tickner, D., Antonelli, F., Babu, S., Borrelli, P., Cheng, L., & Crochetiere, H. (2019). Mapping the world's free-flowing rivers. *Nature, 569*, 215, doi:10.1038/s41586-019-1111-9.

Hassanzadeh, E., Zarghami, M., & Hassanzadeh, Y. (2012). Determining the main factors in declining the Urmia Lake level by using system dynamics modeling. *Water Resources Management, 26*, 129-145, doi:10.1007/s11269-011-9909-8.

Held, I.M., & Soden, B.J. (2006). Robust responses of the hydrological cycle to global warming. *Journal of Climate, 19*, 5686-5699, doi:10.1175/JCLI3990.1.

Ho, J.C., Michalak, A.M., & Pahlevan, N. (2019). Widespread global increase in intense lake phytoplankton blooms since the 1980s. *Nature, 574*, 667-670, doi:10.1038/s41586-019-1648-7.

Ho, M., Lall, U., Allaire, M., Devineni, N., Kwon, H.H., Pal, I., Raff, D., & Wegner, D. (2017). The future role of dams in the United States of America. *Water Resources Research, 53*, 982-998, doi:10.1002/2016WR019905.

Hoerling, M., Eischeid, J., Kumar, A., Leung, R., Mariotti, A., Mo, K., Schubert, S., & Seager, R. (2014). Causes and predictability of the 2012 Great Plains drought. *Bulletin of the American Meteorological Society, 95*, 269-282, doi:10.1175/BAMS-D-13-00055.1.

Huang, C., Chen, Y., Zhang, S., & Wu, J. (2018). Detecting, Extracting, and Monitoring Surface Water From Space Using Optical Sensors: A Review. *Reviews of Geophysics*, 56, 333-360, doi:10.1029/2018RG000598.

Hutchinson, G.E. (1957). A Treatise on. *Limnology, 1*, 243.

Lehner, B., Liermann, C.R., Revenga, C., Vörösmarty, C., Fekete, B., Crouzet, P., Döll, P., Endejan, M., Frenken, K., & Magome, J. (2011). High‐resolution mapping of the world's reservoirs and dams for sustainable river‐flow management. *Frontiers in Ecology and the Environment,* 9, 494-502, doi:10.1890/100125.

Lei, Y., Yao, T., Bird, B.W., Yang, K., Zhai, J., & Sheng, Y. (2013). Coherent lake growth on the central Tibetan Plateau since the 1970s: Characterization and attribution. *Journal of Hydrology, 483*, 61-67, doi:10.1016/j.jhydrol.2013.01.003.

Lei, Y., Yao, T., Yi, C., Wang, W., Sheng, Y., Li, J., & Joswiak, D. (2012). Glacier mass loss induced the rapid growth of Linggo Co on the central Tibetan Plateau. *Journal of Glaciology, 58*, 177-184, doi:10.3189/2012JoG11J025.

Mekonnen, M.M., & Hoekstra, A.Y. (2016). Four billion people facing severe water scarcity. *Science advances*, 2, e1500323, doi:10.1126/sciadv.1500323.

Meng, D. (2019). An improved geography of surface water abundance in lakes and reservoirs.

Messager M L, Lehner B, Grill G, Nedeva I and Schmitt O 2016 Estimating the volume and age of water stored in global lakes using a geo-statistical approach *Nature Communications* 7 13603, doi: 10.1038/ncomms13603.

Micklin, P.P. (1988). Desiccation of the Aral Sea: a water management disaster in the Soviet Union. *science, 241*, 1170, doi:10.1126/science.241.4870.1170.

Müller Schmied, H., Eisner, S., Franz, D., Wattenbach, M., Portmann, F.T., Flörke, M., & Döll, P. (2014). Sensitivity of simulated global-scale freshwater fluxes and storages to input data, hydrological model structure, human water use and calibration. *Hydrology & Earth System Sciences Discussions, 11*, doi:10.5194/hessd-11-1583-2014.

O'Reilly, C.M., Sharma, S., Gray, D.K., Hampton, S.E., Read, J.S., Rowley, R.J., Schneider, P., Lenters, J.D., McIntyre, P.B., & Kraemer, B.M. (2015). Rapid and highly variable warming of lake surface waters around the globe. *Geophysical research letters, 42*, 10,773-710,781, doi:10.1002/2015GL066235.

Oki, T., & Kanae, S. (2006). Global hydrological cycles and world water resources. *science, 313*, 1068-1072, doi:10.1126/science.1128845.

Pekel, J.-F., Cottam, A., Gorelick, N., & Belward, A.S. (2016). High-resolution mapping of global surface water and its long-term changes. *Nature*, 540(7633), 418, doi:10.1038/nature20584.

Rodell, M., Famiglietti, J.S., Wiese, D.N., Reager, J.T., Beaudoing, H.K., Landerer, F.W., & Lo, M.H. (2018). Emerging trends in global freshwater availability. *Nature, 557*, 651-659, doi:10.1038/s41586-018-0123-1.

Rossow, W.B., & Schiffer, R.A. (1999). Advances in understanding clouds from ISCCP. *Bulletin of the American Meteorological Society, 80*, 2261-2287, doi:10.1175/1520-0477(1999)080<2261:AIUCFI>2.0.CO;2.

Schindler, D. (2009). Lakes as sentinels and integrators for the effects of climate change on watersheds, airsheds, and landscapes. *Limnology and Oceanography, 54*, 2349-2358, doi:10.4319/lo.2009.54.6_part_2.2349.

Schwatke, C., Scherer, D., & Dettmering, D. (2019). Automated Extraction of Consistent Time-Variable Water Surfaces of Lakes and Reservoirs Based on Landsat and Sentinel-2. *Remote Sensing, 11*, 1010, doi:10.3390/rs11091010.

Sharma, S., Blagrave, K., Magnuson, J.J., O'Reilly, C.M., Oliver, S., Batt, R.D., Magee, M.R., Straile, D., Weyhenmeyer, G.A., & Winslow, L. (2019). Widespread loss of lake ice around the Northern Hemisphere in a warming world. *Nature Climate Change, 9*, 227-231, doi:10.1038/s41558-018-0393-5.

Sheng, Y., & Yao, T. (2009). Integrated assessments of environmental change on the Tibetan Plateau. *Environmental Research Letters, 4*, 045201, doi:10.1088/1748-9326/4/4/045201.

Smith, L.C., Sheng, Y., MacDonald, G., & Hinzman, L. (2005). Disappearing arctic lakes. *science, 308*, 1429-1429, doi:10.1126/science.1108142.

Song, C., Huang, B., & Ke, L. (2013). Modeling and analysis of lake water storage changes on the Tibetan Plateau using multi-mission satellite data. *Remote Sensing of Environment, 135*, 25-35, doi:10.1016/j.rse.2013.03.013.

Song, C., Huang, B., & Ke, L. (2014a). Inter‐annual changes of alpine inland lake water storage on the Tibetan Plateau: Detection and analysis by integrating satellite altimetry and optical imagery. *Hydrological Processes, 28*, 2411-2418, doi:10.1002/hyp.9798.

Song, C., Huang, B., Richards, K., Ke, L., & Hien Phan, V. (2014b). Accelerated lake expansion on the Tibetan Plateau in the 2000s: Induced by glacial melting or other processes? *Water Resources Research, 50*, 3170-3186, doi:10.1002/2013WR014724.

Syed, T.H., Famiglietti, J.S., Chambers, D.P., Willis, J.K., & Hilburn, K. (2010). Satellite-based global-ocean mass balance estimates of interannual variability and emerging trends in continental freshwater discharge. *Proceedings of the National Academy of Sciences, 107*, 17916-17921, doi:10.1073/pnas.1003292107.

Tong, X., Pan, H., Xie, H., Xu, X., Li, F., Chen, L., Luo, X., Liu, S., Chen, P., & Jin, Y. (2016). Estimating water volume variations in Lake Victoria over the past 22years using multi-mission altimetry and remotely sensed images. *Remote Sensing of Environment, 187*, 400-413, doi:10.1016/j.rse.2016.10.012.

Vahedifard, F., AghaKouchak, A., Ragno, E., Shahrokhabadi, S., & Mallakpour, I. (2017). Lessons from the Oroville dam. *science, 355*, 1139-1140, doi:10.1126/science.aan0171.

Wada, Y., Reager, J.T., Chao, B.F., Wang, J., Lo, M.-H., Song, C., Li, Y., & Gardner, A.S. (2016). Recent Changes in Land Water Storage and its Contribution to Sea Level Variations. *Surveys in Geophysics*, 1-22, doi:10.1007/s10712-016-9399-6.

Wada, Y., Van Beek, L., Viviroli, D., Dürr, H.H., Weingartner, R., & Bierkens, M.F. (2011). Global monthly water stress: 2. Water demand and severity of water stress. *Water Resources Research, 47*, doi:10.1029/2010WR009792.

Walter, B. (2018). An Enhanced Inventory of Global Dams and Reservoirs and Their Contribution to Sea Level.

Wang, J., Sheng, Y., Song, C., Urano, T., Satori, P., & Ford, S. (2015). A high-resolution global lake inventory with classified freshwater and saline types. American Geophysical Union: San Francesco, California, December 14–18, 2015.

Wang, J., Song, C., Reager, J.T., Yao, F., Famiglietti, J.S., Sheng, Y., MacDonald, G.M., Brun, F., Schmied, H.M., Marston, R.A., & Wada, Y. (2018). Recent global decline in endorheic basin water storages. *Nature Geoscience, 11*, 926-932, doi:10.1038/s41561-018-0265-7.

Williamson, C.E., Saros, J.E., Vincent, W.F., & Smol, J.P. (2009). Lakes and reservoirs as sentinels, integrators, and regulators of climate change. *Limnology and Oceanography, 54*, 2273-2282, doi:10.4319/lo.2009.54.6_part_2.2273.

WMO (2016). The Global Observing System for Climate: Implementation Needs*., 200*, 325

Woolway, R.I., & Merchant, C.J. (2019). Worldwide alteration of lake mixing regimes in response to climate change. *Nature Geoscience, 12*, 271-276, doi:10.1038/s41561-019-0322-x.

Wurtsbaugh, W.A., Miller, C., Null, S.E., DeRose, R.J., Wilcock, P., Hahnenberger, M., Howe, F., & Moore, J. (2017). Decline of the world's saline lakes. *Nature Geoscience*, 10, 816–821, doi:10.1038/ngeo3052.

Xu, Z., Gong, T., & Li, J. (2008). Decadal trend of climate in the Tibetan Plateau—regional temperature and precipitation. *Hydrological Processes, 22*, 3056-3065

Yang, K., Yao, F., Wang, J., Luo, J., Shen, Z., Wang, C., & Song, C. (2017). Recent dynamics of alpine lakes on the endorheic Changtang Plateau from multi-mission satellite data. *Journal of Hydrology, 552,* 633-645, doi:10.1016/j.jhydrol.2017.07.024.

Yang, R., Zhu, L., Wang, J., Ju, J., Ma, Q., Turner, F., & Guo, Y. (2016). Spatiotemporal variations in volume of closed lakes on the Tibetan Plateau and their climatic responses from 1976 to 2013. *Climatic Change*, 1-13, 621-33, doi:10.1007/s10584-016-1877-9.

Zhang, B., Wu, Y., Zhu, L., Wang, J., Li, J., & Chen, D. (2011). Estimation and trend detection of water storage at Nam Co Lake, central Tibetan Plateau. *Journal of Hydrology, 405*, 161-170, doi:10.1016/j.jhydrol.2011.05.018.

Zhang, G., Yao, T., Shum, C., Yi, S., Yang, K., Xie, H., Feng, W., Bolch, T., Wang, L., & Behrangi, A. (2017). Lake volume and groundwater storage variations in Tibetan Plateau's endorheic basin. *Geophysical research letters*, 44, 5550-5560, doi:10.1002/2017GL073773.

Zhang, G., Yao, T., Xie, H., Zhang, K., & Zhu, F. (2014). Lakes' state and abundance across the Tibetan Plateau. *Chinese science bulletin, 59*, 3010-3021, doi:10.1007/s11434-014-0258-x.

Zhu, G., Su, Y., Li, X., Zhang, K., & Li, C. (2013). Estimating actual evapotranspiration from an alpine grassland on Qinghai-Tibetan plateau using a two-source model and parameter uncertainty analysis by Bayesian approach. *Journal of Hydrology, 476*, 42-51, doi:10.1016/j.jhydrol.2012.10.006.

Zou, Z., Xiao, X., Dong, J., Qin, Y., Doughty, R.B., Menarguez, M.A., Zhang, G., & Wang, J. (2018). Divergent trends of open-surface water body area in the contiguous United States from 1984 to 2016. *Proceedings of the National Academy of Sciences*, 201719275, doi:10.1073/pnas.1719275115.

Chapter 2 - Lake storage variation on the endorheic Tibetan Plateau and its attribution to climate change since the new millennium

2.1 Introduction

Lakes are important hydrological components in alpine environments, where water budgets are highly vulnerable to climate change (Song et al. 2014b; Williamson et al. 2009). One of the world's largest groups of alpine lakes are located in the remote Changtang Plateau (CP) (Figure 2.1). Here, surface water is landlocked due to arid climate and topographic barriers, forming a cluster of endorheic basins in the northwestern Tibetan Plateau (TP). Different from other arid endorheic basins, the CP possesses a high lake density of 4.6% (Yang et al. 2017), accounting for ~60% of the total lake water storage (LWS) in the entire TP (Messager et al. 2016). Under negligible human disturbance, these alpine lakes act as "sentinels" of regional climate change (Williamson et al. 2014). Influenced by strengthened westerlies through advection of heat and moisture, the CP has undergone evident wetting (Gao et al. 2015) and warming (Hansen et al. 2010; Xu et al. 2008) during the recent decades, which posed inevitable impacts on the water budget in its alpine lakes (Lei et al. 2017; Liu et al. 2009).

Using optical and altimetric satellites, previous studies have revealed that many large lakes on CP experienced dramatic increase in both area and volume during the past couple of decades, especially since the start of the current millennium (Lei et al. 2013; Lei et al. 2012; Song et al. 2013, 2014a; Zhang et al. 2011; Zhang et al. 2017b; Zhou et al. 2015). However, existing approaches for estimating volume variations across the CP are restricted to a limited number of lakes or multi-year to decadal temporal frequencies (Crétaux et al. 2016; Lei et al. 2013; Song et al. 2013; Yang et al. 2016; Zhang et al. 2017b). For example, Zhang et al. (2017b) applied ICESat altimetry and satellite imagery to quantify volume variations in 68 Tibetan lakes annually

from 1989 to 2015. Yang *et al* (Yang et al. 2016) used satellite imagery and digital elevation model (DEM) to estimate volume variations in 114 lakes at 5 to 14-year intervals during 1976–2013, but included only three discrete years (2000, 2005 and 2013) after 2000. Lake dynamics vary across the CP and exhibit different changing rates during different periods. Particularly, in the past few years (since ~2013), expansions of many Tibetan lakes have been decelerated or partially reversed (Crétaux et al. 2016; Pekel et al. 2016; Yang et al. 2017; Zhang et al. 2017b), which suggests the necessity of a continuous, long-term monitoring of their volume variations.

Different from water area change, volume variation is a more direct measure of the mass balance among water fluxes such as precipitation (P), evapotranspiration (ET), and runoff. Thus, an accurate monitoring of CP lake volume is fundamental for a quantitative attribution of lake changing mechanism. Specifically, we aim at applying estimated volume changes to answer: were the observed lake dynamics across the CP (e.g., rapid expansion from ~2000 and then deceleration since ~2013) predominantly driven by the net change in precipitation and evapotranspiration (thereafter net precipitation) or by warming-induced glacier melt or permafrost degradation? Recently, Zhang et al. (2017b) suggested that net precipitation is likely the key driver for lake volume variations on CP during 2003–2009 (when the ICESat observations were available). Nevertheless, the 68 lakes they studied cover ~53% of the total lake area across the CP (Sheng et al. 2016), and the impact of net precipitation after 2009, including the period of decelerated lake expansion, remained unquantified.

Our recent effort (Yang et al. 2017) applied multi-source satellite imagery (Landsat and Huanjing) to produce a detailed mapping of all lakes greater than 1 km^2 (accounting for ~97% of the total lake area (Messager et al. 2016)) across the CP from 2009 to 2014. Despite a limited period, our applied mapping methods and revealed lake area dynamics (see Section 2.2.2.1)

provide a critical basis that allows for an extended and more thorough monitoring of LWS variations across the CP. Thus in this study, we synergized our recent mapping with extended archival imagery and existing global DEMs (SRTM DEM (Survey) and ASTER GDEM (Team 2009)) to estimate water storage variations in the 871 lakes greater than 1 km^2 across the CP annually from 2002 to 2015. This estimate, to our best knowledge, achieved some of the highest spatial and temporal details in LWS monitoring on the climate-sensitive TP. Calculated LWS changes were next validated against the estimates derived from long-term radar altimetry, and then used along with the total water storage (TWS) variations observed by the Gravity Recovery and Climate Experiment (GRACE) satellites to test the hypothesis that "net precipitation is the dominant driver for the recent lake dynamics across the CP". Our goal is to further eliminate the uncertainty in net LWS changes and improve our understanding of the recent and ongoing climate impacts on surface water budgets in the endorheic Tibet.

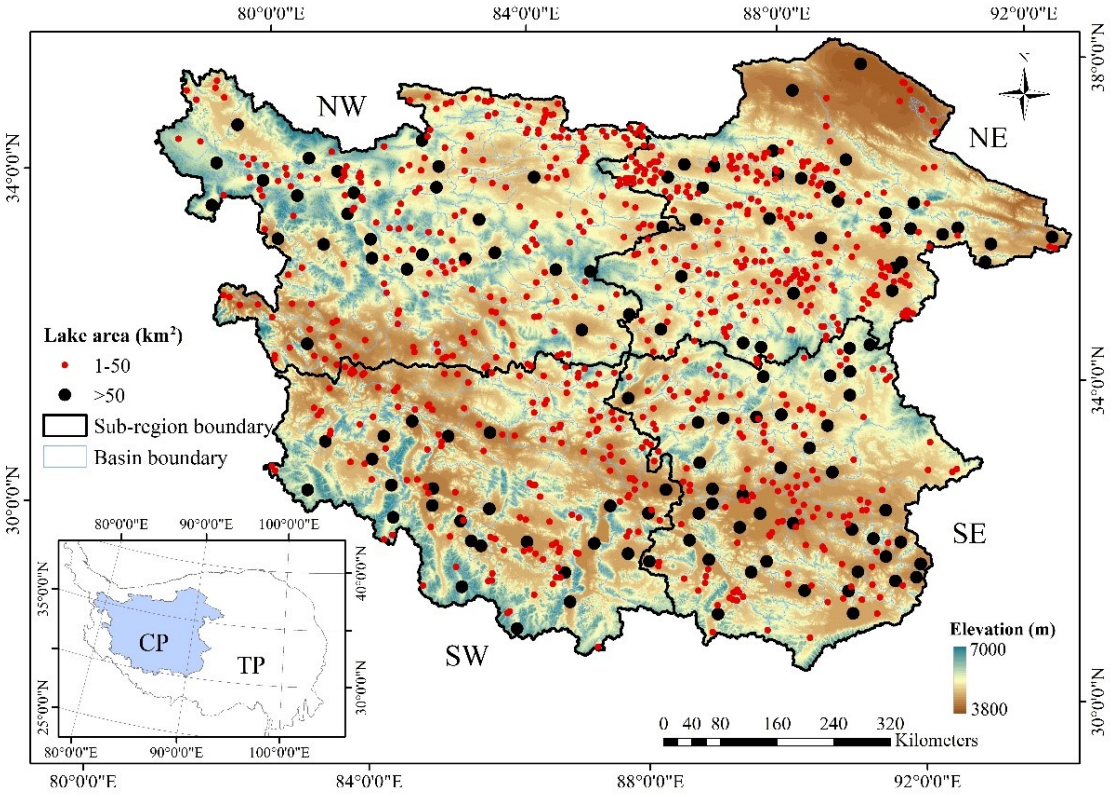

Figure 2.1 Studied alpine lakes across the Changtang Plateau (CP), a total area of ~700 thousand km2 in the northwestern Tibetan Plateau (TP), home to 396 endorheic basins.

2.2 Methods

2.2.1 Monitoring lake water storage (LWS) variations

We calculated the annual time series of water storage variation for each studied lake from 2002 to 2015 through a synergy of water area changes mapped from satellite imagery and bathymetric information retrieved from freely-available DEMs. Detailed methods are explained below.

2.2.1.1 Mapping lake area dynamics

Imagery from the Landsat archive (5, 7 and 8; 16-day repeat cycle) and China's Huanjing satellites (1A and 1B; 2-day repeat cycle) were combined to improve the temporal coverage of cloud-free observations through data blending and fusion. All imagery have the same resolution (30 m) in visible and near-infrared bands (see (Yang et al. 2017) for details), and were collected from September to December during which lake extents on Tibetan Plateau are generally stable (Lei et al. 2013; Lyons and Sheng 2017; Song et al. 2014b; Song et al. 2017; Yang et al. 2017). Combined imagery from Landsat and Huanjing were used to extract annual extents in 871 lakes larger than 1 km^2 from 2009 to 2015. Among them, lake areas from 2009 to 2014 were directly obtained from our previous mapping (Yang et al. 2017). For the period before 2009 (2002–2008) when Huanjing imagery were unavailable, images from Landsat 5 and 7 were fused using the planetary-scale platform Google Earth Engine (GEE) (Gorelick et al. 2017). GEE provides parallel computation for large amounts of satellite data, making fusion of optical images efficient. For each lake, images acquired from September to December were filtered by the SimpleCloudScore algorithm provided in the GEE algorithms API, and then mosaicked using median-value composite. Despite an improved coverage through Landsat image fusion, cloud-free observations were not always feasible for each year and each lake. As a compromise, annual lake areas prior to 2009 were mapped only for 126 lakes larger than 50 km^2.

A self-adaptive lake mapping scheme (similar to Li and Sheng (2012) and Sheng et al. (2016)) was modified to extract lake extents from the optical images (see Yang et al. (2017) for details). In brief, the High Resolution Water Index HRWI (Yao et al. 2015) was applied to enhance the contrast between the water and non-water pixels in each image. Then, an initial threshold (T_0) of HRWI ($T_0 = 0$) was applied to flag possible water bodies. For each possible water body, the HRWI threshold was further fine-tuned by an iterative buffering method which

updates the water extents and its local buffering region until the water extents converge. After that, any remnant errors in the automation results were removed manually with assistance of an interactive editing tool (Wang et al. 2014). Our previous results have shown that lake extents extracted from both Landsat and Huanjing imagery using the proposed approach are highly consistent (slope=1.00, R^2>0.99) (refer to Yang et al. (2017) for details). As our studied minimum lake area (1 km^2) far exceeds the spatial resolution of both imagery (30 m), the error in mapped lake areas was considered to be trivial (Lyons et al. 2013; Pekel et al. 2016; Verpoorter et al. 2014) and thus not included in the uncertainty propagation for lake volume changes (see Section 2.2.3).

2.2.1.2 Calculating lake volume changes

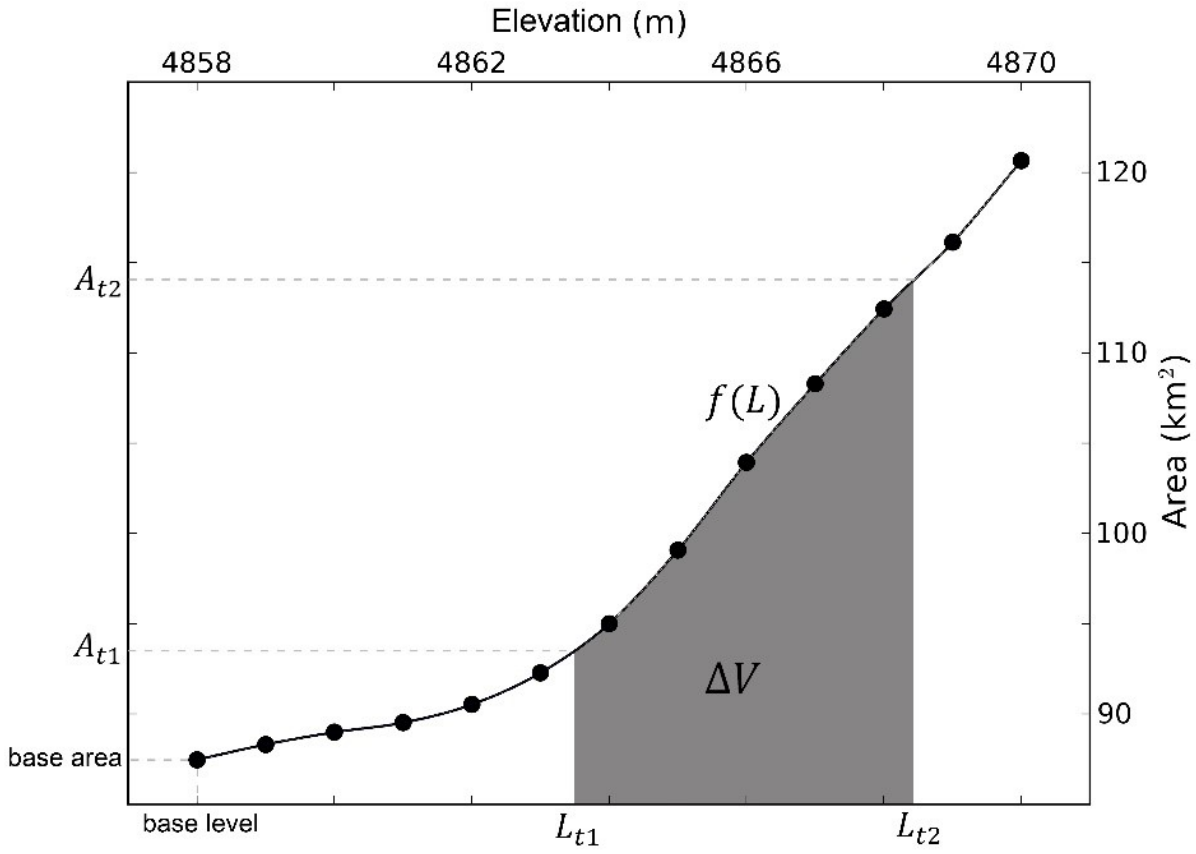

Figure 2.2 Derived hypsometry for Xiangyang Lake (89.42º N, 35.80º E) from the SRTM DEM. The hypsometric curve was calibrated by the monotonic cubic spline fitting.

A DEM may provide useful bathymetric information for inferring lake volume changes if the lakebed topography between the minimum and maximum water levels during the study period was well exposed at the acquisition time of the DEM (Wang et al. 2013a; Yang et al. 2016). As most lakes on the CP have expanded since at least 2000 (Zhang et al. 2017a), the exposed topography surrounding each expanded lake on the SRTM DEM, which was acquired in February 2000, reveals the bathymetry that suffices the estimation of this lake's volume changes during our study period from 2002 to 2015. In other words, the hypsometry (i.e., level-area curve) derived from the SRTM DEM covers the range needed for volume change calculation

without any downward extrapolation. For the remaining lakes where minimum water levels in the study period were higher than those in February 2000, the ASTER GDEM acquired during 2001–2008 was further considered if it could reduce the uncertainties of hypsometry extrapolation.

Specifically, we used the SRTM DEM version 3.0 (Survey) and the ASTER GDEM version 2 (Team 2009), both under the same resolution (1 arc second or ~30 meters). The inundation area of a lake in the SRTM DEM was obtained from the SRTM Water Body Dataset (SWBD) (SWBD 2005) while that in the ASTER GDEM was detected based on surface flatness as in Fujisada et al. (2012). Such a lake area (hereafter referred to as "base area") corresponds to the water level (hereafter referred to as "base level") at the acquisition time of the DEM (Figure 2.2). Given higher vertical accuracy and quality consistency (Rodríguez et al. 2005; Tachikawa et al. 2011), the SRTM DEM was prioritized: it was chosen if 1) the base area is lower than the minimum lake area during the study period, or 2) the base area is lower than that in ASTER GDEM. Otherwise, the ASTER GDEM was applied. Then, base level was simulated to increase at a step of 1 m (the precision for these two DEMs) and the corresponding area below the simulated level in the chosen DEM was calculated until the area is greater than maximum lake area during the study period (Figure 2.2). These level-area pairs were used to construct the hypsometry. If the number of pairs is less than six, base level was further extended until the number reaches six for a better curve fitting purpose. Monotonic cubic spline fitting from the "splines" package of the R software was implemented to fit the hypsometry considering the cubic spline generally outperforms other models (e.g., polynomial) in fitting statistics (Bloomfield 2014; Messager et al. 2016). Finally, lake volume variations were calculated by the integral of the fitted hypsometry (f) as in Equation 1:

$$\Delta V = \int_{L_{t1}}^{L_{t2}} f(L)dL = \int_{A_{t1}}^{A_{t2}} f^{-1}(A)dA \quad (1)$$

where ΔV denotes the water storage change from time ($t1$) with lake area (A_{t1}) and water level (L_{t1}) to time ($t2$) with lake area (A_{t2}) and water level (L_{t2}).

The proposed approach using DEM hypsometry was applied to estimate volume variations in all studied lakes except Zhuonai Lake (35.55º N, 91.94º E) because there was a drastic decline in its water level caused by a moraine dam failure in September of 2011 (Liu et al. 2016). The DEM hypsometry for Zhuonai Lake was, thus, extended by an additional pair of water area and level after the dam failure observed by Landsat 5 imagery and Croysat-2 altimetry, respectively, in order to reduce the error from directly extrapolating the DEM hypsometry.

As previously described, annual time series of volume variation for all 871 lakes larger than 1 km^2 were estimated from the period 2009–2015, while those for the 126 lakes larger than 50 km^2 were further estimated for 2002–2008 during which smaller lakes were not estimated because of a poor temporal coverage caused by the absence of Huanjing imagery before 2009. These 126 larger lakes account for ~83% of the total lake area and ~96% of the total lake volume across the CP (Messager et al. 2016; Yang et al. 2017). Given such dominance, their total volume changes may well represent those in all CP lakes. This is corroborated by a strong linear relationship between the two during the period of 2009–2015 (Figure 2.3b). This relationship was used as a scaling function to infer annual volume variations in all CP lakes from 2002 to 2008 from those in the 126 large lakes (also see Section 2.3.1). The best-fit linear regression was applied to calculate the trends in LWS time series (hereafter referred as "DEM-derived trends"), and the uncertainty analysis is given in Section 2.2.3.

2.2.2 Attributing LWS variations

DEM-derived LWS trends from 2002 to 2015 were validated against the trends during the same period but calculated using available hypsometric curves provided in the LEGOS Hydroweb database (http://hydroweb.theia-land.fr; hereafter Hydroweb-derived trends) (Crétaux et al. 2011). Many hypsometric curves provided by Hydroweb were constructed from multi-decadal records of water levels observed by radar altimeters and water extents mapped from satellite imagery (Crétaux et al. 2016; Crétaux et al. 2011). A total of 18 lakes on the CP with Hydroweb hypsometry were used for the validation. Volume of these lakes varies from ~0.2 to ~100 gigaton (see table S1); collectively, they account for approximately 70% of the total lake volume across the CP (Messager et al. 2016). For a comparison purpose, we also validated the LWS trends from 2002 to 2015 using hypsometric curves constructed from ICESat altimetry and Landsat imagery by Zhang et al. (2017b) (hereafter ICESat-derived trends). This validation is limited to 14 lakes where hypsometric curves are available in both Zhang et al. (2017b) and Hydroweb.

Following standard error propagation rules, uncertainties of our estimated annual LWS changes were integrated from two major sources: (i) the bias of DEM-derived trends, calculated as their discrepancy from Hydroweb-derived trends, and (ii) the uncertainty of estimated volume changes in small lakes during 2002–2008, calculated as the root mean square error (RMSE) of the rescaling relationship between volume variations in large lakes and all lakes (Figure 2.3b). Uncertainties of estimated annual P-ET were directly estimated from the storage errors provided in the GRACE mascon (mass concentration) data, and the additional uncertainties induced by signal leakage in the fringe mascons are further explored in Discussion. Propagated uncertainties

were next applied to infer 95% confidence intervals of the calculated linear trends using a Monte Carlo approach similar to Wang et al. (2017).

2.3 Results and analysis

2.3.1 Accuracy of estimated LWS trends

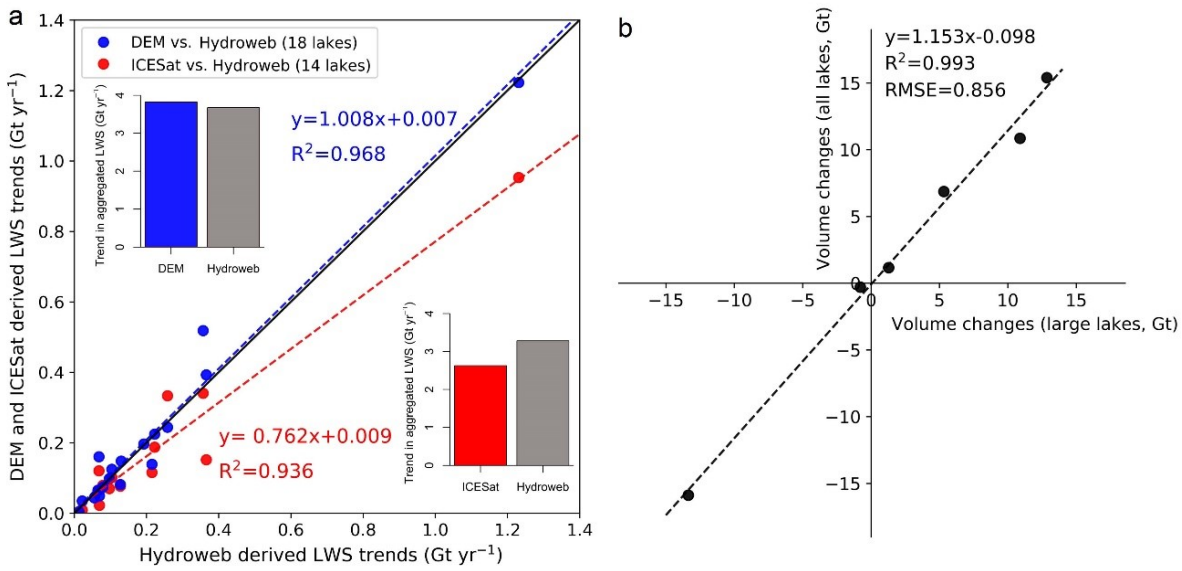

Figure 2.3 Accuracy assessment of estimated lake volume variations. (a) Validation of DEM-derived trends (blue) and ICESat-derived trends (red) in lake volume from 2002 to 2015 by Hydroweb-derived trends. Points represent volume trends in individual lakes (see geographic coordinates in Table 2.1) while histograms represent the aggregated trends in all assessed lakes. (b) Calibrated scaling relationship between annual water storage changes in large lakes (>50 km2) and all lakes (>1 km2) from 2009 to 2015. Dashed lines are best-fit regression lines.

Our DEM-derived LWS trends from 2002 to 2015 are validated against the trends derived from Hydroweb hypsometry (Figure 2.3a). DEM-derived trends in the 18 assessed lakes appear to be highly consistent with the Hydroweb-derived results (slope: 1.008, R^2: 0.968). Their aggregated storage change (the histogram in the upper left corner of Figure 2.3a) shows a minor bias less than 5% of that derived from Hydroweb hypsometry. ICESat-derived trends, by

contrast, are less consistent with the Hydroweb-derived trends (slope: 0.762, R^2: 0.936). The aggregated storage change (the histogram in the lower-right corner of Figure 2.3a) is ~20% lower than that derived from Hydroweb hypsometry. This poorer consistency between ICESat- and Hydroweb-derived storage trends is likely caused by the extrapolation of hypsometric curves constructed from ICESat altimetry levels that are only available during 2003–2009 (Crétaux et al. 2016). This contrast suggests that our proposed approach, using bathymetric information exposed in the DEMs, yields a comparable result with that produced by longer-term radar altimetry measurements, and is fairly reliable for estimating lake volume dynamics across the CP.

Table 2.1 Detailed information of lakes used for volume validation (source: Messager et al. 2016)

Lake Name	Longitude	Latitude	Size (km^2)	Total Volume (Gt)	Elevation (m)
SilingCo	89.05	31.78	1748.21	49.00	4539
NamCo	90.66	30.71	1961.90	87.12	4724
Ayakkum	89.43	37.56	616.65	6.16	3876
LexieWudan	90.21	35.74	220.80	3.68	4870
Aksayquin	79.82	35.22	165.96	1.59	4844
UlanUla	90.36	34.76	480.82	7.98	4855
Dogai Coring	89.00	34.55	360.11	6.63	4818
LumajangdongCo	81.64	34.05	346.93	15.64	4812
Namru	90.84	32.08	207.02	2.63	4568
Ngangla Ringco	83.05	31.57	497.66	5.00	4716
TarongCo	84.33	31.18	473.29	16.15	4567
Zhari Namco	85.64	30.95	957.20	23.95	4612
Tangra	86.50	30.95	824.31	99.01	4535
Dorsoidongco & Migriggyangzhamco	90.25	33.62	877.81	20.15	4936
Dogaicoring-Q*	89.26	35.32	208.99	1.33	4787

DagazeCo*	87.53	31.89	251.37	2.13	4465
PengCo*	90.97	31.51	148.02	1.81	4529
Xuelian*	90.23	34.11	40.22	0.23	5275

* indicates lakes without ICESat hypsometry

As shown in Figure 2.3b, calculated annual volume changes from 2009 to 2015 in all studied 871 lakes (>1 km^2) are closely correlated to those in the 126 large lakes (> 50 km^2) with a slope of 1.153, R^2 of 0.993, and RMSE of 0.856 Gt. Therefore, net annual volume changes in the missing smaller lakes (< 50 km^2) from 2002 to 2008 were inferred by this scaling relationship between volume changes in all lakes and large lakes, and the scaling errors (RMSE) were integrated for propagating LWS change uncertainties (refer to Sections 2.2.3 and 2.4.3).

2.3.2 Spatial distribution of LWS changes

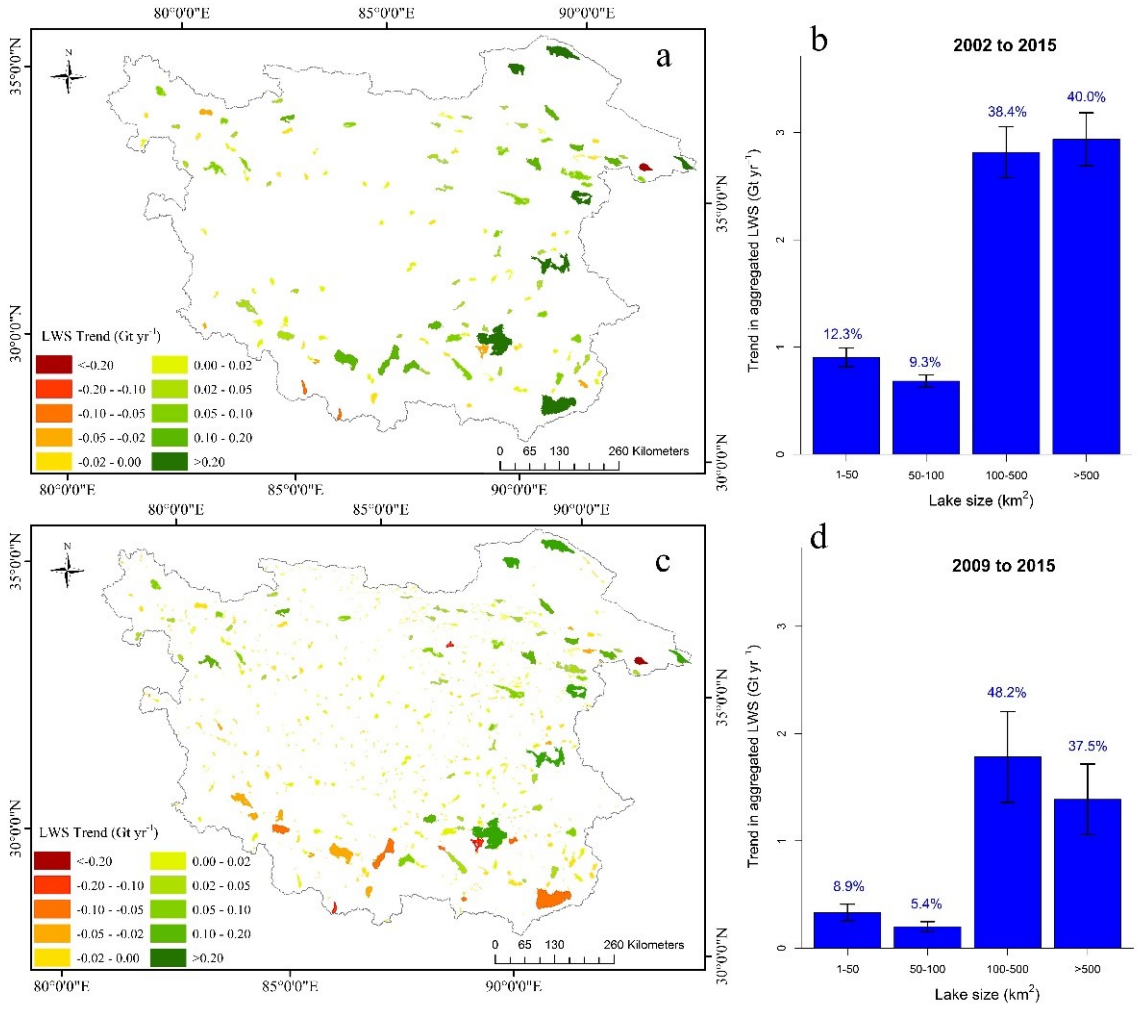

Figure 2.4 Spatial distribution of lake storage changes across the CP. (a) Storage trends in large lakes (>50 km2) from 2002 to 2015. (b) Aggregated lake storage changes in different size groups from 2002 to 2015 (aggregated storage changes in lakes between 1 and 50 km2 were estimated from the calibrated scaling relation as in Figure 2.3b). (c) Storage trends in all lakes (>1 km2) from 2009 to 2015. (d) Aggregated lake storage changes in different size groups from 2009 to 2015. Error bars in (b) and (d) illustrate 95% confidence intervals in the estimations.

Alpine lakes across the CP experienced a widespread storage increase from 2002 to 2015 (Figure 2.4a). The magnitude of volume increase generally reduces along an east-to-west direction, which is consistent with the spatial gradient of decreasing lake abundance and size. As

summarized in Figure 2.4b, LWS increase is proportional to lake size. For example, the largest lake Selingco (31.81°N, 89.07°E) in the southeastern CP experienced the fast volume increase of 1.22 ± 0.10 Gt yr^{-1}, accounting for 17% of the total LWS increase across the CP. About 78% of the total storage increase fed into lakes greater than 100 km^2 (Figure 2.4b), while only 9% occurred in lakes with size between 50-100 km^2 and 12% (estimated from the scaling relation as in Figure 2.3b) occurred in smaller lakes (<50 km^2) (Figure 2.4b).

Figure 2.4c shows storage trends in all 871 lakes greater than 1 km^2 from 2009 to 2015. Storage variations in large lakes vary spatially, whereas the spatial patterns in small lakes are generally much more homogeneous. However, during the last 6-year period (2009–2015), rates of volume changes in all sizes of lakes decreased (Figure 2.4b and 2.4d). Some large lakes in the southern CP, e.g., Namco (30.67°N, 90.60°E) and Tangra Yumco (31.00°N, 86.55°E), even began to shrink (Figure 2.4c).

2.3.3 Trends in LWS across the endorheic Tibetan Plateau and associations with net precipitation

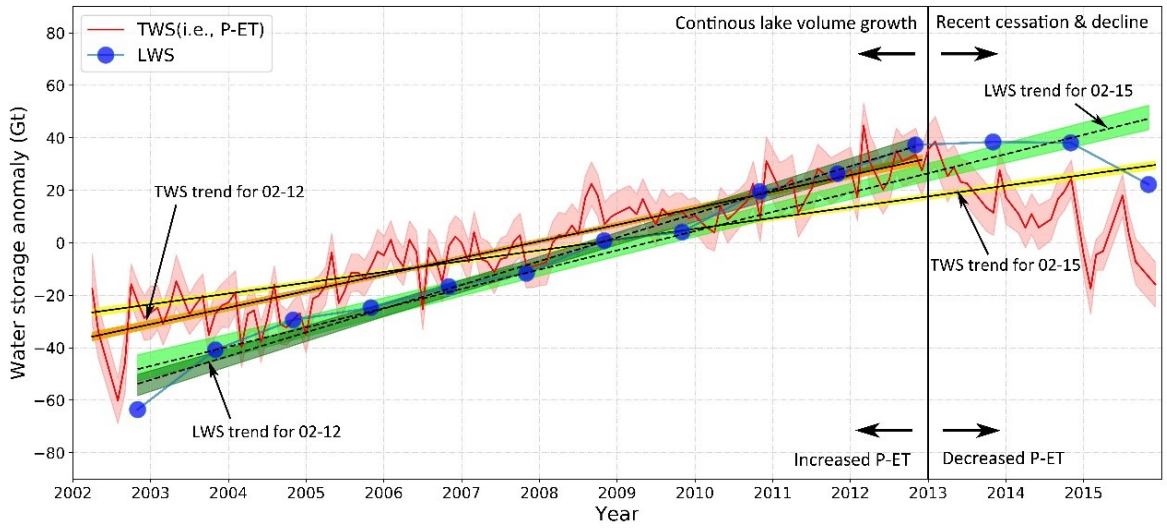

Figure 2.5 Variations in lake water storage (LWS) and total terrestrial water storage (TWS) across the CP from 2002 to 2015. The red curve shows monthly P-ET anomalies (climatology removed) observed by GRACE satellites, while the connected blue dots represent annual LWS anomalies estimated from the proposed approach. All anomalies are relative to the long-term means during 2002–2015. Straight lines (dashed and solid) represent linear trends using best-fit regression for two periods (2002–2012 and 2002–2015). Transparent shades illustrate 95% confidence intervals.

The trajectory of net LWS across the CP exhibits three distinct phases (Figure 2.5): a monotonic increase from 2002 to 2012, a general cessation and pause in 2013 and 2014, and then an evident decline from 2015. Coherently, net precipitation (i.e., P-ET) generally increased from 2002 to 2012 but declined from 2013 to 2015. Increasing net precipitation from 2002 to 2012 concurred with rapid lake expansion and the decreasing net precipitation after 2013 concurred with the recent cessation of lake expansion and the subsequent LWS loss. However, the decreased net precipitation did not seem to trigger an immediate decline in LWS. Instead, LWS started to decline in 2015, about two years after the turning point of net precipitation in 2013.

This time lag indicates that NLWS (e.g., warming-induced glacier melting and permafrost thawing) may have compensated for the LWS reduction caused by immediate net precipitation decrease in the early period, but was unable to completely offset the long-term effect of net precipitation decline.

As further summarized in Table 2.2, net precipitation on the CP increased at an average rate of 4.11 ± 0.19 Gt yr^{-1} during our study period (2002–2015), which explains 56.0 ± 5.4 % of the concurrent increase in LWS (7.34 ± 0.62 Gt yr^{-1}). From 2002 to 2012, net precipitation increased at 6.31 ± 0.27 Gt yr^{-1}, accounting for 69.7 ± 5.8 % of the rapid LWS increase of 9.05 ± 0.65 Gt yr^{-1}, while net precipitation declined at a rate of -13.61 ± 2.03 Gt yr^{-1} from 2013 to 2015, which completely explains the concurrent LWS decline (-8.09 ± 3.37 Gt yr^{-1}). Given these calculations, net precipitation appears to be the first-order contributor to the recent LWS changes across the CP.

Table 2.2 Summary of changes in lake water storage (LWS), P-ET (net precipitation) and non-lake water storage (NLWS) on the CP. Uncertainties indicate 95% confidence intervals.

Periods	LWS	P-ET		NLWS	
	Gt yr^{-1}	Gt yr^{-1}	% of ΔLWS	Gt yr^{-1}	% of ΔLWS
Increasing P-ET period (2002–2012)	9.05 ± 0.65	6.31 ± 0.27	69.72 ± 5.83	-2.74 ± 0.70	-30.28 ± 8.08
Decreasing P-ET period (2013–2015)	-8.09 ± 3.37	-13.61 ± 2.03	168.23 ± 74.44	-5.52 ± 3.93	-68.23 ± 56.33
Entire study period (2002–2015)	7.34 ± 0.62	4.11 ± 0.19	56.00 ± 5.39	-3.23 ± 0.65	-44.01 ± 9.58

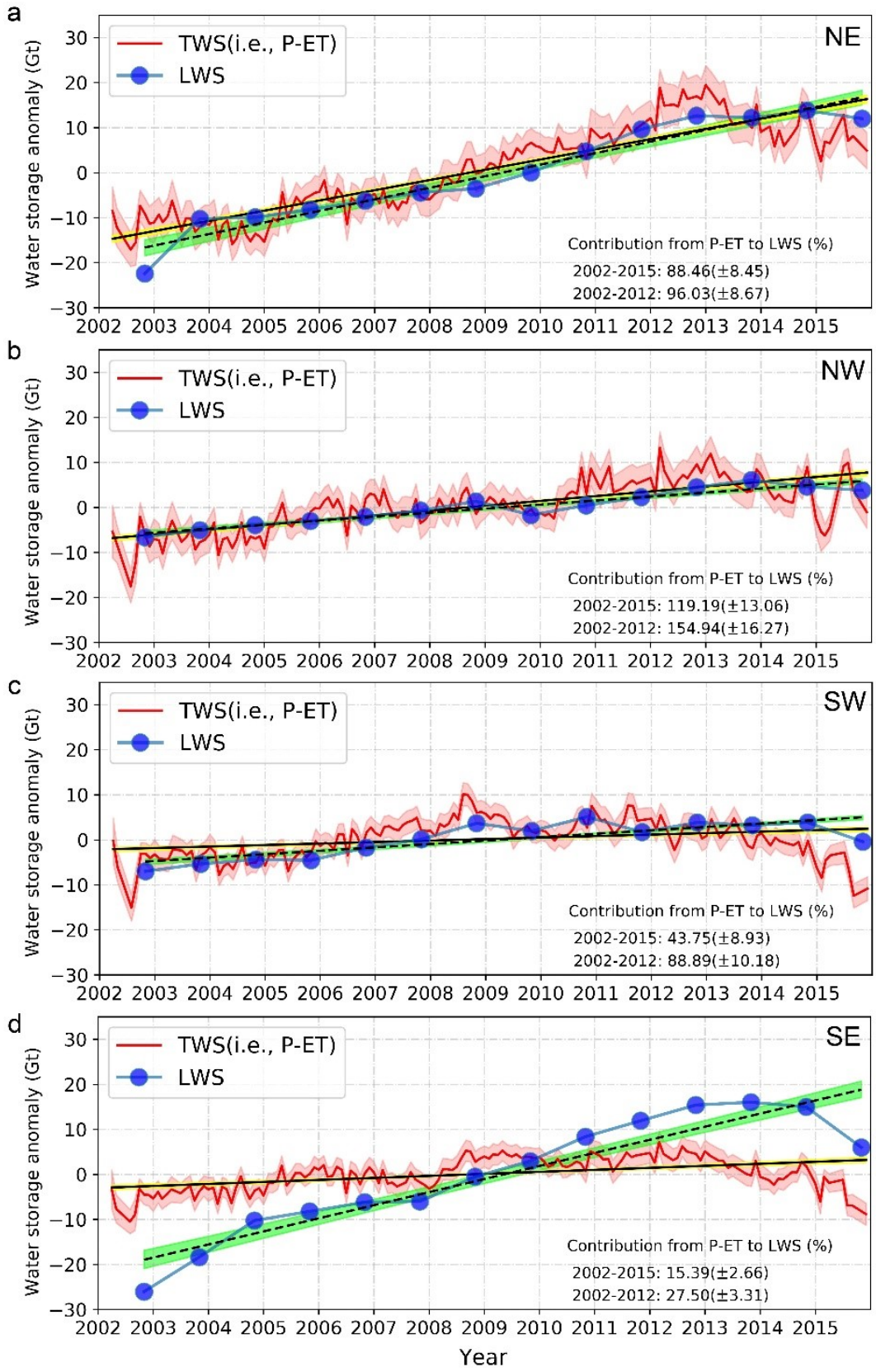
a
NE
TWS(i.e., P-ET)
LWS
Water storage anomaly (Gt)
Contribution from P-ET to LWS (%)
2002-2015: 88.46(±8.45)
2002-2012: 96.03(±8.67)
b
NW
TWS(i.e., P-ET)
LWS
Water storage anomaly (Gt)
Contribution from P-ET to LWS (%)
2002-2015: 119.19(±13.06)
2002-2012: 154.94(±16.27)
c
SW
TWS(i.e., P-ET)
LWS
Water storage anomaly (Gt)
Contribution from P-ET to LWS (%)
2002-2015: 43.75(±8.93)
2002-2012: 88.89(±10.18)
d
SE
TWS(i.e., P-ET)
LWS
Water storage anomaly (Gt)
Contribution from P-ET to LWS (%)
2002-2015: 15.39(±2.66)
2002-2012: 27.50(±3.31)
Year

Figure 2.6 Variations in the lake water storage (LWS) and total terrestrial water storage (TWS) from 2002 to 2015 for northeastern (NE) (a), northwestern (NW) (b), southwestern (SW) (c) and southeastern (SE) (d) CP. Symbol and color illustrations are the same as in Figure 2.5.

2.4 Discussion

Our results indicate a dominant role of net precipitation on the recent decadal lake dynamics on the CP, which is consistent with several existing studies (Lei et al. 2014; Lei et al. 2013; Song et al. 2015; Song et al. 2014b; Zhang et al. 2017b; Zhou et al. 2015). However, this finding may contradict those of some other studies. For instance, Li et al. (2014) found limited impacts of glacier retreat and hypothesized that permafrost thawing was the primary cause for Tibetan lake expansion in recent decades, although Zhang et al. (2017) concluded that the magnitude of permafrost thawing is not substantially more than that of glacier retreat. Jiang et al. (2017) also suggested the important role of permafrost on rapid lake expansion in the northeastern CP. Thus, we here compare the relationships between LWS and net precipitation in four sub-regions of the CP (Figure 2.6). In northeastern, northwestern, and southwestern CP, rapid lake expansion accompanied with dramatic increase in P-ET during 2002 to 2015 (Figure 2.6a-2.6c), which confirms the dominant contribution of net precipitation. However, the covariation between LWS and net precipitation is not evident in the southeastern CP (Figure 2.6d). This may be caused by the substantial contribution from glacier retreat, as indicated in previous studies (Wang et al. 2013b; Zhu et al. 2010).

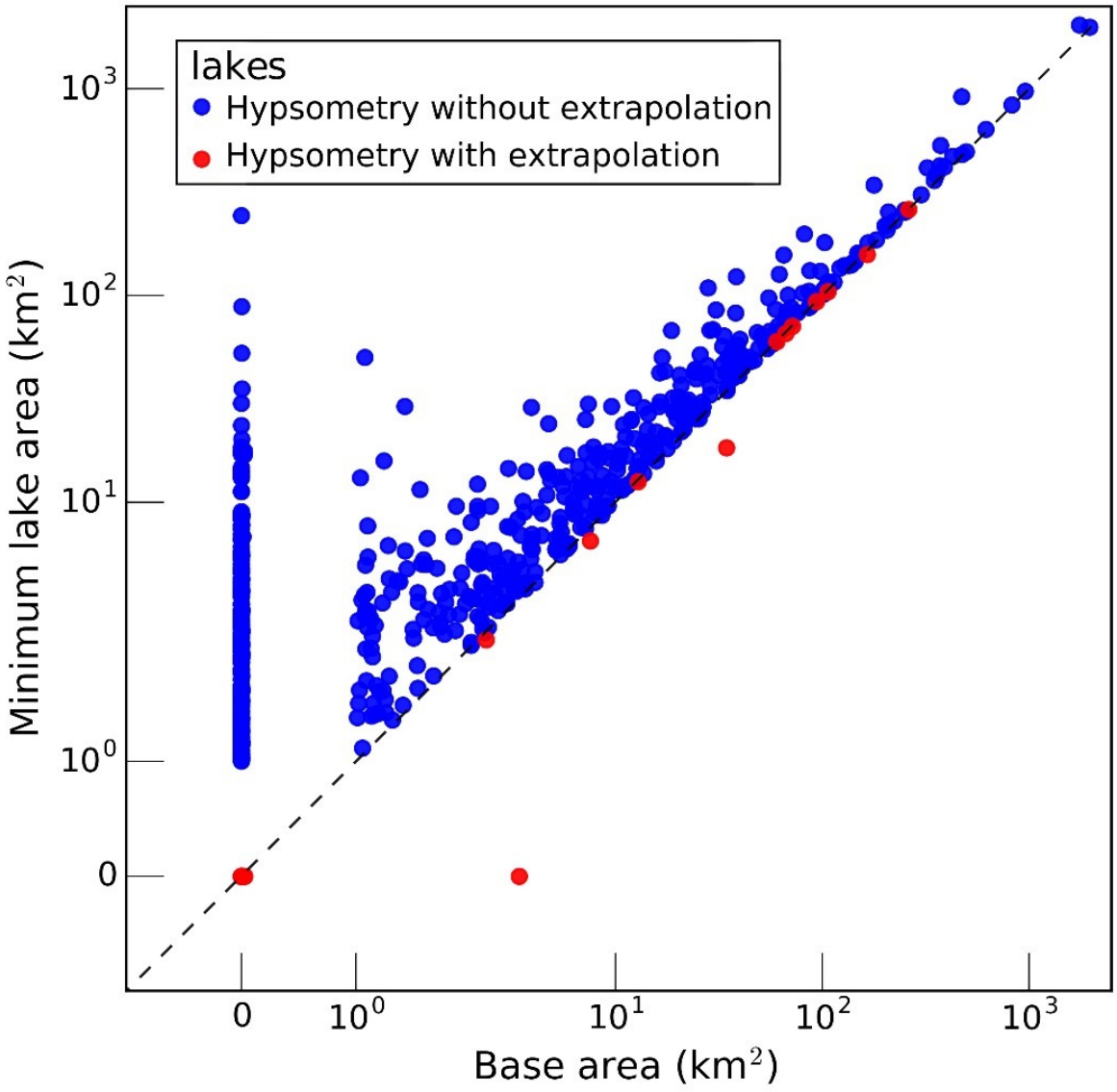

Figure 2.7 Base areas and minimum areas for 871 studied lakes. Lakes with extrapolated hypsometry are those with minimum areas less than base areas (red dots below the diagonal line).

Several error sources limit our results and contribute to the uncertainty of this study. First, we ignored the additional uncertainty from hypsometry extrapolation for 6% of studied lakes (Figure 2.7), where neither of the two DEM products could reveal the complete bathymetry required for storage change recovery during the study period. However, these lakes only account for less than 4% of the total lake area on CP (Sheng et al. 2016), so their hypsometry

extrapolation should not substantially affect our estimated net LWS variations. Second, except the errors provided by the RL05M mascon data, we did not explicitly quantify the uncertainty in GRACE-derived TWS anomalies arising from signal leakage from the surrounding basins in the fringe mascons (which override the CP boundaries). To perceive this uncertainty, we here explore two solutions that implement the same procedure as described in Section 2.2.2 to partition TWS variations into changes in LWS and NLWS. The first solution only includes mascons that are fully contained by the CP (Table 2.3), while the second solution applies the mascon set of 0.5-degree scale factors simulated by the Community Land Model (CLM) (Watkins et al. 2015) (Table 2.4). It is worth noting that, despite a partial recovery of the signal variation within each mascon, the scale factors may not be suitable for deriving TWS trends at sub-mascon resolutions. This is because 1) the CLM does not include lake or glacier components so the simulated surface storage variations on the CP may be highly uncertain, and 2) the least-square correction involved in the factor calculation tends to be dominated by the annual cycles of water storage variations (Landerer and Swenson 2012; Watkins et al. 2015). For these reasons, we did not apply the scale factors in the calculations as reported in Section 2.3, but only used them for inferring possible uncertainty scales induced by signal leakage in the fringe mascons. Results of both solutions are consistent with our previous findings. The increase in net precipitation (TWS) accounts for most (~70% or more) of the LWS increase from 2002 to 2012 and the net precipitation decrease fully explains the LWS loss from 2013 to 2015. Therefore, potential uncertainties due to signal leakage are not likely to alter our primary conclusion that LWS changes are predominantly attributed to the variations in net precipitation. Finally, limited by data availability, the attribution of lake storage changes in this study were based on the net impacts of potential drivers (i.e. net precipitation and NLWS including glaciers and permafrost).

The quantified impact of glaciers and permafrost reflect their integrated storage changes rather than their actual amounts of melting runoff to the lakes. The difference between their net storage change and melting runoff mainly depends on how net precipitation is intercepted by or stored as glaciers and permafrost. While being difficult to quantify, such an impact seems to be relatively trivial because only less than 10% of precipitation fell during the winter (Xu et al. 2008; Yang et al. 2017). Additionally, the LWS across the inner Tibet ceased in expansion right after the turning point of net precipitation around 2013, and it eventually declined in 2015 when the net precipitation continued to drop. This evidence also supports that the net precipitation has the dominant determinant of the recent lake storage changes across the inner Tibet.

Table 2.3 Trends in lake water storage (LWS), P-ET (net precipitation) and non-lake water storage (NLWS) in full mascons within the CP

Periods	LWS	P-E		NLWS	
	Gt yr^{-1}	Gt yr^{-1}	% of ΔLWS	Gt yr^{-1}	% of ΔLWS
Increasing P-ET period (2002–2012)	3.59 ± 0.28	2.51 ± 0.19	69.92 ± 7.60	-1.08 ± 0.34	-30.08 ± 9.71
Decreasing P-ET period (2013–2015)	-2.43 ± 1.01	-4.57 ± 1.38	188.06 ± 96.62	-2.14 ± 1.71	88.07 ± 79.33
Entire study period (2002–2015)	2.86 ± 0.24	1.46 ± 0.13	51.05 ± 6.25	-1.40 ± 0.27	-48.95 ± 10.39

Table 2.4 Summary of changes in lake water storage (LWS), P-ET (net precipitation, estimated from mascon data with GLDAS-modeled scale factors) and non-lake water storage (NLWS) across the CP. All uncertainties are 95% confidence intervals.

Periods	LWS	P-ET		NLWS	
	Gt yr^{-1}	Gt yr^{-1}	% of ΔLWS	Gt yr^{-1}	% of ΔLWS
Increasing P-ET period (2002–2012)	9.05 ± 0.65	6.89 ± 0.27	76.13 ± 5.83	-2.16 ± 0.70	-23.87 ± 8.08
Decreasing P-ET period (2013–2015)	-8.09 ± 3.37	-14.98 ± 2.03	185.17 ± 74.44	-6.89 ± 3.93	-85.17 ± 56.33
Entire study period (2002–2015)	7.34 ± 0.62	4.66 ± 0.18	63.49 ± 5.39	-2.68 ± 0.65	-36.51 ± 9.58

2.5 Summary and concluding remarks

This study provides a comprehensive estimate of LWS variations across the CP from 2002 to 2015, by synergizing satellite imagery (Landsat and Huanjing) and freely-available DEMs (SRTM DEM and ASTER GDEM). The sheer number of lakes (871) analyzed in our estimate, which account for 97% of total lake area across the CP (Sheng et al. 2016), is substantially greater than any number recently studied for lake volume changes on the Tibetan Plateau (e.g., 68 lakes in Zhang et al. (2017b) and 114 lakes in Yang et al. (2016)). Compared with existing estimates (Song et al. 2013; Zhang et al. 2017b) using hypsometric curves extrapolated from short-term ICESat observations (available during 2003–2009), our LWS trends are more consistent with values derived from longer-term radar altimetry measurements (slope=1.01, R^2=0.97). This indicates that volume change estimates using extrapolated hypsometry may need to be interpreted with cautions. Given such improved spatiotemporal coverage and reduced

estimation biases, this study advances our understanding of recent variations in lake water budget across the remote Tibetan Plateau. Our produced lake area and storage change data set is publicly available at the scientific data repository PANGAEA (doi:10.1594/PANGAEA.888706).

From 2002 to 2015, the net LWS increased at an average rate of 7.34 ± 0.62 Gt yr^{-1} (cumulatively 95.42 ± 8.06 Gt), manifested as a dramatic monotonic increase of 9.05 ± 0.65 Gt yr^{-1} before 2012, a deceleration and pause in 2013–2014, and then an intriguing decline after 2014. Using TWS anomalies from GRACE observations and a water balance model, we quantified that ~70% of the monotonic LWS increase before 2012 was attributed to the increase in net precipitation (P-ET). Despite a smaller total influence, warming-induced NLWS changes, including glacier retreat and permafrost thawing, might compensate for the LWS reduction caused by the initial net precipitation decrease in 2013–2014, which is manifested by a 2-year time lag between net precipitation and LWS declines. However, the impact of NLWS was unable to offset the longer-term effect of net precipitation decline, leading to an evident LWS decrease in 2015: the first major reverse of a double-decadal lake expansion on the CP (Zhang et al. 2017b). To this end, we conclude that net precipitation (i.e., P-ET) is a first-order contributor to alpine lake dynamics across the CP since at the least the new millennium.

2.6 References

Williamson C E, Saros J E, Vincent W F and Smold J P 2009 Lakes and reservoirs as sentinels, integrators, and regulators of climate change *Limnology and Oceanography* **54** 2273-82, doi: 10.4319/lo.2009.54.6_part_2.2273

Song C, Huang B, Richards K, Ke L and Hien Phan V 2014 Accelerated lake expansion on the Tibetan Plateau in the 2000s: induced by glacial melting or other processes? *Water Resources Research* **50** 3170-86, doi: 10.1002/2013WR014724

Yang K, Yao F, Wang J, Luo J, Shen Z, Wang C and Song C 2017 Recent dynamics of alpine lakes on the endorheic Changtang Plateau from multi-mission satellite data *Journal of Hydrology* **552** 633-45, doi: 10.1016/j.jhydrol.2017.07.024

Messager M L, Lehner B, Grill G, Nedeva I and Schmitt O 2016 Estimating the volume and age of water stored in global lakes using a geo-statistical approach *Nature Communications* **7** 13603, doi: 10.1038/ncomms13603

Williamson C E, Brentrup J A, Zhang J, Renwick W H, Hargreaves B R, Knoll L B, Overholt E P and Rose K C 2014 Lakes as sensors in the landscape: optical metrics as scalable sentinel responses to climate change *Limnology and Oceanography* **59** 840-50, doi:10.4319/lo.2014.59.3.0840

Gao Y, Li X, Leung L R, Chen D and Xu J 2015 Aridity changes in the Tibetan Plateau in a warming climate *Environmental Research Letters* **10** 034013, doi:10.1088/1748-9326/10/3/034013

Hansen J, Ruedy R, Sato M and Lo K 2010 Global surface temperature change *Reviews of Geophysics* **48** RG4004, doi:10.1029/2010RG000345

Xu Z, Gong T and Li J 2008 Decadal trend of climate in the Tibetan Plateau—regional temperature and precipitation *Hydrological Processes* **22** 3056-65, doi:10.1002/hyp.6892

Liu J, Wang S, Yu S, Yang D and Zhang L 2009 Climate warming and growth of high-elevation inland lakes on the Tibetan Plateau *Global and Planetary Change* **67** 209-17, doi:10.1016/j.gloplacha.2009.03.010

Lei Y, Yao T, Yang K, Sheng Y, Kleinherenbrink M, Yi S, Bird B W, Zhang X, Zhu L and Zhang G 2017 Lake seasonality across the Tibetan Plateau and their varying relationship with regional mass changes and local hydrology *Geophysical Research Letters* **44** 892-900, doi:10.1002/2016GL072062

Zhang B, Wu Y, Zhu L, Wang J, Li J and Chen D 2011 Estimation and trend detection of water storage at Nam Co Lake, central Tibetan Plateau *Journal of Hydrology* **405** 161-70, doi:10.1016/j.jhydrol.2011.05.018

Song C, Huang B and Ke L 2014 Inter-annual changes of alpine inland lake water storage on the Tibetan Plateau: Detection and analysis by integrating satellite altimetry and optical imagery *Hydrological Processes* **28** 2411-8, doi:10.1002/hyp.9798

Lei Y, Yao T, Bird B W, Yang K, Zhai J and Sheng Y 2013 Coherent lake growth on the central Tibetan Plateau since the 1970s: Characterization and attribution *Journal of Hydrology* **483** 61-7, doi: 10.1016/j.jhydrol.2013.01.003

Lei Y, Yao T, Yi C, Wang W, Sheng Y, Li J and Joswiak D 2012 Glacier mass loss induced the rapid growth of Linggo Co on the central Tibetan Plateau *Journal of Glaciology* **58** 177-84, doi:10.3189/2012JoG11J025

Song C, Huang B and Ke L 2013 Modeling and analysis of lake water storage changes on the Tibetan Plateau using multi-mission satellite data *Remote Sensing of Environment* **135** 25-35, doi:10.1016/j.rse.2013.03.013

Zhang G, Yao T, Shum C, Yi S, Yang K, Xie H, Feng W, Bolch T, Wang L and Behrangi A 2017 Lake volume and groundwater storage variations in Tibetan Plateau's endorheic basin *Geophysical Research Letters* **44** 5550–60, doi:10.1002/2017GL073773

Zhou J, Wang L, Zhang Y, Guo Y, Li X and Liu W 2015 Exploring the water storage changes in the largest lake (Selin Co) over the Tibetan Plateau during 2003–2012 from a basin-wide hydrological modeling *Water Resources Research* **51** 8060-86, doi:10.1002/2014WR015846

Crétaux J-F, Abarca-del-Río R, Berge-Nguyen M, Arsen A, Drolon V, Clos G and Maisongrande P 2016 Lake volume monitoring from space *Surveys in Geophysics* **37** 269-305, doi:10.1007/s10712-016-9362-6

Yang R, Zhu L, Wang J, Ju J, Ma Q, Turner F and Guo Y 2016 Spatiotemporal variations in volume of closed lakes on the Tibetan Plateau and their climatic responses from 1976 to 2013 *Climatic Change* **140(3-4)** 621-33, doi:10.1007/s10584-016-1877-9

Pekel J-F, Cottam A, Gorelick N and Belward A S 2016 High-resolution mapping of global surface water and its long-term changes *Nature* **540** 418-22, doi:10.1038/nature20584

Sheng Y, Song C, Wang J, Lyons E A, Knox B R, Cox J S and Gao F 2016 Representative lake water extent mapping at continental scales using multi-temporal Landsat-8 imagery *Remote Sensing of Environment* **185** 129-41, doi:10.1016/j.rse.2015.12.041

Shuttle Radar Topography Mission (SRTM) 1 Arc-Second Global Digital Elevation Model (DEM) [dataset]. Hosted by the U.S. Geological Survey. Available at https://lta.cr.usgs.gov/SRTM1Arc

NASA JPL and Japan ASTER Science Team (2009) ASTER Global Digital Elevation Model version 2 [dataset]. Available at https://doi.org/10.5067/aster/astgtm.002

Lehner B, Verdin K and Jarvis A 2008 New global hydrography derived from spaceborne elevation data Eos, Transactions American Geophysical Union 89(10) 93-4, doi:10.1029/2008EO100001

Song C, Sheng Y, Wang J, Ke L, Madson A and Nie Y 2017 Heterogeneous glacial lake changes and links of lake expansions to the rapid thinning of adjacent glacier termini in the Himalayas Geomorphology 280 30-8, doi:10.1016/j.geomorph.2016.12.002

Lyons E A and Sheng Y 2017 LakeTime: Automated Seasonal Scene Selection for Global Lake Mapping Using Landsat ETM+ and OLI Remote Sensing 10 54, doi:10.3390/rs10010054

Gorelick N, Hancher M, Dixon M, Ilyushchenko S, Thau D and Moore R 2017 Google Earth Engine: Planetary-scale geospatial analysis for everyone Remote Sensing of Environment 202 18-27, doi: 10.1016/j.rse.2017.06.031

Li J and Sheng Y 2012 An automated scheme for glacial lake dynamics mapping using Landsat imagery and digital elevation models: A case study in the Himalayas International Journal of remote sensing 33 5194-213, doi:10.1080/01431161.2012.657370

Yao F, Wang C, Dong D, Luo J, Shen Z and Yang K 2015 High-resolution mapping of urban surface water using ZY-3 multi-spectral imagery Remote Sensing 7 12336-55, doi:10.3390/rs70912336

Wang J, Sheng Y and Tong T S D 2014 Monitoring decadal lake dynamics across the Yangtze Basin downstream of Three Gorges Dam Remote Sensing of Environment 152 251-69, doi: 10.1016/j.rse.2014.06.004

Verpoorter C, Kutser T, Seekell D A and Tranvik L J 2014 A global inventory of lakes based on high‐resolution satellite imagery Geophysical Research Letters 41 6396-402, doi:10.1002/2014GL060641, doi: 10.1002/2014GL060641

Lyons E A, Sheng Y, Smith L C, Li J, Hinkel K M, Lenters J D and Wang J 2013 Quantifying sources of error in multitemporal multisensor lake mapping International journal of remote sensing 34 7887-905, doi: 10.1080/01431161.2013.827343

Wang X, Chen Y, Song L, Chen X, Xie H and Liu L 2013 Analysis of lengths, water areas and volumes of the Three Gorges Reservoir at different water levels using Landsat images and SRTM DEM data Quaternary International 304 115-25, doi:10.1016/j.quaint.2013.03.041

Zhang G, Yao T, Piao S, Bolch T, Xie H, Chen D, Gao Y, O'Reilly C M, Shum C and Yang K 2017 Extensive and drastically different alpine lake changes on Asia's high plateaus during the past four decades Geophysical Research Letters 44 252-60, doi:10.1002/2016GL072033

SWBD (2005) Shuttle Radar Topography Mission Water Body Data set [Dataset]. Available at http://www2.jpl.nasa.gov/srtm/index.html.

Fujisada H, Urai M and Iwasaki A 2012 Technical methodology for ASTER global DEM IEEE Transactions on Geoscience and Remote Sensing 50 3725-36, doi:10.1109/TGRS.2012.2187300

Rodríguez E, Morris C, Belz J, Chapin E, Martin J, Daffer W and Hensley S 2005 An assessment of the SRTM topographic products Jet Propulsion Laboratory D31639 143 pp

Tachikawa T, Kaku M, Iwasaki A, Gesch D B, Oimoen M J, Zhang Z, Danielson J J, Krieger T, Curtis B and Haase J 2011 ASTER global digital elevation model version 2-summary of validation results. Compiled by D. Meyer. The NASA Land Processes Distributed Active

Archive Center and the Joint Japan-US ASTER Science Team, 26 pp. Available at https://lpdaacaster.cr.usgs.gov/GDEM/Summary_GDEM2_validation_report_final.pdf

Bloomfield V A 2014 Using R for Numerical Analysis in Science and Engineering vol 1: CRC Press)

Liu B, Du Y e, Li L, Feng Q, Xie H, Liang T, Hou F and Ren J 2016 Outburst flooding of the moraine-dammed Zhuonai Lake on Tibetan Plateau: causes and impacts IEEE Geoscience and Remote Sensing Letters 13 570-4, doi:10.1109/LGRS.2016.2525778

Zhu G, Su Y, Li X, Zhang K and Li C 2013 Estimating actual evapotranspiration from an alpine grassland on Qinghai-Tibetan plateau using a two-source model and parameter uncertainty analysis by Bayesian approach Journal of hydrology 476 42-51, doi:10.1016/j.jhydrol.2012.10.006

Muskett R 2008 GRACE equivalent water mass balance of the Himalayas and Tibet Plateau region EGU General Assembly 10 EGU2008-A-01606

Immerzeel W W, Van Beek L P and Bierkens M F 2010 Climate change will affect the Asian water towers Science 328 1382-5, doi:10.1126/science.1183188

Moiwo J P, Yang Y, Tao F, Lu W and Han S 2011 Water storage change in the Himalayas from the Gravity Recovery and Climate Experiment (GRACE) and an empirical climate model Water Resources Research 47 W07521, doi:10.1029/2010WR010157

Watkins M M, Wiese D N, Yuan D N, Boening C and Landerer F W 2015 Improved methods for observing Earth's time variable mass distribution with GRACE using spherical cap mascons Journal of Geophysical Research: Solid Earth 120 2648-71, doi:10.1002/2014JB011547

Scanlon B R, Zhang Z, Save H, Wiese D N, Landerer F W, Long D, Longuevergne L and Chen J 2016 Global Evaluation of New GRACE Mascon Products for Hydrologic Applications Water Resources Research 52 9412–29, doi:10.1002/2016WR019494

Chen J, Pekker T, Wilson C, Tapley B, Kostianoy A, Cretaux J F and Safarov E 2017 Long‐term Caspian Sea level change Geophysical Research Letters 44 6993-7001, doi:10.1002/2017GL073958

Wiese D N, Landerer F W and Watkins M M 2016 Quantifying and reducing leakage errors in the JPL RL05M GRACE mascon solution Water Resources Research 52 7490-502, doi:10.1002/2016WR019344

Crétaux J-F, Jelinski W, Calmant S, Kouraev A, Vuglinski V, Bergé-Nguyen M, Gennero M-C, Nino F, Del Rio R A and Cazenave A 2011 SOLS: A lake database to monitor in the Near Real Time water level and storage variations from remote sensing data Advances in space research 47 1497-507, doi: 10.1016/j.asr.2011.01.004

Wang J, Sheng Y and Wada Y 2017 Little impact of the Three Gorges Dam on recent decadal lake decline across China's Yangtze Plain Water Resources Research 53 3854–3877, doi:10.1002/2016WR019817

Song C, Huang B and Ke L 2015 Heterogeneous change patterns of water level for inland lakes in High Mountain Asia derived from multi‐mission satellite altimetry Hydrological Processes 29 2769-81, doi: 10.1002/hyp.10399

Lei Y, Yang K, Wang B, Sheng Y, Bird B W, Zhang G and Tian L 2014 Response of inland lake dynamics over the Tibetan Plateau to climate change Climatic Change 125 281-90, doi:10.1007/s10584-014-1175-3

Li Y, Liao J, Guo H, Liu Z and Shen G 2014 Patterns and potential drivers of dramatic changes in Tibetan lakes, 1972–2010 PloS one 9 e111890, doi:10.1371/journal.pone.0111890

Jiang L, Nielsen K, Andersen O B and Bauer-Gottwein P 2017 Monitoring recent lake level variations on the Tibetan Plateau using CryoSat-2 SARIn mode data Journal of Hydrology 544 109-24, doi: 10.1016/j.jhydrol.2016.11.024

Zhu L, Xie M and Wu Y 2010 Quantitative analysis of lake area variations and the influence factors from 1971 to 2004 in the Nam Co basin of the Tibetan Plateau Chinese Science Bulletin 55 1294-303

Wang X, Siegert F, Zhou A-g and Franke J 2013 Glacier and glacial lake changes and their relationship in the context of climate change, Central Tibetan Plateau 1972–2010 Global and Planetary Change 111 246-57, doi:10.1016/j.gloplacha.2013.09.011

Landerer F W and Swenson S 2012 Accuracy of scaled GRACE terrestrial water storage estimates Water resources research 48 W04531, doi:10.1029/2011WR011453

Chapter 3 - Constructing long-term high-frequency time series of global lake and reservoir areas using Landsat imagery

3.1 Introduction

Lakes and reservoirs cover about 2-3% of Earth's non-glaciated land area and store the largest mass of liquid freshwater on the terrestrial surface (Feng et al. 2016; Lehner and Döll 2004; Messager et al. 2016; Sheng et al. 2016; Verpoorter et al. 2014). Due to easy accessibility and a broad spatial distribution, these inland water bodies serve as one of the primary water sources for irrigation, industrial, and domestic purposes (Alsdorf et al. 2007). However, their uneven distribution and vulnerability to environmental changes (e.g., warming and climate variability) result in temporally and spatially variable abundance that often does not meet local water demands (Crétaux et al. 2016). In recent decades, stress on surface water has been significantly intensified by population growth and climate change (Oki and Kanae 2006). Due to the ever-growing water demand, more than half of the global river systems are regulated by reservoirs (Grill et al., 2019; Lehner et al. 2011; Pokhrel et al. 2012), but two-thirds of the world's population are facing severe water shortage at least one month per year (Mekonnen and Hoekstra 2016). Under recent global warming, extreme events such as floods and droughts have become more intense and frequent, which further increases the unevenness of the distribution of surface water reserves (Alexander et al. 2013; Wang et al. 2018). Improved monitoring of extent variations in lakes and reservoirs is critical for assessing human and climate impacts on terrestrial water resources (Gao et al. 2012; Haddeland et al. 2014; Wang et al. 2017b; Zhan et al. 2019). Such knowledge is fundamental for evaluating global water availability, projecting future water stress, and formulating sustainable management plans (Gleick 2010; Van Beek et al. 2011).

Remote sensing provides a unique and effective way to monitor spatial and temporal variability of surface water extents at broad geographic scales. Water extraction methods using optical sensors are well established (Donchyts et al. 2016; Du et al. 2014; Feng et al. 2016; Feyisa et al. 2014; Haas et al. 2009; Hui et al. 2008; Jiang et al. 2014; Li and Sheng 2012; McFeeters 1996; Murray et al. 2019; Pekel et al. 2014; Sheng et al. 2016; Verpoorter et al. 2014; Wang et al. 2014; Yamazaki et al. 2015; Yang et al. 2017b; Yao et al. 2015). However, most of the established methods involve a practical tradeoff between spatial and temporal resolutions (Cooley et al. 2017; Huang et al. 2018). As a result, existing water extent products often do not meet the desirable spatial or temporal resolutions, such as 20 m and a daily frequency suggested by the Global Climate Observing System (GCOS) 2016 Implementation Plan (WMO 2016). High temporal resolution sensors, such as the Moderate Resolution Imaging Spectroradiometer (MODIS) Terra and Aqua, have been used to assess water extents at daily to 16-day timescales (Bergé-Nguyen and Crétaux 2015; Gao et al. 2012; Khandelwal et al. 2017; Klein et al. 2017; Sun et al. 2011; Wang et al. 2014; Wang et al. 2018). Yet, areal changes in many small water bodies (e.g., 10–50 km^2 or less) and the larger ones with irregular shapes, may not be discernible owing to the coarse resolution of MODIS imagery (250-500 m in visible and near-infrared bands) (Tao et al. 2015). Compared with MODIS, Landsat imagery (e.g., Landsat 5 Thematic Mapper (TM), 7 Enhanced Thematic Mapper Plus (ETM), and 8 Operational Land Imager (OLI)) have a much finer spatial resolution (30 m) and a nominal temporal resolution of 16 days (or finer if multiple Landsat sensors are combined). But due to cloud contamination (Rossow and Schiffer 1999), the temporal frequencies of previous Landsat-based water mapping are typically much lower than the nominal resolution, and could extend to one year for lakes with prolonged ice cover (Yao et al. 2018; Zhang et al. 2017). The Multispectral Instruments (MSI) onboard the

recently launched twin satellites Sentinel 2A and 2B provide a 10-m resolution in visible and near-infrared bands at 5- to 10-day intervals. However, their observations are currently limited to the latest 4 years (since 2015) and cannot yet considerably benefit decadal-scale monitoring.

In addition to the tradeoff between spatial and temporal resolutions, several other factors challenge high-resolution monitoring of long-term changes in global surface water extent (Klein et al. 2017). They include (i) intrinsic heterogeneity in spectral reflectance of water itself and (ii) spectral contaminations by atmosphere (clouds and aerosols), topographic shadows, aquatic vegetation, and ice/snow covers. An integration of multiple techniques is usually required to provide a robust water extraction under these complex scenarios. Recently, Pekel et al. (2016) used an extensive training dataset and combined expert systems with visual analytics, to identify the existence/absence of surface water on a monthly basis for every pixel in archival Landsat imagery during 1984-2015. The product was entitled the European Commission Joint Research Centre (JRC) Global Surface Water dataset (hereafter referred to as GSW). Despite remarkable achievements, GSW was based on cloud-free pixels, so the mapped extent of a specific water body is only complete when the cloud cover in a monthly-composite image is low. A follow-up study by Busker et al. (2019) extracted monthly areas in 137 lakes/reservoirs using a subset of the GSW dataset with cloud covers lower than 5%. The produced areas for nearly half of the lakes/reservoirs show correlations greater than 0.8 with water levels measured by radar altimetry. Nevertheless, temporal frequencies of the produced area time series are still limited by the availability of cloud-free images, and the time series discontinued after October 2015 due to the current availability of the GSW.

A potential way to increase the temporal frequency for Landsat-based lake mapping is to estimate water areas from contaminated images (e.g., affected by clouds or observation gaps).

Although these images have relatively poor quality, the partial lake extents exposed in them may provide useful information to infer the complete extents. Recently, Zhao and Gao (2018) applied monthly water mappings in the GSW dataset to produce area time series for 6817 reservoirs documented by the Global Reservoir and Dam Database (Lehner et al. 2011) from 1984 to 2015. Their method includes a novel recovery of full reservoir extents from partial observations due to cloud contamination, by segmenting the pixels of water occurrence probability provided in the GSW. Compared to the result of Busker et al. (2019), their produced area time series increased the number of observation by ~80%. However, dependence on the existing GSW dataset constrained their reservoir area records to the period from 1984 to 2015, and the validation of their recovery method was limited to nine reservoirs with time-variable water levels.

Here we propose a new mapping method that aims to produce temporally continuous inundation areas for both lakes and reservoirs globally at 30-m resolution during the past nearly three decades (from 1992 to 2018). The proposed method leveraged six spectral water indices, and used water extent time series extracted from high-quality Landsat images to recover the missing water areas under contaminations, thus enabling a monthly to bi-monthly monitoring frequency closer to Landsat's nominal temporal resolution. Our algorithm was implemented automatically on the Google Earth Engine (Gorelick et al. 2017), a cloud-based platform for planetary-scale geospatial analysis with free access to the entire Landsat archive. To evaluate the performance of this mapping method, we applied it to 428 lakes and reservoirs worldwide (Figure 3.1) that currently have time-variable water level measurements by multi-mission satellite radar altimeters, as provided in three major altimetry archives (see Section 3.2.1). The robustness of the method was further tested for 25 water bodies (14 lakes and 11 reservoirs) under five challenging scenarios. These scenarios considered different combinations of spatial

location, water body type, and disturbing factors of water mapping. Our overall objectives are: (i) to improve the temporal frequency and accuracy of long-term water mapping using Landsat imagery, (ii) to produce an update-to-date high-resolution record of global lake/reservoir area time series (GLATS), and (iii) to suggest a generic method that can assist in temporally continuous water area monitoring based on similar spectral or synthetic aperture radar (SAR) images.

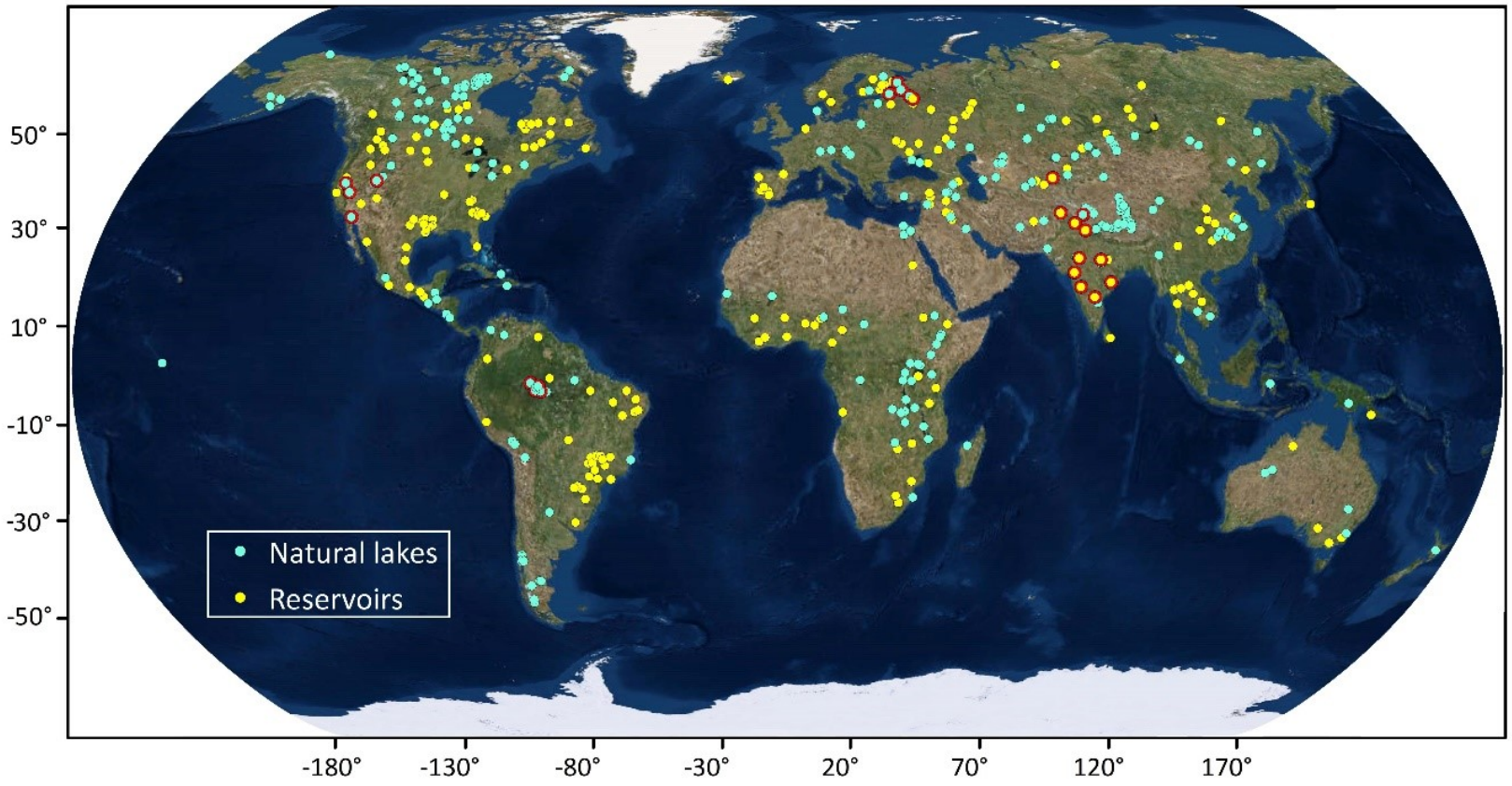

Figure 3.1 Distribution of 428 water bodies worldwide (223 lakes and 205 reservoirs) that are used for evaluating the proposed water mapping method. Robustness of the method was further tested on 25 water bodies (14 lakes and 11 reservoirs, highlighted by red circles) under various scenarios (refer to Section 3.3.2 and Table 3.2).

3.2 Methodology

3.2.1 Data

3.2.1.1 Landsat images

This study used orthorectified top-of-atmosphere (TOA) reflectance data (L1T) Tier 1 from Landsat 5 TM, 7 ETM+ and 8 OLI sensors. We opted to use the TOA data rather than surface reflectance data, which is consistent with some existing studies on global surface water extents and dynamics (Allen and Pavelsky 2018; Donchyts et al. 2016; Pekel et al. 2016; Sheng et al. 2016). We also compared the mapping performance using TOA data with that from surface reflectance data, and confirmed that the latter does not lead to evident improvement in mapping accuracy or temporal coverage (see Figure 3.2 for details). All applied images have 30-m spatial resolution and were acquired during October 1, 1992 to October 31, 2018. The period was set with regard to the availability of the validation dataset (see Section 3.2.1.2). Different from most existing studies (Busker et al. 2019; Sheng et al. 2016; Yang et al. 2017a), we considered the entire Landsat archive over the past 26 years (1992-2018) for each of the studied 428 lakes and reservoirs, including those with reasonable contaminations of clouds, aerosols, mountain shadows and the ETM+ Scan Line Corrector (SLC) errors (more details in Section 3.2.2.1). Inclusion of contaminated images could further increase the temporal resolution of water mapping. For water bodies in high-latitude or high-altitude regions, we excluded the images during the freezing period considering that water extents and boundaries can hardly be detected when they were severely covered by snow/ice (Cooley et al. 2017; Yao et al. 2018) (also refer to Discussion). All used images were accessed online from the Google Earth Engine (https://earthengine.google.com).

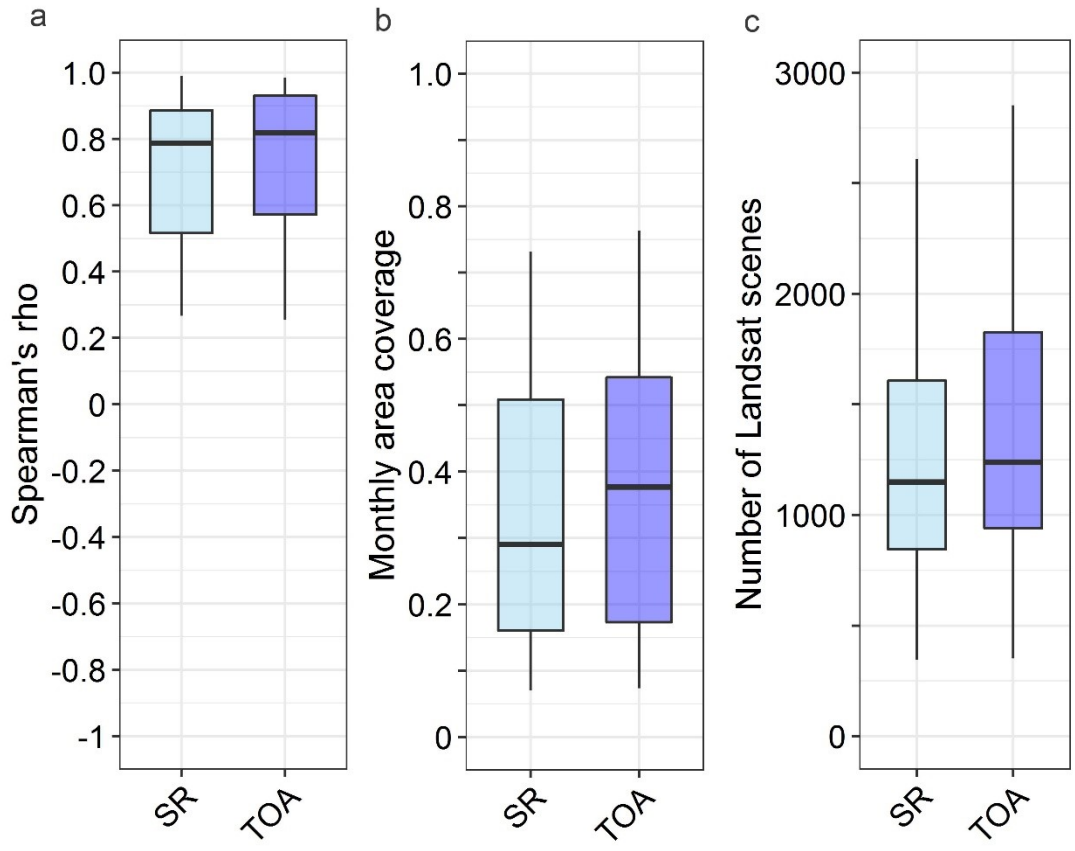

Figure 3.2 Comparison of the performances of the proposed method on top of atmosphere (TOA) images vs surface reflectance (SR) images for 50 randomly selected water bodies. (a) Area-level rank correlation (Spearman's rho). (b) Temporal coverage of extracted area time series. (c) The number of Landsat scenes in the Tier 1 collection. The results show that using SR imagery, the strength of area-level correlations is not improved (Figure 3.2a), and the temporal coverage of area time series is lower (Figure 3.2b), partially owing to fewer Landsat scenes compared with TOA images (Figure 3.2c).

3.2.1.2 Altimetry levels

As part of the validation procedure, we compared our produced lake/reservoir area time series with water levels measured by satellite radar altimeters. Level time series were acquired from three major altimetry archives including the Hydroweb (http://hydroweb.theia-land.fr) (Crétaux et al. 2011), the Global Reservoir and Lake Monitor database (G-REALM; https://ipad.fas.usda.gov/cropexplorer/global_reservoir) (Birkett et al. 2011), and the Database

for Hydrological Time Series of Inland Waters (DAHITI; https://dahiti.dgfi.tum.de/en) (Schwatke et al. 2015). While most level time series in Hydroweb and DAHITI were processed from multi-mission altimetry measurements at a (sub-)monthly basis, G-REALM implemented a more frequent but less accurate Interim Geophysical Data Record (IGDR) altimeter to produce 10-day level products (Birkett et al. 2011). Thus, levels from Hydroweb and DAHITI were prioritized here. If a lake or reservoir has level products from both Hydroweb and DAHITI, the longer record was used. Typically, the accuracy of radar altimetry levels ranges from a few centimeters (e.g., for large lakes and reservoirs) to several decimeters (e.g., for small or narrow water bodies) (Crétaux et al. 2016).

3.2.2 Monthly water area mapping

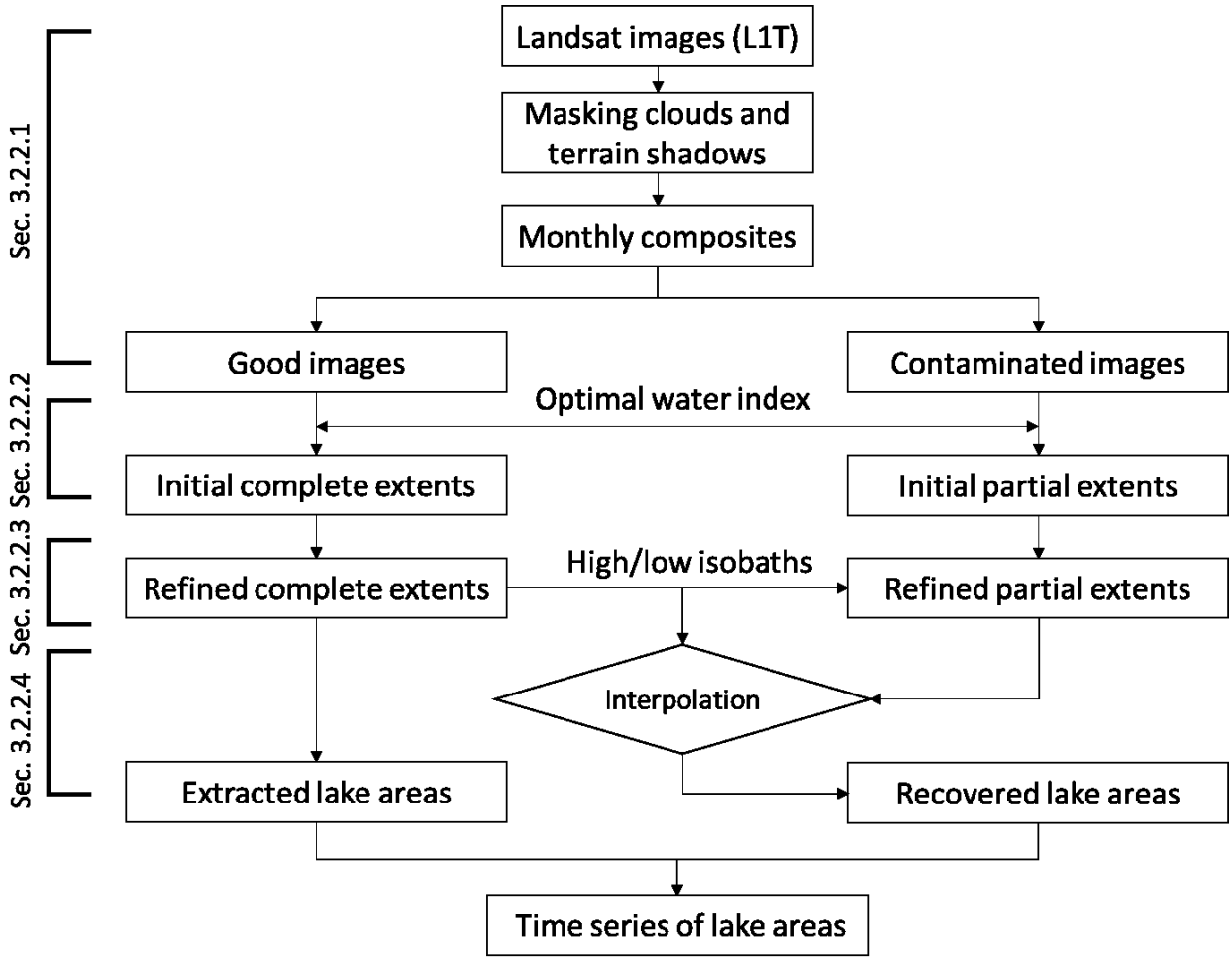

Figure 3.3 Schematic workflow of the proposed water mapping and recovery method.

We follow the schematic flowchart in Figure 3.3 to demonstrate the procedure of mapping and recovering water areas for each studied lake/reservoir. In brief, our method started with maximizing the proportion of available high-quality observations, by masking cloud and terrain shadow contaminations in individual Landsat scenes and then mosaicking them to monthly composite imagery (Section 3.2.2.1). Next, the initial water extent from each composite image was optimized by comparing the mapping results of six water indices (Section 3.2.2.2). Remnant mapping errors in the initial water extents from both good (contamination-free) and

contaminated composite images were further reduced by a refining process (Section 3.2.2.3). Then, the complete water areas for the partial lake/reservoir extents affected by cloud and SLC-error contaminations, were recovered by the complete water extents (isobaths) mapped from good images (Section 3.2.2.4). Finally, complete water areas, both directly mapped from good images and recovered from bad images, were combined to construct the area time series. Details of each step are elaborated below.

3.2.2.1 Compositing monthly images

We applied the *SimpleCloudScore* algorithm provided in the Google Earth Engine to mask cloud covers in the individual TOA reflectance images acquired by Landsat 5 TM, 7 ETM+ and 8 OLI sensors. The *SimpleChouldScore* algorithm is a widely-used thresholding method for detecting clouds in Landsat TOA imagery (Donchyts et al. 2016; Gorelick et al. 2017; Wang et al. 2017a; Wayand et al. 2018). The detection was based on the "simple cloud-likelihood score", which is determined by a combination of brightness, temperature and Normalized Difference Snow Index (NDSI) (Gorelick et al. 2017). The brightness score reflects that clouds are bright in visible bands. The temperature score reflects that clouds have a cool temperature measured by thermal bands. The NDSI score was used to separate clouds from snow. We set the threshold score to be 30 according to previous references (Wang et al. 2017a; Wayand et al. 2018) and our own visual inspections. In addition to clouds, deep terrain shadows can also contaminate the TOA reflectance, and thus were masked out from individual scenes before the composition. We applied the 30-m resolution SRTM digital elevation model (Farr et al. 2007) to generate slope and hillshade at the image acquisition time using the provided solar angles. The slope and hillshade information was then used to generate mountain shadow masks as per Li and Sheng (2012). The masked TOA images were then mosaicked using median-value

composite on a monthly basis during our study period (October 1, 1992 to October 31, 2018). The monthly composite images, by combining cloud-free pixels in multiple scenes, improved the overall proportion for high-quality observations. Masked pixels that remain in each composite image are hereafter referred to as “contaminations”, which are a combination of cloud covers, deep mountain shadows, and missing observations such as due to the SLC error.

3.2.2.2 Extracting initial water extents

For each lake or reservoir, its time-variable water areas were extracted from a fixed region of interest (ROI) on the monthly TOA composite images. The ROI was defined as a buffer region that contains a reference extent of this water body as depicted in the circa-2000 global lake inventory (Sheng et al. 2016). We set this ROI to be roughly double to triple the size of the reference extent in order to fully encompass the largest possible inundation extent of this water body during the study period. We also ensured that other major water bodies except the studied one were excluded from the ROI. To optimize the accuracy of water extraction, we considered six commonly applied water indices including the Normalized Difference Water Index (NDWI) (McFeeters 1996), the Modified Normalized Difference Water Index (MNDWI) (Xu 2006), the High Resolution Water Index (HRWI) (Yao et al. 2015), the 2015 Water Index (WI2015) (Fisher et al. 2016), and two Automatic Water Extraction Indices ($AWEI_{nsh}$ and $AWEI_{sh}$) (Feyisa et al. 2014). Detailed index configurations are given in Table 3.1.

Table 3.1 Six water indices considered for initial water extent extraction

Water index	Reference	Configuration
NDWI	McFeeters (1996)	(G–NIR)/(G+NIR)
MNDWI	Xu (2006)	(G-SWIR1)/(G+SWIR1)
$AWEI_{nsh}$	Feyisa et al (2014)	4×(G-SWIR1) -(0.25×NIR+2.75×SWIR1)
$AWEI_{sh}$	Feyisa et al (2014)	B+2.5×G-1.5×(NIR+SWIR1) -0.25×SWIR2
HRWI	Yao et al (2015)	6×G – R - 6.5×NIR + 0.2
WI2015	Fisher et al (2016)	1.7204+171×G+3×R-70×NIR-45×SWIR1-71×SWIR2

Note: B, G, R, NIR, SWIR1, SWIR2 represent Landsat's blue, green, red, near infrared, short-wave infrared 1, and short-wave infrared 2 bands, respectively.

For each lake/reservoir with altimetry levels, the available water levels were applied to identify the best-performing water index. On typical conditions, lake inundation areas are positively correlated to water levels, and this correlation would decrease if the mapping error increases. Therefore, the strength of correlation to water level, here measured as Spearman's rank correlation (Lyerly 1952), was used to rank the performance of different water indices. For high-quality composite images (here defined as <5% contaminations within the ROI, thereafter "good" images), each of the six indices was employed to extract two sets of water area time series within the ROI, one at a default threshold (here defined as 0) and the other at adaptive thresholds. We considered adaptive thresholds to segment water and land pixels because default thresholds may not always yield satisfactory water extraction due to various image qualities (presence of aerosols, water vapor, water turbidity, mineral and chlorophyll contents, and surrounding settings across space and time (Li and Sheng 2012; Sheng et al. 2016; Wang et al. 2014). The adaptive thresholds were determined by the Otsu's method(Otsu 1979) using the

pixels of each monthly composite image within the ROI, so the threshold is automatically adapted to the spectral condition for each month (see Li and Sheng (2012) for details). This generated 12 sets of water area time series for this lake/reservoir. The set of water areas that exhibit the strongest correlation to water levels, were used as the initial extents of this lake/reservoir. Preliminary tests on 86 randomly selected lakes/reservoirs with altimetry levels confirm that the water areas optimized by the consideration of multiple indices yield a higher average accuracy than those produced by any one of the six indices at either default or adaptive thresholds (Figure 3.4). For contaminated images (>=5% contaminations within the ROI, thereafter "bad" image), adaptive thresholds can be sensitive to the disturbance of clouds and cloud shadows (Fisher 2014). Therefore, the initial lake/reservoir extents were generated by the selected best-performing index at the default threshold.

For the purpose of method validation (Section 3.2.4), all 428 lakes/reservoirs in this study have altimetry level measurements. However, the rationale of the above index selection can be similarly applied to water bodies without level measurements. A feasible solution is to replace the numeric levels by an ordinal sequence of water levels inferred from the positions of the mapped shorelines. This is based on the fact that rising and falling shorelines of a lentic water body constitute a set of elevation isobaths (contours). If a water index is effective, the mapped water area is expected to increase as the isobath expands outward. The correlation between water areas and shoreline orders would decrease if the index introduces more omission or commission errors (as illustrated in Figure 3.5a). For this reason, the optimal index solution can be determined as the one yielding the strongest rank correlation between the mapped lake areas and shoreline orders.

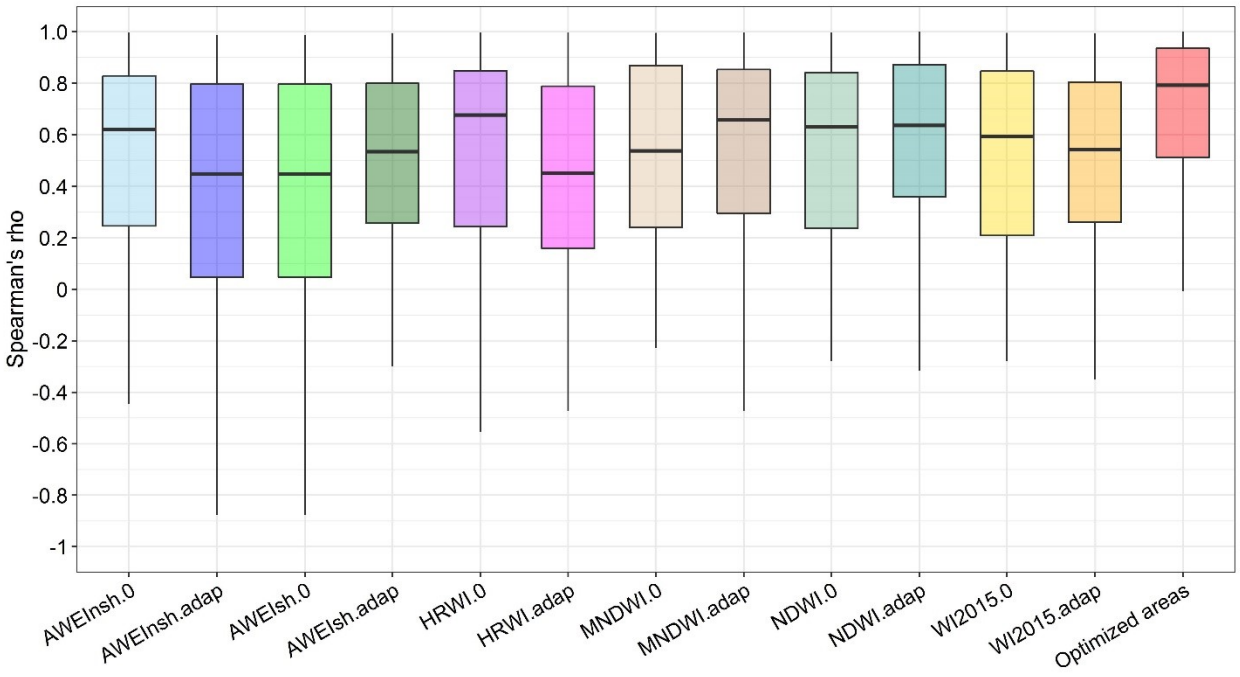

Figure 3.4 Comparison between initial water mappings optimized by multiple index solutions and those using only one of the solutions. The comparison is based on rank correlations (Spearman's rho) between altimetry levels and water areas mapped from good imagery for 86 randomly sampled lakes and reservoirs. Each box and whisker diagram represents the distribution of area-level correlations for all 86 lakes/reservoirs, where water areas were mapped using (1) any one of the six water indices (Table 1) at either the default threshold (0) or the adaptive thresholds (the first 12 diagrams), and (2) the areas optimized by the best-performing index solution for each lake/reservoir (the last diagram). Bottom, middle, and top lines of each box illustrate the 25th, 50th (median), and 75th percentiles, respectively. Bottom and top whiskers illustrate the 5th and 95th percentiles, respectively.

3.2.2.3 Refining water extents in good imagery

Despite the consideration of multiple water index solutions, remnant mapping errors could still occur due to minor contaminations such as sporadic clouds, cloud/terrain shadows, and aquatic vegetation. The expansion and shrinkage of a water body is constrained by its bathymetry, which could be used to reduce the remnant errors (Khandelwal et al. 2017). For a lentic water body, the edge or shoreline of its water extent can be treated as an isobath. A smaller water extent, which is typically associated with a lower/inner isobath, should be contained by a larger extent associated with a higher/outer isobath. The water extents/isolines were thus ranked by their containment topology based on the overall positions of the pixels along the shorelines. This design also reduces the influence of the shorelines that may occasionally intersect due to mapping errors or severe hysteresis (unstable lake surfaces). For each water extent mapped from a good image, the two higher isobaths and two lower isobaths that are closest to this extent were used to reduce commission and omission errors. As illustrated in Figure 3.5a, if the mapped extent contains an "island" which is however inundated by both lower isobaths, the "island" was treated as an omission error and thus corrected to water. Similarly, if this water extent has a portion beyond both higher isobaths, this portion was treated as a commission error and removed.

3.2.2.4 Recovering lake areas in contaminated imagery

Although extracted shorelines from contaminated/bad images are incomplete, the positions of these partial shorelines still indicate a sequence in elevation (Figure 3.5b and 3.5c). Following the same rationale as described in Section 3.2.2.3, if a shoreline segment (the solid yellow line in Figure 3.5b) locates between a lower isobath and a higher isobath (green and purple in Figure 3.5b), we expect that the complete shoreline (the solid and dash yellow line in

Figure 3.5b) recovered from this segment will be bound/enclosed by the isobaths on both sides of the segment. Correspondingly, the complete water extent for this segment should also fall between the smaller extent associated with the lower isobath and the larger extent with the higher isobath. The closer the bounding isobaths are, the less uncertain the recovered area is. For this reason, the complete water area associated with this shoreline segment can be estimated as an interpolation between the areas of the minimum bounding isobaths. Here, the minimum bounding isobaths are defined as a pair of complete water shorelines mapped from good images, which are immediately above and below the incomplete shoreline (purple and green in Figure 3.5b and 3.5c) so that the interpolation uncertainty can be minimized.

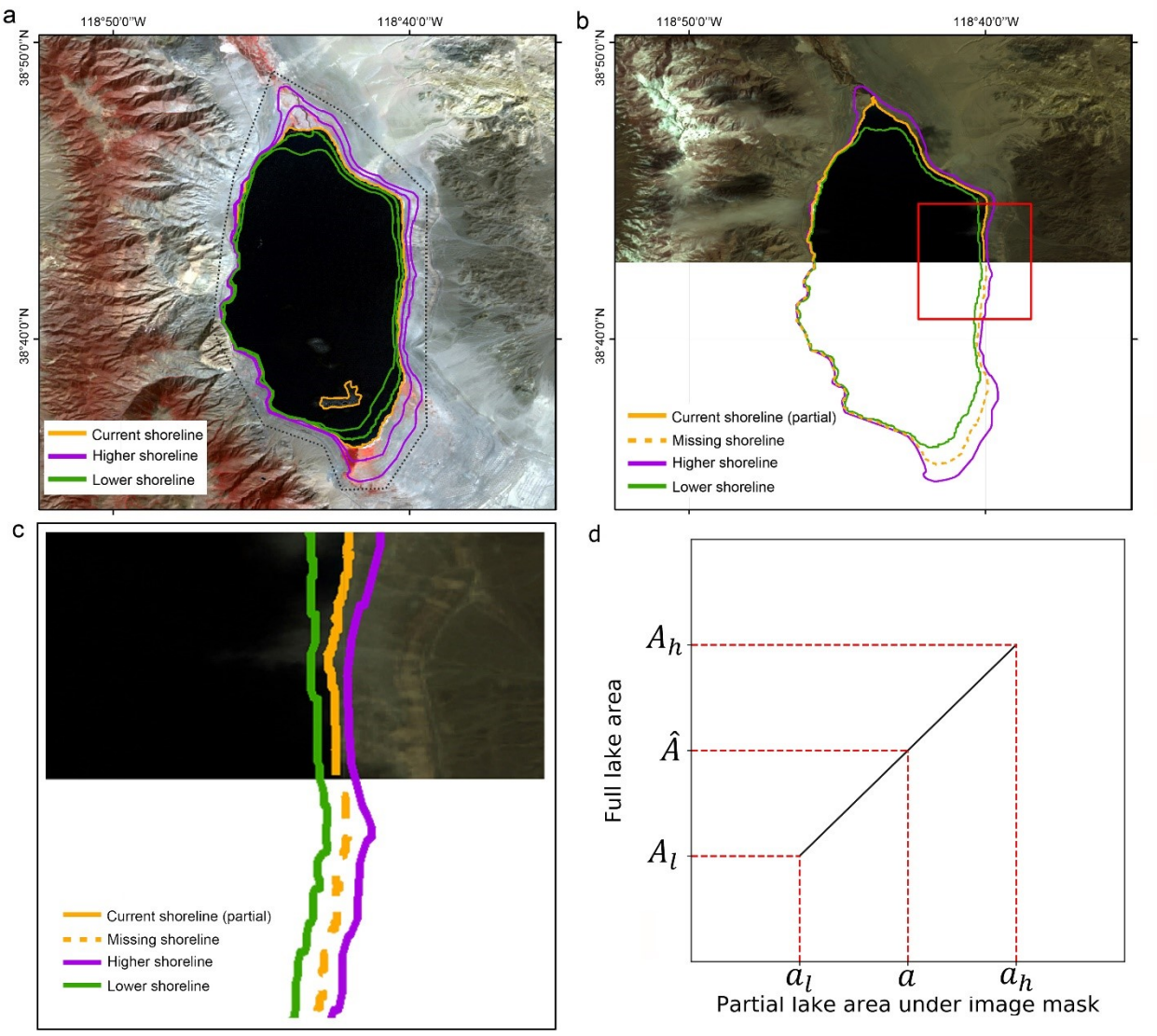

Figure 3.5 Illustration of the proposed lake/reservoir area recovery method using a case study of Walker Lake (38.70°N, 118.71°W) in Nevada, USA. (a) Refinement of lake area extracted from good imagery. Black dash line shows the extent of this lake ROI. Small yellow polygon represents omission errors. A total of 254 isobaths (complete shorelines) were mapped for this lake (see Figure 3.16g), but only a few were shown in this figure for the clarity of method illustration. (b) Recovery of partial lake area from bad imagery. (c) Enlargement of the red box region in (b). (d) Estimation of the full lake area from partial lake extents.

Similar to Section 3.2.2.3, the bounding isobaths were first applied to remove any mapping errors from the partial lake/reservoir extent (Figure 3.5b). Assuming that between the

bounding isobaths, the variation of water areas in the good/valid portion of a bad image is proportional to that of their full areas (Figure 3.5d), the full area ($\hat{A}$) associated with the partial extent (a) was recovered as:

$$\hat{A} \cong \frac{A_h - A_l}{a_h - a_l}(a - a_l) + A_l \quad [1]$$

Where A_h and A_l represent the full areas of the higher and lower minimum bounding isobaths, respectively, and a_h and a_l the partial areas of the bounding isobaths observed in the valid portion of the bad image. As implied in Equation 1, our area recovery was based on a linear interpolation between the water extents of the closest isobaths. This design enables an efficient estimation of lake areas based on shoreline positions with considerable accuracy (see Results). By using our own mapping of complete extents/isobaths, this recovery method is less dependent on other inundation products (e.g., GSW as applied in Zhao and Gao (2018)), and thus more generic to potential applications using other sensors and for extended periods (e.g., beyond 2015) (see Discussions). However, it is worth noting that in occasional cases, incomplete shoreline segments may go beyond the maximum (or minimum) extents mapped from available good imagery during our study period. If this happened, the maximum (or minimum) water extents recorded in GSW were considered as the highest (or lowest) bounding isobaths for our interpolation.

The full water areas, either recovered from bad images or directly mapped from good images, were combined to generate the area time series for each lake/reservoir. Similar to Zhao and Gao (2018), we measured the improvement in temporal coverage for each time series by "improvement ratio", defined as the number of recovered water areas divided by the number of complete areas observed in good images. We here only used imagery with effective observations (free of clouds, terrain shadows, and SLC errors) greater than 50% within an ROI. By doing so,

the areas of observation are larger than those of interpolation, so the reliability of our area recovery is better assured. Since the accuracy of delineated water extents may decrease as the cloud percentage increases, we further excluded the images where cloud cover exceeds 20% of the valid pixels (excluding no data gaps) within the ROI. This cloud cover threshold gives a reasonable tradeoff between the mapping accuracy and the increase of observation number (more details in Discussions).

3.2.3 Quality assurance and quality control (QA/QC)

Outliers in the produced area time series may exist due to imagery quality and unavoidable mapping errors (Pekel et al. 2016; Sheng et al. 2016). To assure the quality of our produced time series, we visually inspected the results for each of the 428 lakes and reservoirs. For each inspected water extent, if classification errors were substantial, the image was reclassified by using other water indices until the satisfactory result was achieved. If none of the water indices could achieve a reasonable accuracy, the area outlier was removed. A total of 289 areas were identified as outliers, accounting for 0.4% of all water areas in our produced time series for the 428 water bodies. This low outlier occurrence suggests that our mapping and recovery methods are reliable under most circumstances. However, we found relatively more outliers for six saline lakes (Lake Urmia (45.50°W, 37.64°N), Great Salt Lake (112.57°W, 41.13°N), Salton Sea (115.82°W, 33.31°N), Aral Sea East (59.82°W, 44.90°N), Aral Sea West (58.72°W, 45.02°N), and Lake Khyargas (93.38°W, 49.16°N)) owing to misclassification of salty lake bed as clouds. For these six saline lakes, we applied the proposed method on the surface reflectance data where cloud mask appears more accurate.

3.2.4 Accuracy assessment

3.2.4.1 Validation methods

We assessed our recovered lake/reservoir areas in two aspects. One is a direct validation against observed lake areas, and the other is a comparison with altimetry water levels. For the first validation, complete lake areas mapped from good images were used to assess the recovered areas from simulated partial observations in the same images. Specifically, we randomly selected 10 good images for each reservoir or lake. For each image, we randomly masked a proportion (i.e., between 5%-50%) of the pixels within the lake/reservoir ROI to simulate a partial contamination. The remaining pixels in the ROI served as the simulated partial observation, from which the complete water area was recovered using the proposed method in Section 3.2.2. The recovered areas were then compared with the actual areas directly mapped from good images using linear regression. The slope, R^2 value, and root mean square error (RMSE) of the linear regression were used to assess the fidelity of our proposed mapping/recovery method.

Alternatively, the performance of the proposed method was evaluated by the hypsometric relationship between our produced lake/reservoir areas and their altimetry water levels. For each of the 428 studied lakes/reservoirs, we calculated the correlation between altimetry levels and our produced areas from both good and bad images, and then compared it with the area-level correlation using good images alone. The correlation was measured as Spearman's rank correlation, given that lake area and level do not necessarily follow a linear relationship. We also assessed the change of "relative hypsometric range" owing to the use of recovered water areas. Here, relative hypsometric range is defined as the difference between the maximum and minimum water levels that are paired with available water areas, divided by the full range of the observed altimetry levels. An increase of hypsometric range indicates a more complete depiction

of the lake/reservoir bathymetry, and thus improved accuracy in deriving water volume changes. To further evaluate our proposed method with recent approaches, we compared our results with those of Busker et al. (2019), who calculated water areas for 137 lakes/reservoirs using a subset of the GSW water classifications from only good Landsat images. If any of our studied 428 lakes/reservoirs is not included in their study, we applied their approach on that lake/reservoir.

3.2.4.2 Overall accuracy

The overall accuracy of the proposed method was assessed by applying the above two validations on all the 428 lakes and reservoirs with available altimetry water levels. These water bodies have a diverse range of size from about 2 km^2 to 82,000 km^2 (Sheng et al. 2016) and are located in various geographic and climatic zones (Figure 3.1).

3.2.4.3 Robustness

We further evaluated the proposed method by testing its robustness on 25 out of the 428 lakes/reservoirs that represent five scenarios with regard to spatial location, lake type, and mapping difficulty. These five scenarios include fluvial lakes in the Amazon basin, reservoirs in (sub-)tropical India, lakes and reservoirs in High Mountain Asia, saline lakes in western United States, and high-latitude lakes in northwestern Russia (dots highlighted by red circles in Figure 3.1). These scenarios cover a wide range of disturbing factors for water mapping, such as cloud and cloud shadow contaminations (particularly in humid regions), complicated shoreline geometries (e.g., dendritic reservoir shapes), terrain shadows (e.g., in mountainous regions), high mineral concentrations (e.g., in saline lakes), and snow/ice covers (e.g., in high-latitude lakes). In order to objectively evaluate the mapping robustness, these 25 lakes/reservoirs were sampled among some of the most challenging examples for each scenario.

3.3 Results

3.3.1 Overall performance of the proposed method

3.3.1.1 Accuracy of water area recovery

The recovered lake/reservoir areas from simulated partial observations agree well with the actual areas observed from good images. The mean relative RMSE is only 2.2%, and the slope and R^2 values of the linear fitting between simulations and observations both approach 1 (Figure 3.6a). As further summarized in Figure 3.6b, R^2 values for each of the 428 studied lakes/reservoirs reach a median value of 0.99, with over 75% of them above 0.90. The offset in slope among the lakes/reservoirs is 2%, where over 90% of them are within ±10%. The median relative RMSE is only 0.3%, with over 75% of them below 1%. These results suggest that our proposed area recovery method is overall reliable.

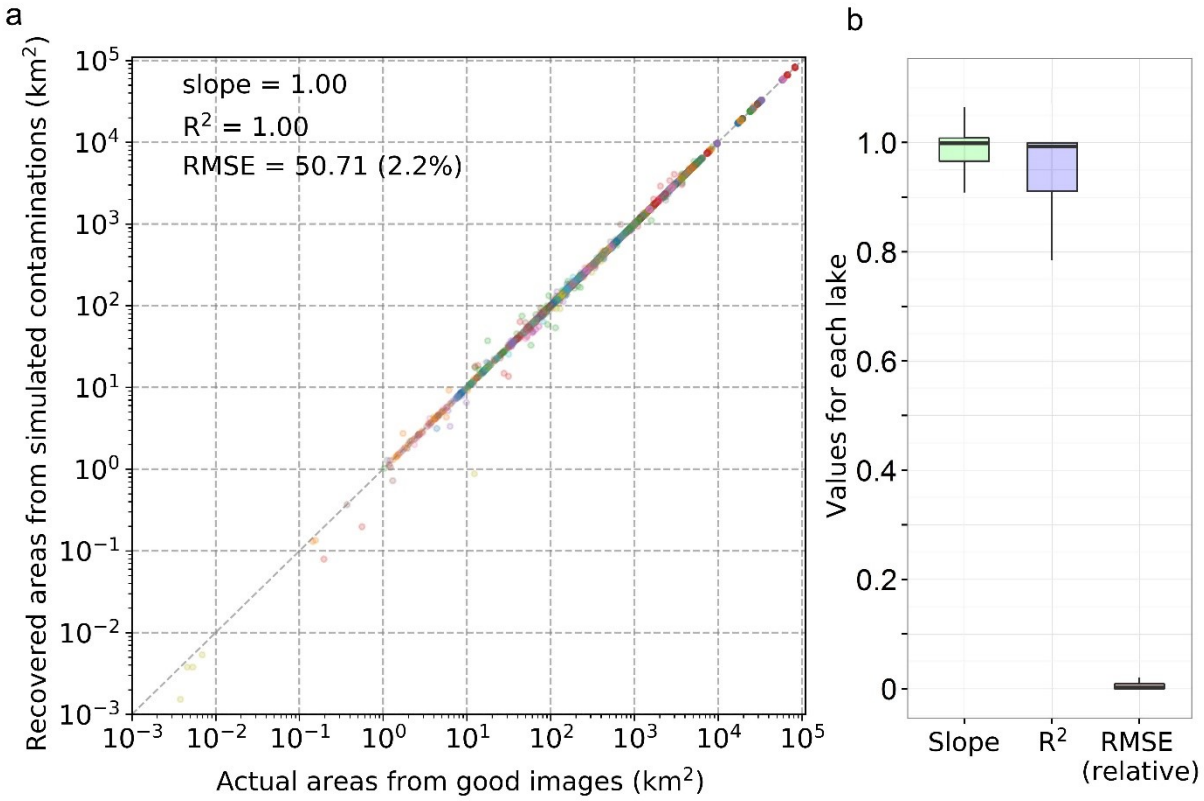

Figure 3.6 Validation of recovered lake/reservoir areas from simulated contaminations on good images. (a) Overall agreement for all lakes/reservoirs. Different colors represent each of the 428 lakes/reservoirs. A total of 4, 280 validation samples is shown. (b) Agreements for individual lakes/reservoirs. The box and whisker diagrams summarize the fitting R2 and slopes between recovered and observed areas of each of the 428 lakes/reservoirs. Statistical interpretation of the box and whisker diagrams is as in Figure 3.4.

3.3.1.2 Correlation with altimetry water levels

Among the 428 lakes and reservoirs, the upper quartile, median and lower quartile of the correlation (Spearman's rho) between measured altimetry levels and mapped/recovered water areas from both good and bad images are 0.94, 0.79 and 0.44, respectively. These are comparable to the area-level correlations by using good images alone (upper quartile, median, lower quartile are 0.95, 0.80 and 0.47, respectively) (Figure 3.7a). For more than 80% of the lakes/reservoirs, adding recovered water areas from bad images yielded comparable or improved

area-level correlations (Figure 3.8a). This was partially owing to the increased area-level pairs and thus a more complete representation of their covariation. However, a few lakes/reservoirs (12%, red dots in Figure 3.8a) show some degree of decrease in area-level correlation (Spearman's rho reduced by 0.1 or more). This was primarily affected by low area variations (<2%) and mapping challenges posed by snow and ice in high-latitude or altitude regions (see Figure 3.8a and Section 3.3.2.5). Compared with the GSW-based estimate using good imagery only (Busker et al. 2019), our median area-level correlation was improved from 0.64 to 0.79, and the interquartile range (i.e., interval between 25 to 75 percentiles) of the area-level correlations reduced from 0.64 to 0.50 (Figure 3.7a).

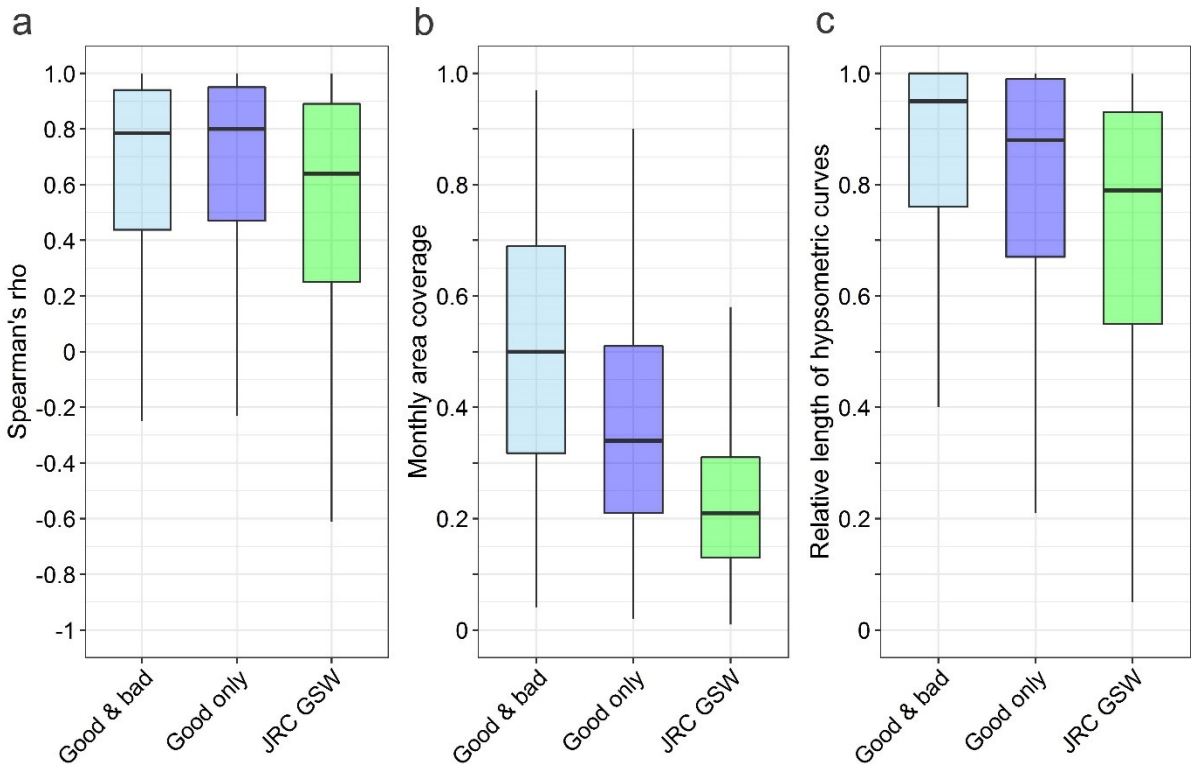

Figure 3.7 Evaluation of the proposed lake/reservoir mapping method by altimetry water levels. (a) Comparison of rank correlations (Spearman's rho) between altimetry levels and water areas estimated from good images alone (this study), both good and bad images (this study), and the study of Busker et al. (2019) using a subset of GSW water mappings based on good images. (b) Comparison of monthly coverages among the three results (as in a). Values indicate the number of months with available mapping as a fraction of the total number of months during the study period (1992-2018). (c) Comparison of relative hypsometric ranges among the three results (as in a). Each box and whisker diagram summarizes the distribution of the results from each of the 428 studied lakes and reservoirs. Statistical interpretation of the diagrams is as in Figure 3.4.

3.3.1.3 Improvements of temporal coverage and hypsometric range

Including recovered lake/reservoir areas from contaminated images increased the average monthly coverage during our study period (1992-2018) from 37% to 50%, achieving a mean improvement ratio of 43% (Figure 3.7b and 3.8b). Particularly, high improvement ratios (e.g., >50%) generally occur in tropical and sub-tropical regions where cloud covers are high (Figure 3.8b). Compared with a GSW-based estimate using good imagery only (Busker et al. 2019), our monthly coverage during the overlapping period (Oct 1992- Oct 2015) increases substantially by an average of 78% (Figure 3.7b).

In addition to the improved temporal coverage, our recovered water areas from bad images also increased the ranges of the hypsometric curves (area-level relationships) (Figure 3.7c). For the studied 428 lakes/reservoirs, more than half of their hypsometric curves now cover at least 95% of the level variations observed by altimetry satellites. As previously stated, extended hypsometric curves better represent the lake/reservoir bathymetric information, and thus allow for more accurate estimates of lake volume variations (Crétaux et al. 2016).

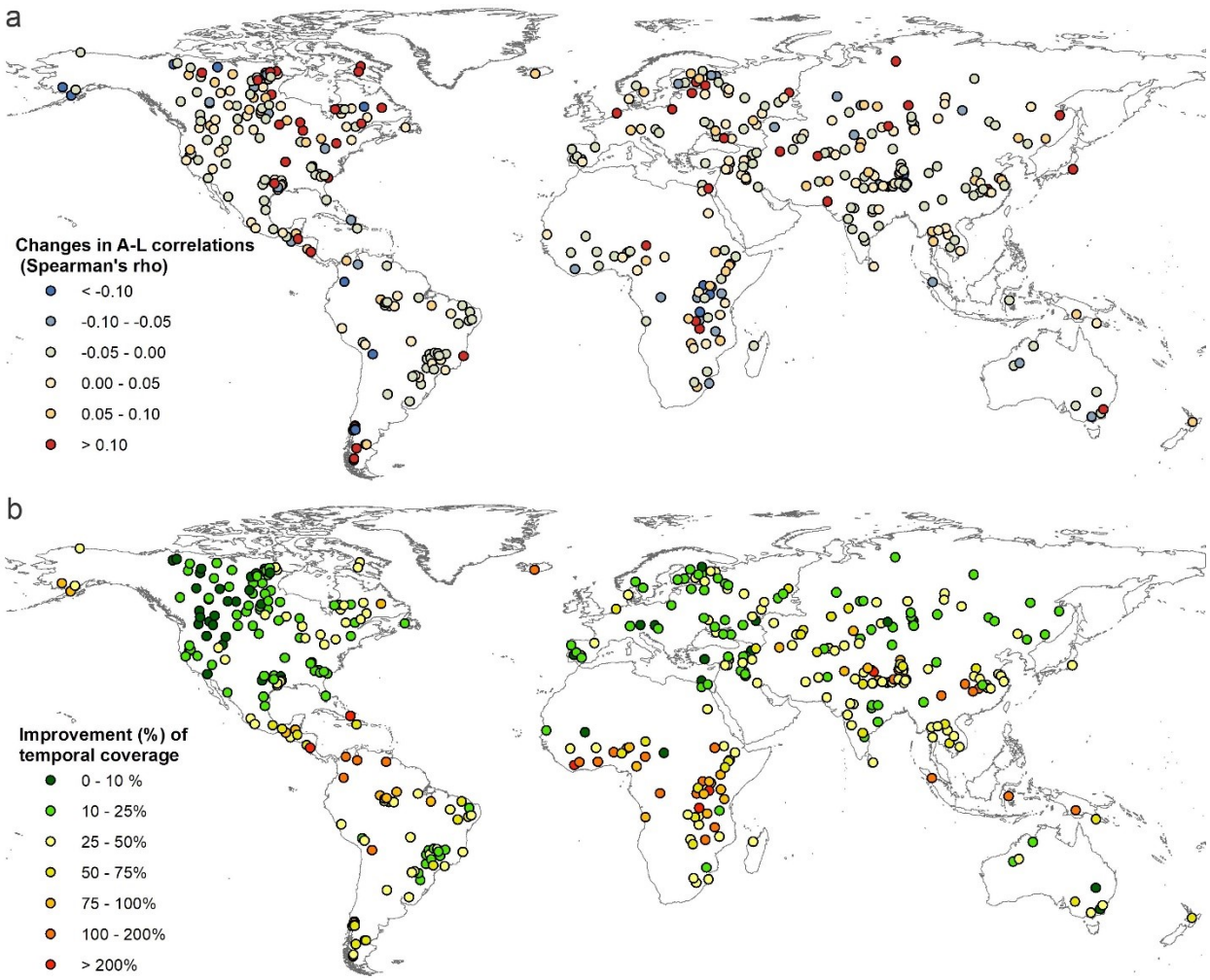

Figure 3.8 Impacts of water area recovery from contaminated imagery on area-level correlations and temporal coverage for the studied 428 lakes/reservoirs. (a) Changes in area-level (A-L) correlation (in Spearman's rho). Values indicate correlations before including recovery subtracted by correlations after including recovery. (b) Improvement of temporal coverage at monthly timescale (in %).

3.3.2 Robustness under different scenarios

3.3.2.1 Fluvial lakes in the Amazon

Fluvial lakes are usually shallow fresh water bodies formed on floodplains and deltas by fluvial processes (Cohen 2003). Water levels in fluvial lakes are often influenced by the stage of the connected rivers, which leads to highly dynamic inundation areas in these lakes (Wang et al. 2017b). Increasing the mapping frequency for fluvial lakes is significant to the monitoring of freshwater availability and potential flood managements, particularly in humid regions. However, high-frequency mapping of fluvial lakes is notoriously difficult due to enduring and frequent cloud covers in humid regions, such as the Amazon. So for our first scenario, five fluvial lakes in the Amazon Basin with sizes in between ~100–1000 km^2 (Table 3.2) were selected to evaluate the performance of our proposed mapping method.

As shown in Figure 3.9a, lake areas recovered from simulated contaminations are generally consistent with the actual areas, with a negligible relative error of 1.1%. The combined water area time series from both good and bad images improved the mapping frequency for nearly all of these fluvial lakes (except for Amana) to a bi-monthly level (Table 3.2; Figure 3.10). Such an improved temporal frequency reveals new details on the seasonal cycles of these fluvial lakes (Figure 3.10).

The combined area time series (from both good and bad images) achieve fairly strong correlations with altimetry levels (Spearman's rho between 0.78 and 0.95), which are highly comparable to the area-level correlations using good images alone (Spearman's rho between 0.82 and 0.95) (Table 2 and Figure 3.10). This is further illustrated in the example for Lake Badajos (Figure 3.11) that shows the water extents extracted from a good image and a bad image of roughly equal water levels. The water extent from the bad image (Figure 3.11d) is incomplete

due to contaminations by both sporadic clouds and the ETM+ SLC error (the linear strips). As a result, the extracted water extent is only 85% of that extracted from the good image (Figure 3.11b). But after our area recovery, the estimated full lake area for the bad image matches 98% of the area in the good image. The above results indicate that our area recovery method substantially improves the monitoring frequency for these fluvial lakes, without a significant sacrifice of the mapping accuracy.

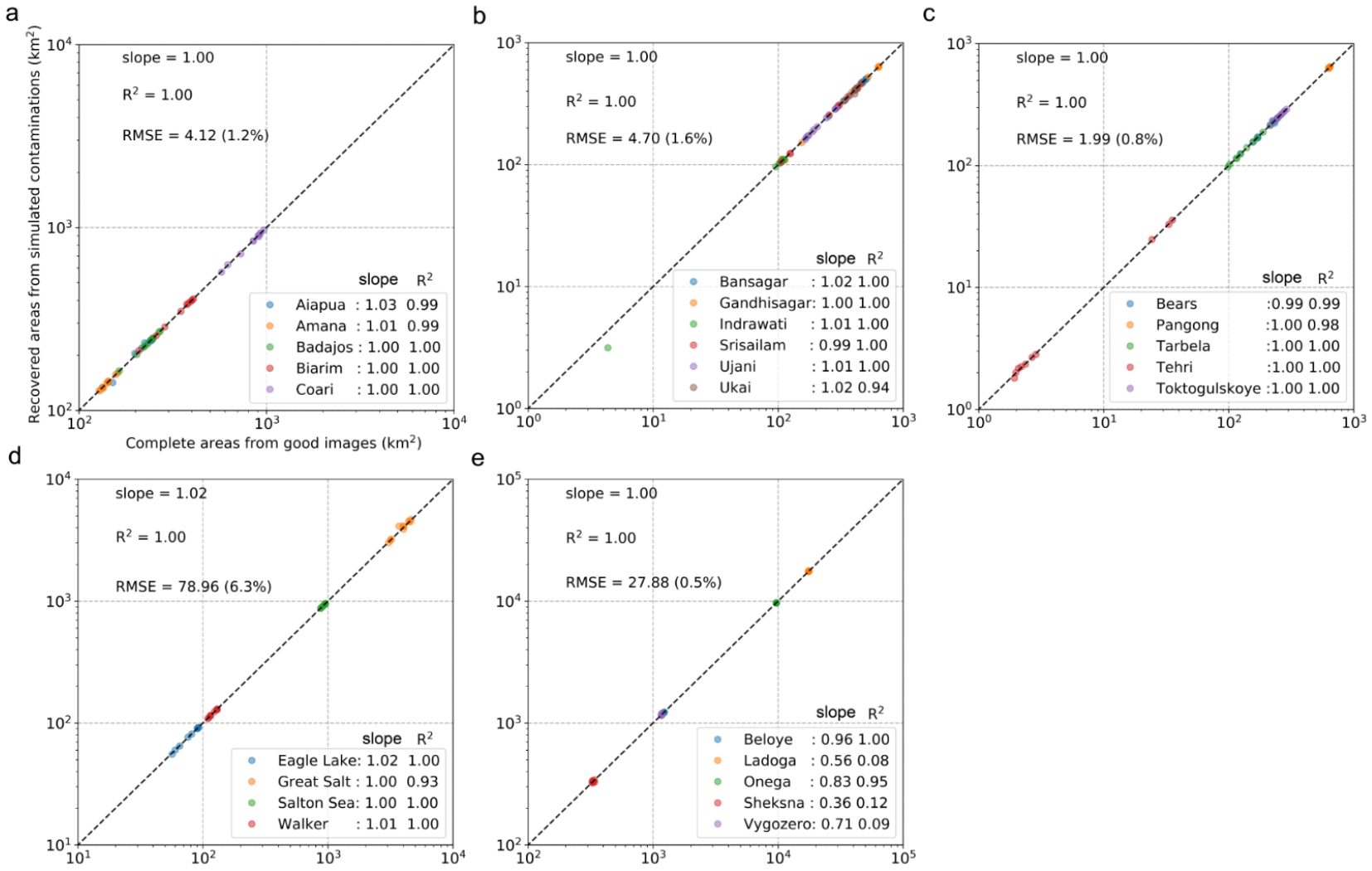

Figure 3.9 Validation of recovered lake/reservoir areas from simulated contaminations on good images for different scenarios. (a) Five fluvial lakes in the Amazon basin. (b) Six reservoirs in India. (c) Five lakes and reservoirs in High Mountain Asia. (d) Four saline lakes in western United States. (e) Five high-latitude lakes in northwestern Russia.

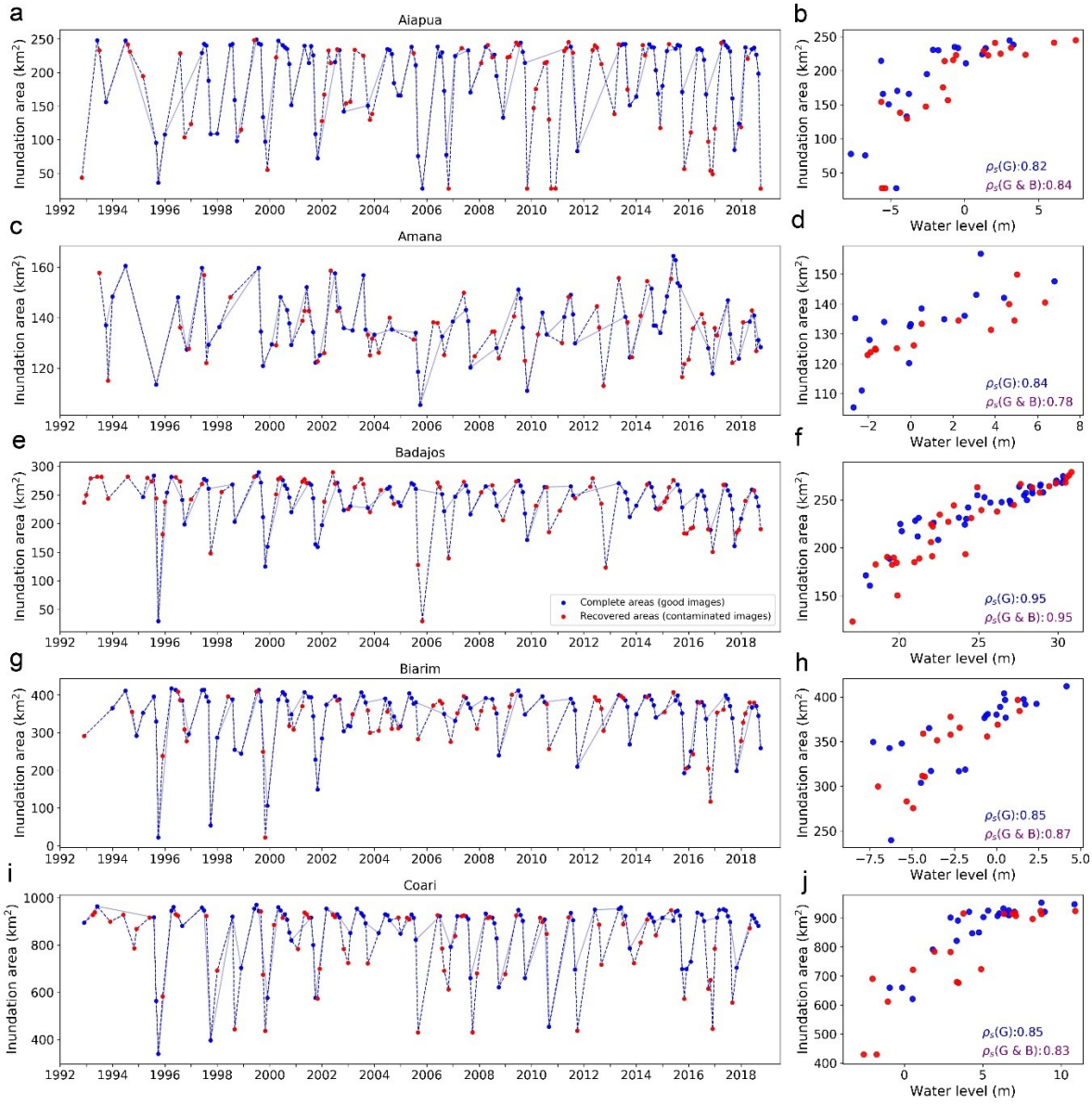

Figure 3.10 Produced water area time series for five fluvial lakes in the Amazon and their relationships with altimetry water levels. (a)-(b) Lake Aiapua. (c)-(d) Lake Amana. (e)-(f) Lake Badajos. (g)-(h) Lake Biarim. (i)-(j) Lake Coari. Refer to Table 2 for their geographic coordinates. Area time series are shown in the left panel, while hypsometric (area-level) relationships in the right panel. Lake areas mapped from good imagery are shown in blue circles, and areas recovered from contaminated (bad) images in red circles.

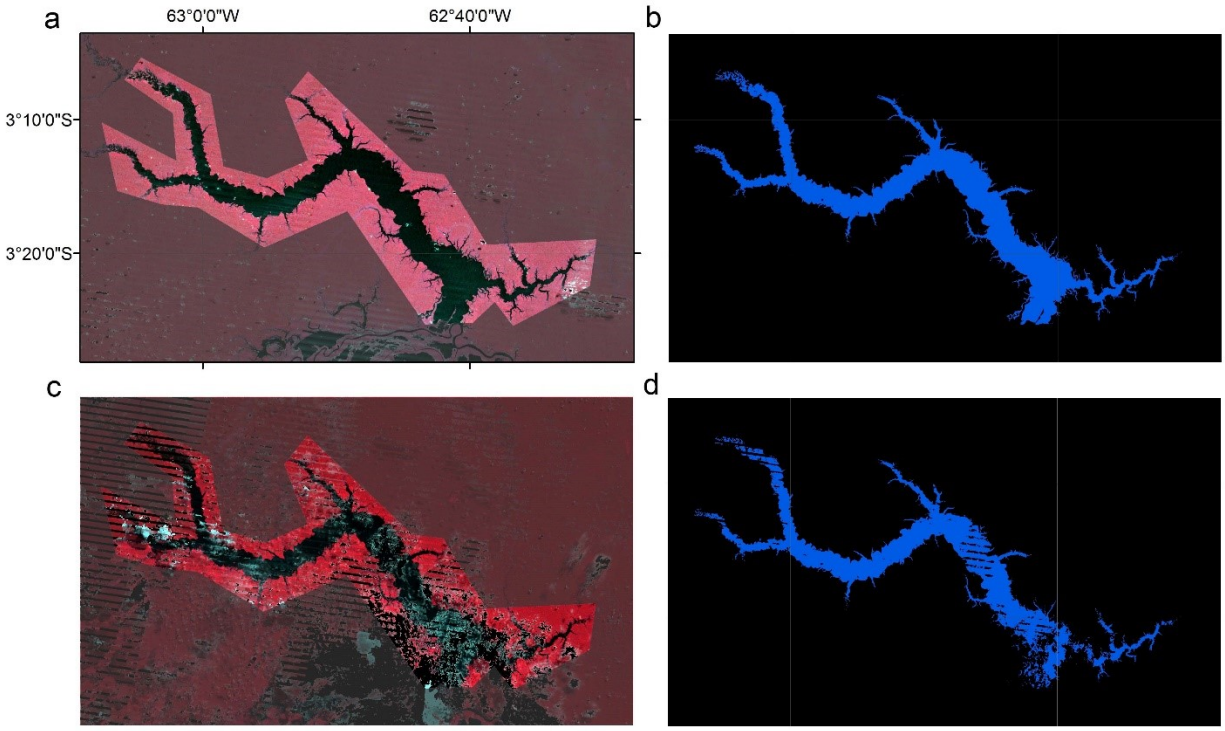

Figure 3.11 Comparison between extracted water extents for Lake Badajos (3.24°S, 62.78°W) under nearly equal levels from good and contaminated images. (a) Good image in July 2009 (cloud cover: 0.5%, water level: 30.73 m). (b) Extracted water extent of (a). (c) Contaminated image in June, 2014 (cloud/SLC-error cover: 15%, water level: 30.57 m). (d) Extracted partial water extent of (c). Landsat images are displayed in conventional false color composite (near-infrared, red, and green as RGB). Contaminations are masked in black and regions beyond the lake ROI is masked in transparent grey (same for Figures. 3.12, 3.14, 3.16, and 3.18). The recovered area (i.e., 268.1 km2) of (d) is close to the area (274.6 km2) of (b).

Table 3.2 Summary of monthly area coverages and area-level correlations (Spearman's rho) for the selected 25 lakes and reservoir under different scenarios

				Monthly area coverage			A-L correlation (Spearman's rho)		
Name (Location)	Type	Area (km^2)	CV (%)	Good images	Good and bad images	GSW (Good images)	Good images	Good and bad images	GSW (Good images)
Fluvial lakes in the Amazon Basin									
Aiapua (4.44°S, 62.16°W)	lake	234	34.98	0.31	0.52	0.22	0.82	0.84	0.80
Amana (2.56°S, 64.69°W)	lake	152	9.13	0.22	0.40	0.16	0.84	0.78	0.65
Badajos (3.24°S, 62.78°W)	lake	274	16.53	0.27	0.50	0.17	0.95	0.95	0.88
Biarim (3.50°S, 63.32°W)	lake	407	22.26	0.32	0.51	0.20	0.85	0.87	0.83
Coari (4.09°S, 63.36°W)	lake	862	17.26	0.30	0.51	0.17	0.85	0.83	0.85
Mean		386	20.03	0.28	0.49	0.18	0.86	0.85	0.80
Reservoirs in India									
Bansagar (24.11°N, 81.08°E)	reservoir	137	71.62	0.54	0.65	0.41	1.00	1.00	0.99
Gandhisagar (24.44°N, 75.50°E)	reservoir	421	48.02	0.57	0.73	0.43	0.99	0.99	0.98
Indrawati (19.24°N, 82.83°E)	reservoir	108	46.89	0.53	0.63	0.34	0.96	0.96	0.95
Srisailam (16.00°N, 78.29°E)	reservoir	507	61.18	0.36	0.56	0.25	0.97	0.97	0.97
Ujani (18.21°N, 75.01°E)	reservoir	215	19.93	0.49	0.66	0.35	0.85	0.87	0.84
Ukai (21.35°N, 73.81°E)	reservoir	469	22.54	0.50	0.72	0.36	0.93	0.93	0.93
Mean		310	45.03	0.50	0.66	0.36	0.95	0.95	0.94
Water bodies in High Mountain Asia									
Bears (32.00°N, 76.03°E)	reservoir	179	26.00	0.50	0.70	0.31	0.94	0.93	0.94
Pangong (33.73°N, 79.29 °E)	lake	627	2.76	0.25	0.36	0.16	0.69	0.69	0.08
Tarbela (34.23°N, 72.82°E)	reservoir	175	23.10	0.35	0.68	0.26	0.87	0.90	0.94
Tehri (30.41°N, 78.46°E)	reservoir	19	73.60	0.35	0.61	0.39	0.95	0.96	0.93
Toktogulskoye(24.11°N, 81.08°E)	reservoir	224	13.12	0.28	0.41	0.26	0.99	0.99	0.96
Mean		245	27.72	0.35	0.55	0.28	0.89	0.89	0.77
Saline lakes in the Western United States									
Eagle (40.64°N, 120.74°W)	lake	102	12.87	0.59	0.65	0.45	0.95	0.95	0.96
Great Salt (41.19°N, 112.54°W)	lake	3555	16.07	0.66	0.89	0.31	0.87	0.84	0.85
Salton (33.31°N, 115.82°W)	lake	942	3.01	0.90	0.95	0.65	0.99	0.99	0.96
Walker (38.69°N, 118.71°W)	lake	142	7.47	0.81	0.93	0.57	0.99	0.99	0.98
Mean		1185	9.86	0.74	0.86	0.50	0.95	0.94	0.94
High-latitude lakes in northwestern Russia									
Beloye (60.18°N, 37.63°E)	lake	1187	0.65	0.25	0.29	0.16	0.54	0.56	0.27
Ladoga (60.83°N, 31.48°E)	lake	17349	0.23	0.27	0.36	0.15	0.65	0.4	-0.08
Onega (61.79°N, 35.42°E)	lake	9531	0.22	0.28	0.35	0.14	0.03	0.03	-0.01
Sheksna (59.66°N, 38.44°E)	reservoir	315	1.78	0.22	0.27	0.15	0.08	0.05	-0.13
Vygozero (63.58°N, 34.78°E)	lake	1217	0.88	0.2	0.27	0.11	0.21	0.27	0.02
Mean		5920	0.75	0.24	0.31	0.14	0.30	0.26	0.01

Note: Values in “Area” field represent the average lake/reservoir area inferred by the circa-2000 global lake inventory (Sheng et al. 2016). “CV” stands for coefficient of variation.

3.3.2.2 Reservoirs in (sub-)tropical India

Reservoirs are artificial water impoundments on the natural rivers, in order to provide different purposes such as hydropower generation, water supply, flood control, and navigation. Timely monitoring of reservoir inundation extents is important for local food security and water managements (Crétaux et al. 2015; Zhang et al. 2014). In addition to cloud contamination, accurate detection of area changes in reservoirs is challenging because their shorelines are usually underdeveloped and thus complex in geometry. Thus for the second scenario, we selected six reservoirs with complex geometric shapes in tropical/sub-tropical India (Table 2). Areas of these reservoirs range from 108 to 507 km^2 (Sheng et al. 2016).

Figure 8b shows that inundation areas of the six reservoirs recovered from simulated contaminations are highly comparable to the actual areas mapped from good images, with an average error of 1.6% and both fitting slopes and R^2 values close to 1. Including recovered areas from bad images improved the number of observations in the final time series by 19-56% (Table 2 and Figure 3.12). As a result, the average monthly coverage for the six reservoirs reaches 66% (exceeding a bi-monthly frequency). The accuracy of our produced time series are also corroborated by the area-level correlations (Table 2; Figure 3.12), which remain strong (Spearman's rho >0.85) for all six reservoirs even after inclusion of recovered areas. For the Srisailam reservoir, visual inspection on the mapped extents from two significantly contaminated images show satisfactory results (Figure 3.13). After applying area recovery, recovered areas from contaminated imagery show a similar pattern in area-level relationship as areas from good imagery (Figure 3.12h). The area-level correlation is very high (spearman's rho: 0.97) even after areas from contaminated imagery are included (Figure 3.12h).

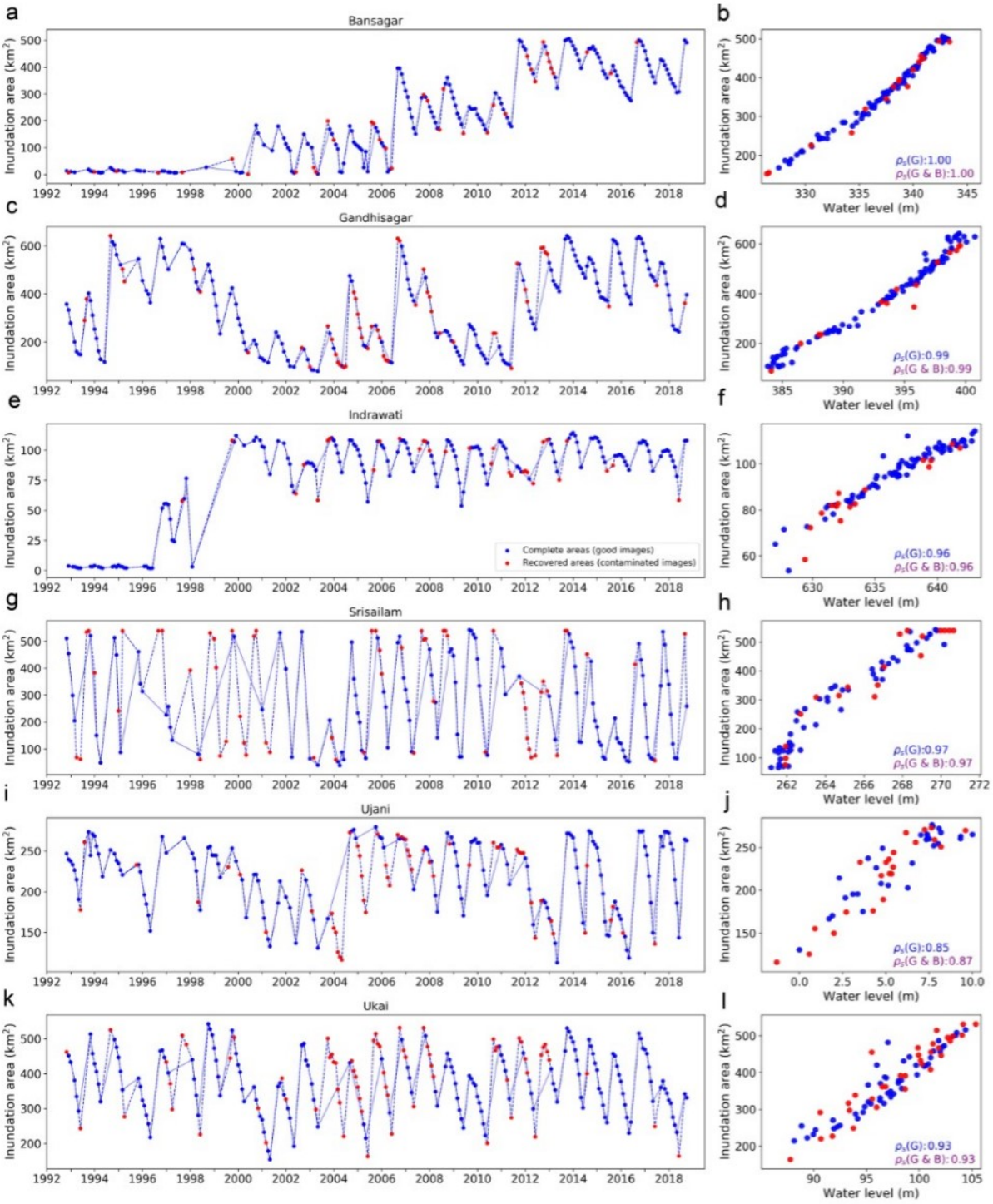

Figure 3.12 Produced water area time series for six reservoirs in India (left panel) and their relationships with altimetry water levels (right panel). (a)-(b) Reservoir Bansagar. (c)-(d) Reservoir Gandhisagar. (e)-(f) Reservoir Indrawati. (g)-(h) Reservoir Srisailam. (i)-(j) Reservoir Ujani. (k)-(l) Reservoir Ukai. Refer to Table 3.2 for their geographic coordinates. Reservoir areas mapped from good imagery are shown in blue circles, and areas recovered from contaminated images in red circles.

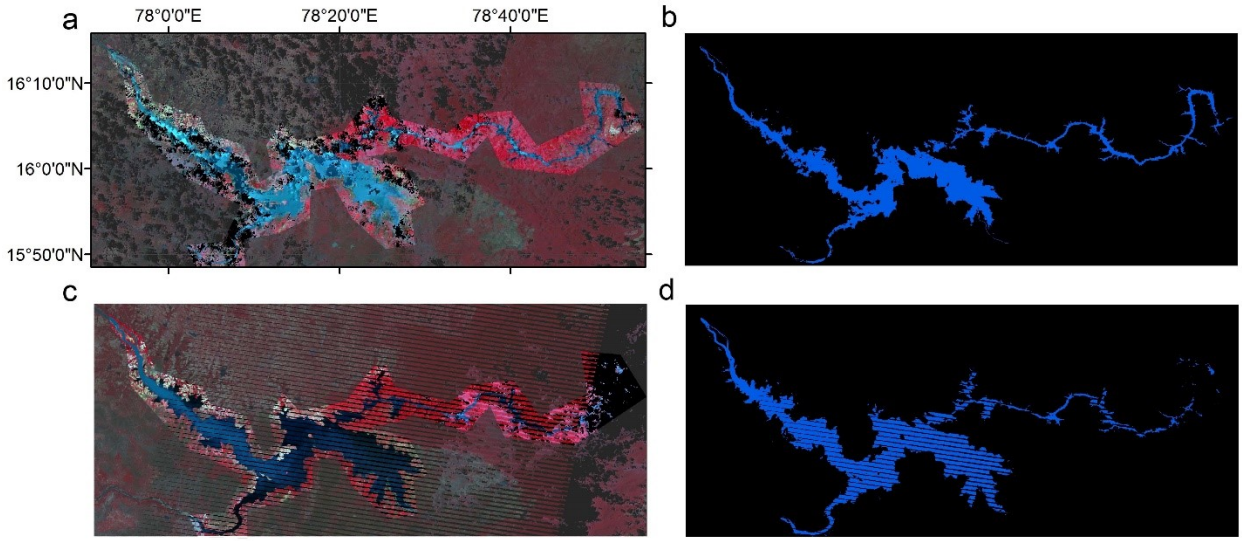

Figure 3.13 Extracted water extents of Srisilam reservoir (16.00°N, 78.29°E) from two contaminated images. (a) Contaminated image in August 2016 with conventional false-color composite (cloud cover: 14%). (b) Extracted water extent of (a). This incomplete extent (382.81 km2, shown here) was recovered to a full area of 413.89 km2 as in Figure 2.11g. (c) Contaminated image in September 2008 (cloud/SLC-error cover: 26%). (d) Extracted water extent of (c). This incomplete extent (419.17 km2) was recovered to a full area of 539.19 km2 as in Figure 3.12g.

3.3.2.3 Lakes and reservoirs in High Mountain Asia

Lakes and reservoirs are also common landscape features in mountain regions, and serve as climate indicators and important water sources for the downstream users (Nie et al., 2018; Song et al., 2017; Yang et al., 2017). However, mountain shadows often cause commission errors in water misclassification and impede the understanding of water area dynamics (Li and Sheng 2012). Five lakes and reservoirs in High Asia were selected to assess the performance of our method in mountain regions. These water bodies have various sizes ranging from 19 km^2 to 627 km^2 (Sheng et al. 2016).

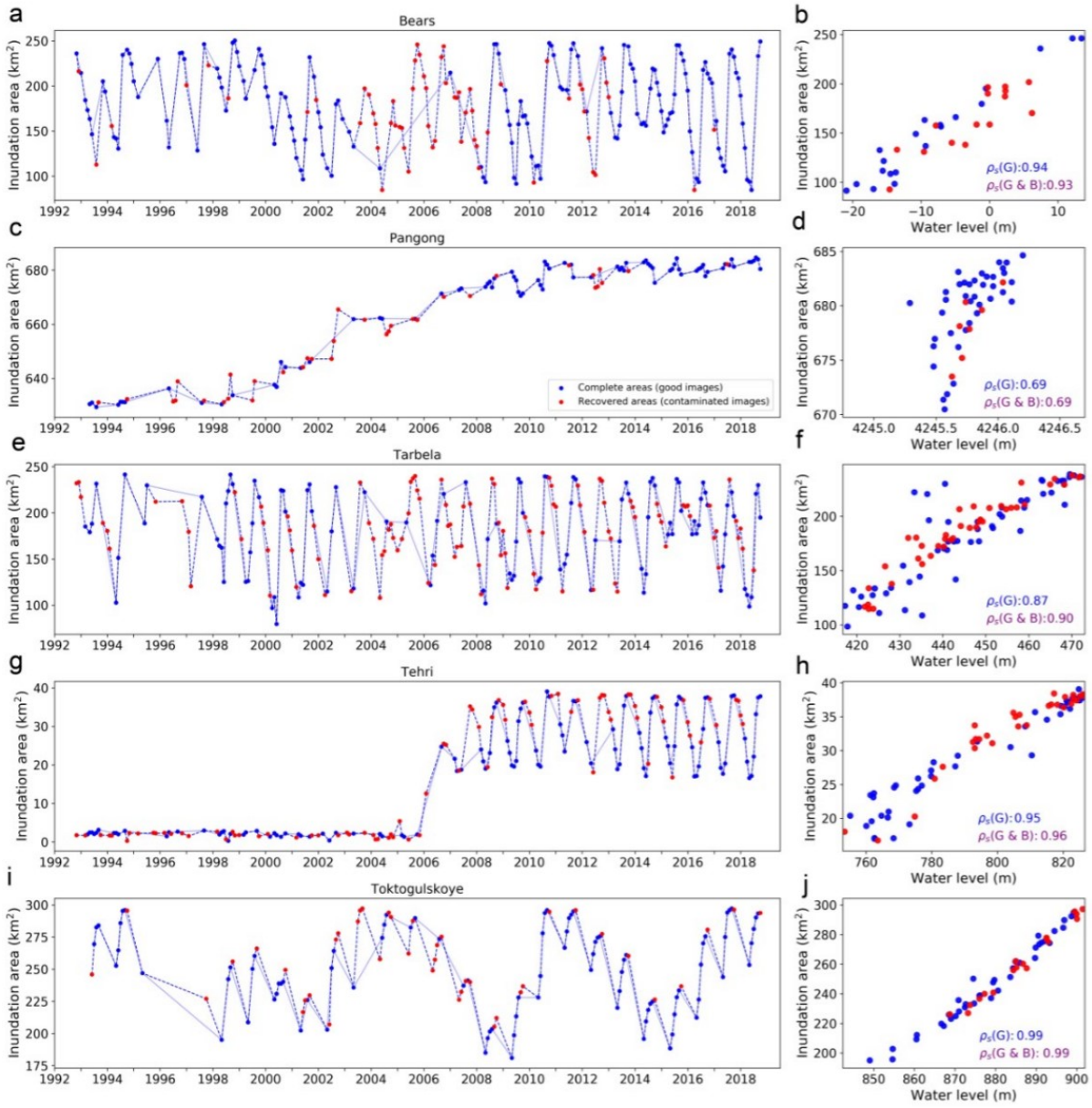

Figure 3.14 Produced water area time series for five water bodies in High Mountain Asia (left panel) and their relationships with altimetry water levels (right panel). (a)-(b) Lake Bears. (c)-(d) Pangong Lake. (e)-(f) Tarbela Lake. (g)-(h) Tehri Lake. (i)-(j) Toktogulskoye. Refer to Table 3.2 for their geographic coordinates. Reservoir areas mapped from good imagery are shown in blue circles, and areas recovered from contaminated (bad) images in red circles.

The produced time series well reveal the seasonality of the water area in these five mountain lakes (Figure 3.14). Recovered water areas from contaminated images improve the

temporal coverage by an average of 60%. Strong area-level correlation (spearman's rho>0.8) exists for all water bodies except Pangong Lake. The relative lower correlation (spearman's rho of 0.69) for Pangong Lake is because altimetry levels for this lake were only available after 2008 but its areas or levels have changed little since then (Figure 3.14 c-d). However, our result for Pangong Lake still substantially outperformed that based on good images in GSW (Busker et al. 2019) (Table 3.2). The impacts of mountain shadows are more severe in winter when the solar altitudes are lower. Two winter images with significant mountain shadow contamination (~15% of the ROI area) were shown for Lake Tarbela (Figure 3.15). Visual inspection of the extracted water extents does not find any evident commission errors caused by mountain shadow, suggesting that our algorithm appears to be robust in mountainous regions. After applying area recovery, the recovered areas from contaminated images further improved the strength of area-level correlation (Figure 3.14f).

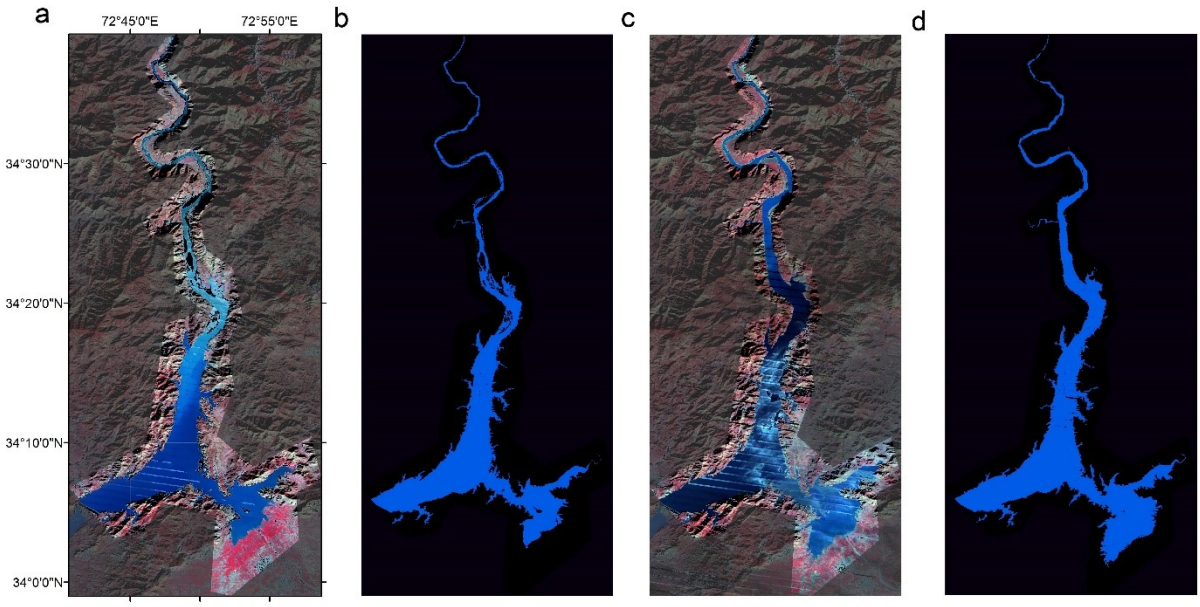

Figure 3.15 Extracted water extents of Lake Tarbela (34.26°N, 72.83°E) for two winter images substantially contaminated by terrain shadows. (a) Contaminated image in January 2018 with conventional false-color composite (cloud/terrain shadow cover: 16%). (b) Extracted water extent of (a). This incomplete area (166.97 km2, shown here) was recovered to a full area of 182.95 km2 as in Figure 3.14e. (c) Contaminated image in January 2016 (cloud/terrain shadow cover: 14%). (d) Extracted water extent of (c). This incomplete area of 204.30 km2 was recovered to a full area of 207.96 km2 as in Figure 3.14e.

3.3.2.4 Saline lakes in arid United States

Saline lakes are mostly found in arid/semiarid endorheic basins. They are considered as basin-scale integrators of hydrological and climatic conditions, and are sensitive to climate change and direct human water management (Wang et al., 2018; Wurtsbaugh et al. 2017). Due to high mineral concentration and evaporite deposits, many saline lakes exhibit different spectral characteristics from freshwater lakes, especially in shallow regions (e.g., bays and playas). In our third scenario, we selected four saline lakes located in arid/semiarid western United States, including Great Salt Lake in Utah, Lake Walker in Nevada, and Salton Sea and Lake Eagle in

California (Table 2). Sizes of these saline lakes range from about 100 to nearly 4000 km^2 (Sheng et al. 2016).

For all these four saline lakes, the produced inundation areas are well correlated with altimetry water levels (Spearman rho mostly greater than 0.9) (Table 2, Figure 3.16), which indicates that lake area variations were well captured by the proposed method. However, the areas recovered from simulated contaminations show a larger relative error (5.8%) compared with other scenarios (Figure 3.9c). This is primarily because the recent decline of the Great Salt Lake, the largest among the four, has led to more disintegration of its surface water area. As a result, the area changes in some detached small water bodies in the peripheral region were no longer synchronous with the main water body (Figure 3.17). Although constraining the ROI of the Great Salt Lake to the main water body may reduce the error, the current relative error (5.8%) seems to be acceptable given the magnitude of area changes (a coefficient of variation (CV) of 16.07%). Additionally, the area-level correlation for the Great Salt Lake remains strong (Spearman's rho: 0.84) even after inclusion of recovered areas (Figure 3.16d). Owing to dryness, the Great Basin in the western United States has low cloud fraction which leads to more good images compared with the other scenarios. As a result, including contaminated images improved the number of lake area observations by an average of only 16% (Table 2 and Figure 3.16).

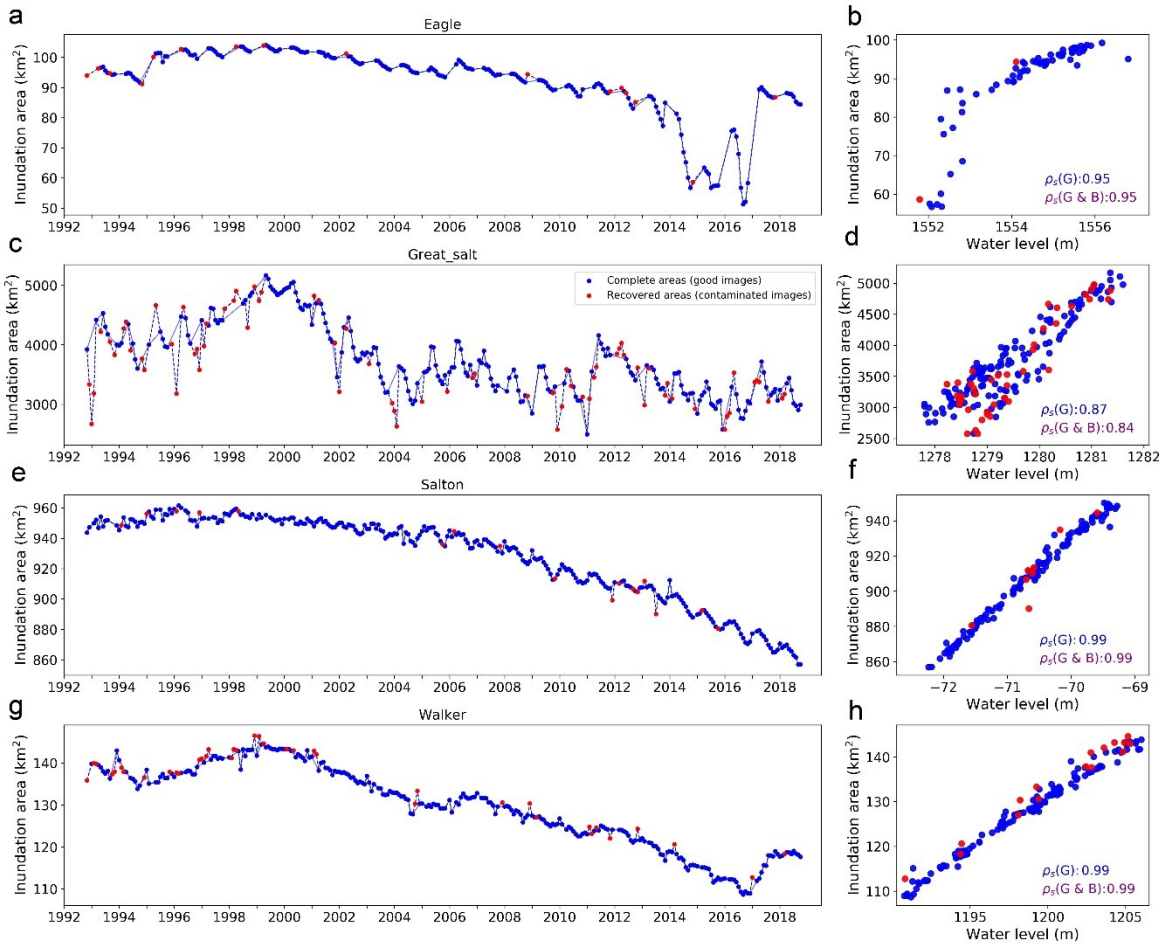

Figure 3.16 Produced water area time series for four saline lakes in western United States (left panel) and their relationships with altimetry water levels (right panel). (a)-(b) Lake Eagle. (c)-(d) Great Salt Lake. (e)-(f) Salton Sea. (g)-(h) Lake Walker. Refer to Table 3.2 for their geographic coordinates. Lake areas mapped from good imagery are shown in blue circles, and areas recovered from contaminated (bad) images in red circles.

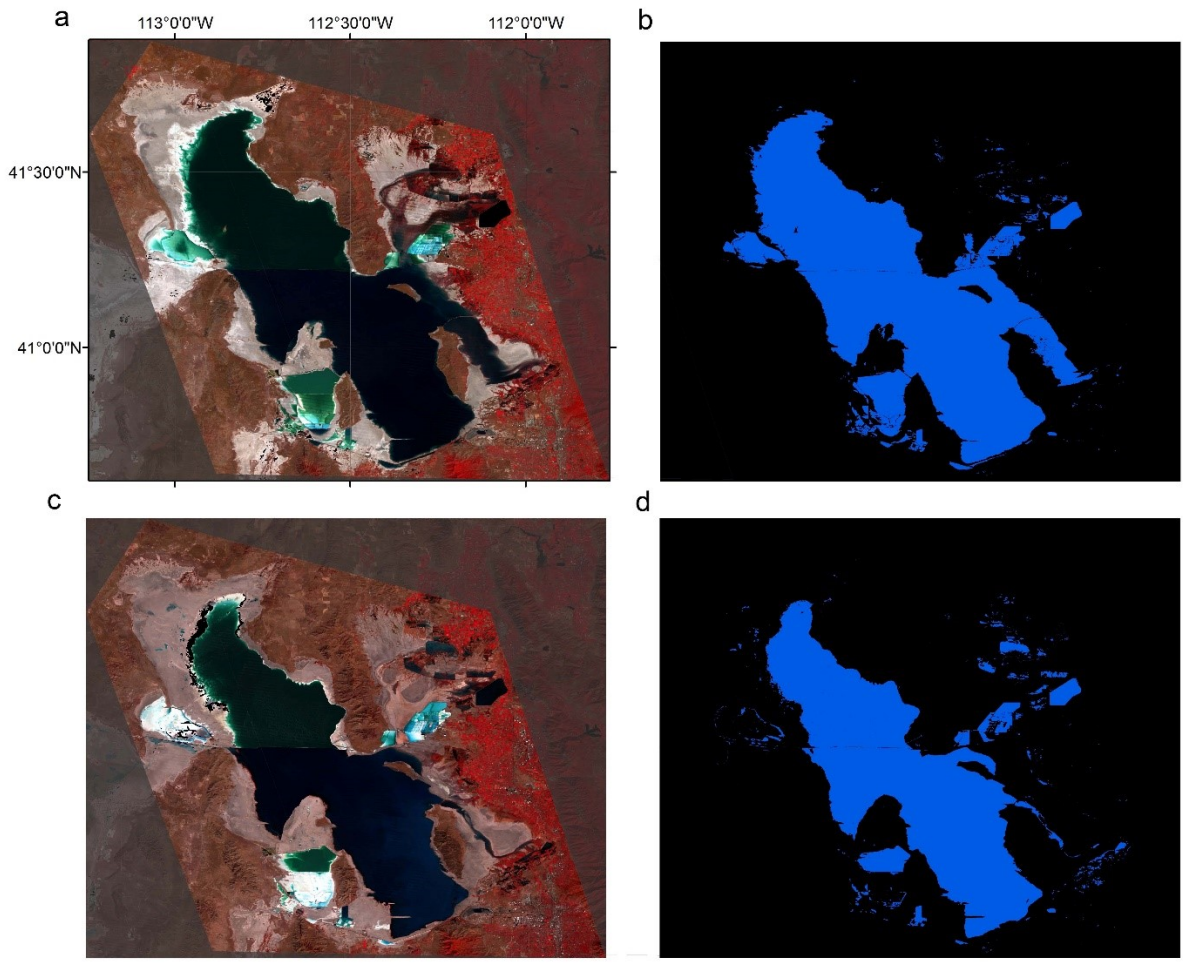

Figure 3.17 Two extracted water extents from good images for the Great Salt Lake (41.19°N, 112.54°W). (a) Good image in July 2005 with conventional false-color composite (cloud cover: 0%). (b) Extracted water extent of (a). (c) Good image in September 2016 (cloud cover: 1%). (d) Extracted partial water extent of (c). The main lake area decreased in the second image, but the areas of detached smaller water bodies, particularly on the eastern side, did not seem to decrease.

3.3.2.5 High-latitude lakes in northwestern Russia

High-latitude lakes encompass a various range of aquatic ecosystems and have global significance to the carbon cycle, biome, and climate change (Hinkel et al., 2012; Smith et al., 2005; Vincent and Laybourn-Parry 2008; Wang et al., 2012). Because of low temperature, these inland waters and their surrounding land are frequently covered by snow and ice which challenge accurate water extractions from optical sensors. In the last scenario, five lakes (including one reservoir) in northwestern Russia (above 60° N) that cover a large size range from 315 to 17,349 km^2 (Sheng et al. 2016) were selected to evaluate our proposed method on high-latitude lakes (Table 2).

The produced area time series, with inclusion of contaminated images, reaches a mean monthly coverage of 31% (Table 2 and Figure 3.18). This coverage suggests that on average, our recovery method enables a seasonal mapping frequency for high-latitude water bodies. Although coarser than the other scenarios, this improved temporal frequency, particularly compared to ~14% in Busker et al. (2019), offers incremental advancement to the depiction of inter-annual trends for pan-Arctic water bodies.

The accuracy of recovered lake areas from simulated contaminations vary among the five lakes (Figure 3.9e). For example, the R^2 values between recovered and actual areas range from 0.08 (for Ladoga Lake) to 1.00 (for Beloye Lake) with an average of 0.45. From the one hand, these relatively low accuracies are partially explained by rather small area variations (CV under 2%). From the other hand, the combined spectral disturbance from ice, snow, aerosols, cloud, and cloud shadow poses substantial challenges to accurate extent delineations. As a result, the area-level correlation is generally low even for using good imagery alone. In the example of Figure 3.19, our mapping results from two good images are given for Sheksna Reservoir. A

careful visual examination suggests that our delineated water extents are reasonable, but the complex surface conditions (such as snow, ice, aerosol, and shadow) constrained the possibility of further mapping improvements, at least from an automated perspective. Therefore, the area-level correlation for this reservoir remains low (0.08). Inclusion of recovered areas from contaminated imagery further decreases the mean area-level correlation from 0.30 to 0.26. (Table 2, Figure 3.18). Nevertheless, compared with the method that applied GSW mapping such as Busker et al. (2019), our proposed method improved the area-level correlations for these high-latitude lakes by an average of 0.25 (Table 2), which is the highest improvement of area-level correlation among all five scenarios. In addition, despite lower accuracies for some of the individual lakes, the average bias (relative RMSE) in the recovered areas from simulated contaminations is as small as 0.4% (Figure 3.9e), which suggests that our method may work fairly well in estimating aggregated lake areas for high-latitude lakes.

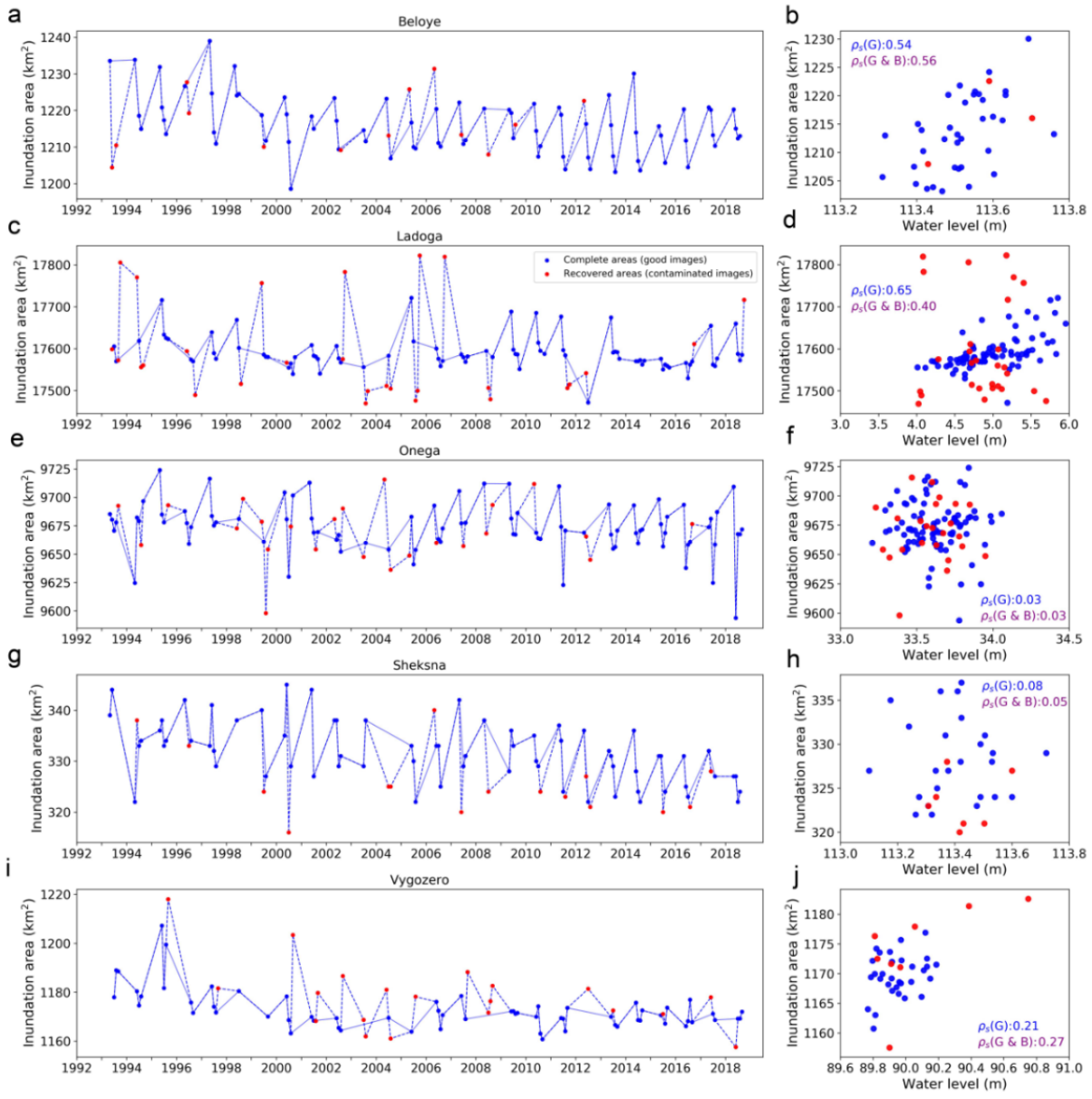

Figure 3.18 Produced water area time series for five high-latitude lakes in northwestern Russia (left panel) and and their relationships with altimetry water levels (right panel). (a)-(b) Lake Beloye. (c)-(d) Lake Ladoga. (e)-(f) Lake Onega. (g)-(h) Reservoir Sheksna. (i)-(j) Lake Vygozero. Refer to Table 3.2 for their geographic coordinates. Areas mapped from good imagery are shown in blue circles, and areas recovered from contaminated (bad) images in red circles.

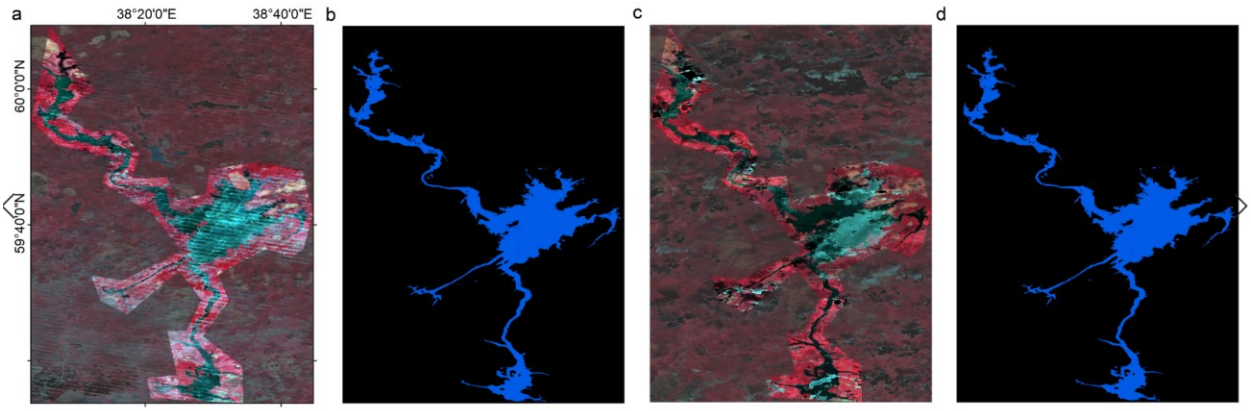

Figure 3.19 Two extracted water extents from good images for Sheksna Reservoir (59.66°N, 38.44°E). (a) Good image in July 2013 with conventional false-color composite (cloud cover: 0%). (b) Extracted water extent of (a). (c) Good image in June 2000 (cloud cover: 3%). (d) Extracted partial water extent of (c). Note that the mapping quality in (d) is impaired by ground conditions (such as snow, ice, aerosol, shadow).

3.4 Discussion

3.4.1 Comparison with existing Landsat water mapping methods

Our proposed method shows several merits compared with some recent water mapping or recovery methods using Landsat images. First, our water mapping was based on multiple water indices and adaptive thresholding, and does not require the collection of extensive training datasets such as applied in the GSW production (Pekel et al. 2016). Second, compared with Busker et al. (2019) who used a subset of the GSW product from good images (with contaminations <5%), our method leveraged archival Landsat images since 1992 with contaminations up to 50%. Our recovered water areas under contaminations achieved a small average error of 2.2%. The combined area time series from both good and contaminated images improved the temporal coverage from good images alone by an average of 43%. The improvement ratios appear even higher (e.g., >50%) across humid tropical and sub-tropical regions where cloud contamination is more frequent. Additionally, our lake/reservoir mapping

achieved much stronger areal-level correlations with extended hypsometric ranges, suggesting an improved potential for inferring volumetric changes. Third, compared with the water recovery method as proposed in Zhao and Gao (2018), our method did not rely on the a priori knowledge provided by the GSW inundation probability (as observed during 1984–2015). Almost concurrent with our study, Schwatke et al. (2019) applied a longer-term inundation probability map to generate area time series for 32 selected lakes/reservoirs during 1984–2018. Their method of water area recovery is similar to that of Zhao and Gao (2018), except that Schwatke et al. (2019) mapped their own inundation probabilities using Landsat and Sentinel-2 images. Despite many merits in both studies, the raster map of inundation probability is a mosaic of pixelized water occurrence under cloud-free observations. The probability of each pixel was computed independently from the other pixels. Due to uneven or insufficient cloud-free observations (e.g., gaps and biases) within the water body, an "isoline" of similar probabilities may not correspond to a realistic isobath or water shoreline. Alternatively, our area recovery was based on a set of complete isobaths/shorelines as observed from cloud-free images. Although the isobaths density is also determined by the sufficiency of cloud-free observations, the bounding isobaths for any partial shoreline are likely more realistic, and the recovery of its full area was based on an interpolation gauged by the area proportion visible between the bounding isobaths (refer back to Equation 1). Last but not the least, although tested on Landsat images, the area recovery procedure demonstrated in our method is generic and potentially replicable for estimating water/reservoir areas using other sensors (e.g., Sentinel-2 and Surface Water and Ocean Topography (SWOT)) (see Section 3.4.2 for more discussion).

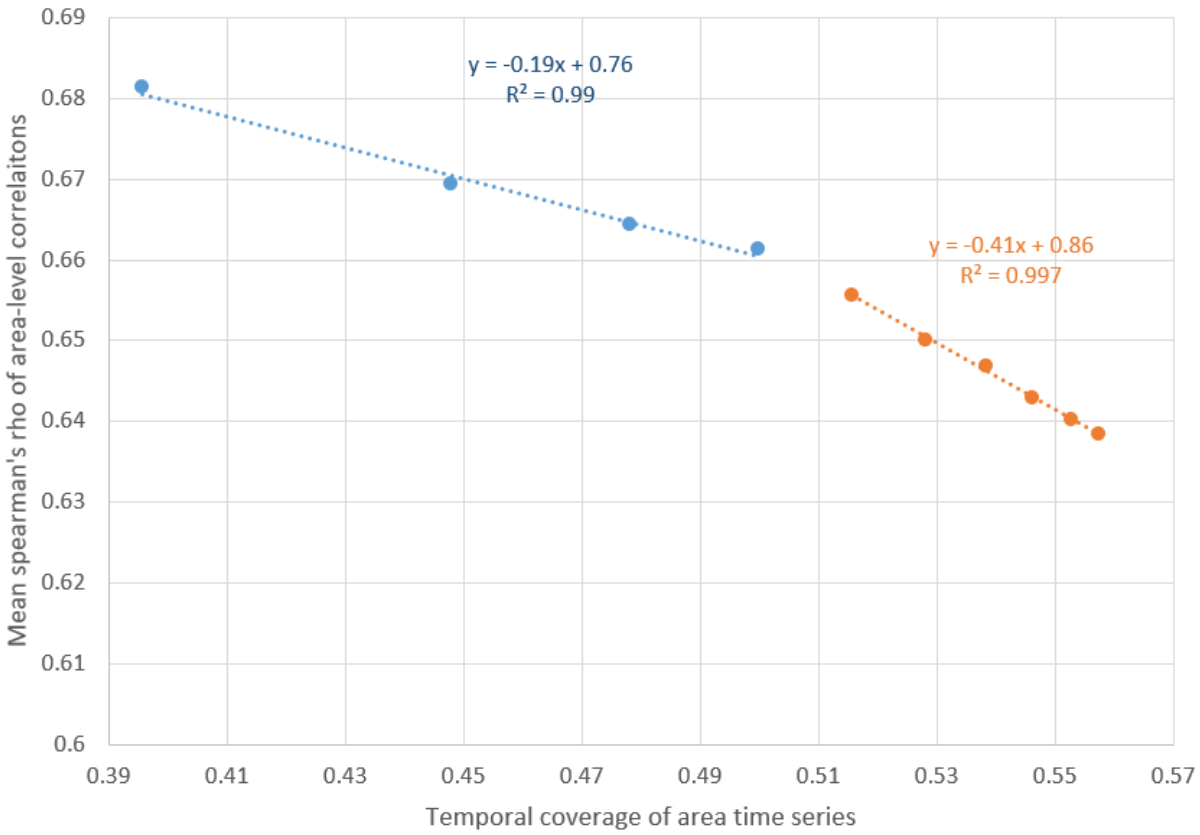

Figure 3.20 Performance of the proposed method as cloud cover threshold increases from 5% (the leftmost point) to 50% (the rightmost point) within the lake ROIs. The rightmost blue dot denotes cloud cover 20% which is used in current study. By using images with cloud cover from 5% to 20% (blue dots), the mean area-level correlation decreases from 0.68 to 0.66, but the improvement ratio on temporal coverage improves by an average of 43%. If the cloud cover threshold further increases to 50% (orange dots), the gain of temporal coverage appears marginal but the decrease in area-level correlation is more apparent.

In this study, we used images with contaminations (e.g., cloud covers and no data gaps such as due to the SLC error) lower than 50% for generating area time series, whereas Zhao and Gao (2018) estimated water areas using images with contaminations up to 95%. Using more contaminated images could further improve the temporal frequency but may have a cost in accuracy. To illustrate this, we compared the area-level corrections and temporal coverages among this study (using images with contaminations <50%), Zhao and Gao (2018) (with contaminations <95%), and Busker et al. (2019) (with contaminations <5%) for the four

reservoirs with area-level correlations reported by Zhao and Gao (2018). Compared with Busker et al. (2019), Zhao and Gao (2018) substantially improved the number of area observations by 53–135%, but reduced the R^2 values for the area-level relations by 0.07–0.31 (Table 3.3). These reductions in correlation indicate that the inclusion of severely contaminated images likely decreased their overall area accuracy. By using images with contaminations lower than 50%, our algorithm achieved slightly higher area-level correlations than those in Busker et al. (2019), and improved the mean monthly coverage from 36% to 67% (Table 3.3). Thus, our algorithm substantially increases the temporal frequency without sacrificing the accuracy. This good performance is owing to the merits as highlighted above and our meticulous testing in order to find a reasonable tradeoff between the mapping accuracy and the volume of images applied (Figure 3.20). It is important to note that we also excluded the images where cloud cover exceeds 20% on the valid pixels (i.e., those excluding no data gaps) within each ROI. Applying our algorithm on severely cloudy images is technically possible, but as we demonstrated in Figure 3.20, this may sacrifice the reliability of the recovered areas and thus require additional manual quality control.

Table 3.3 Summary of monthly area coverages and area-level relations for four reservoirs included in this study, Zhao and Gao (2018), and (Busker et al. 2019) during the period that all studies overlapped (1992 to 2015).

Reservoir name	R^2 in the area-level relation			Monthly area coverage		
	This study	Zhao and Gao (2018)	Busker et al (2019)	This study	Zhao and Gao (2018)	Busker et al (2019)
Massingir, Mozambique (23.89°S, 32.04°E)	0.98	0.89	0.96	65%	72%	47%
Mosul, Iraq (36.75°N, 42.74°E)	0.94	0.69	0.94	66%	54%	32%
Sobradinho, Brazil (9.69°S, 41.65°W)	0.94	0.82	0.91	75%	96%	43%
Xiaolangdi, China (35.08°N, 111.91°E)	0.95	0.63	0.94	61%	54%	23%

Given the availability of existing altimetry level records at a global scale, we only examined the performance of the proposed method on relatively sizable water bodies (larger than 2 km^2). Our method was built upon the fine spatial resolution Landsat imagery, and thus could be potentially used to monitor numerous small water bodies. This is a potential advantage compared to previous methods using coarse resolution imageries (e.g., MODIS) (Khandelwal et al. 2017; Klein et al. 2017). To explore the performance on small water bodies, we here apply our method in three smaller reservoirs (~1 km^2 or so) gauged by the US Geological Survey (USGS) (accessed from https://waterdata.usgs.gov). As shown in Figure 3.21, the results are promising in terms of both accuracy (correlations between areas and gauging levels greater than 0.95) and temporal frequency (monthly coverage greater than 50%).

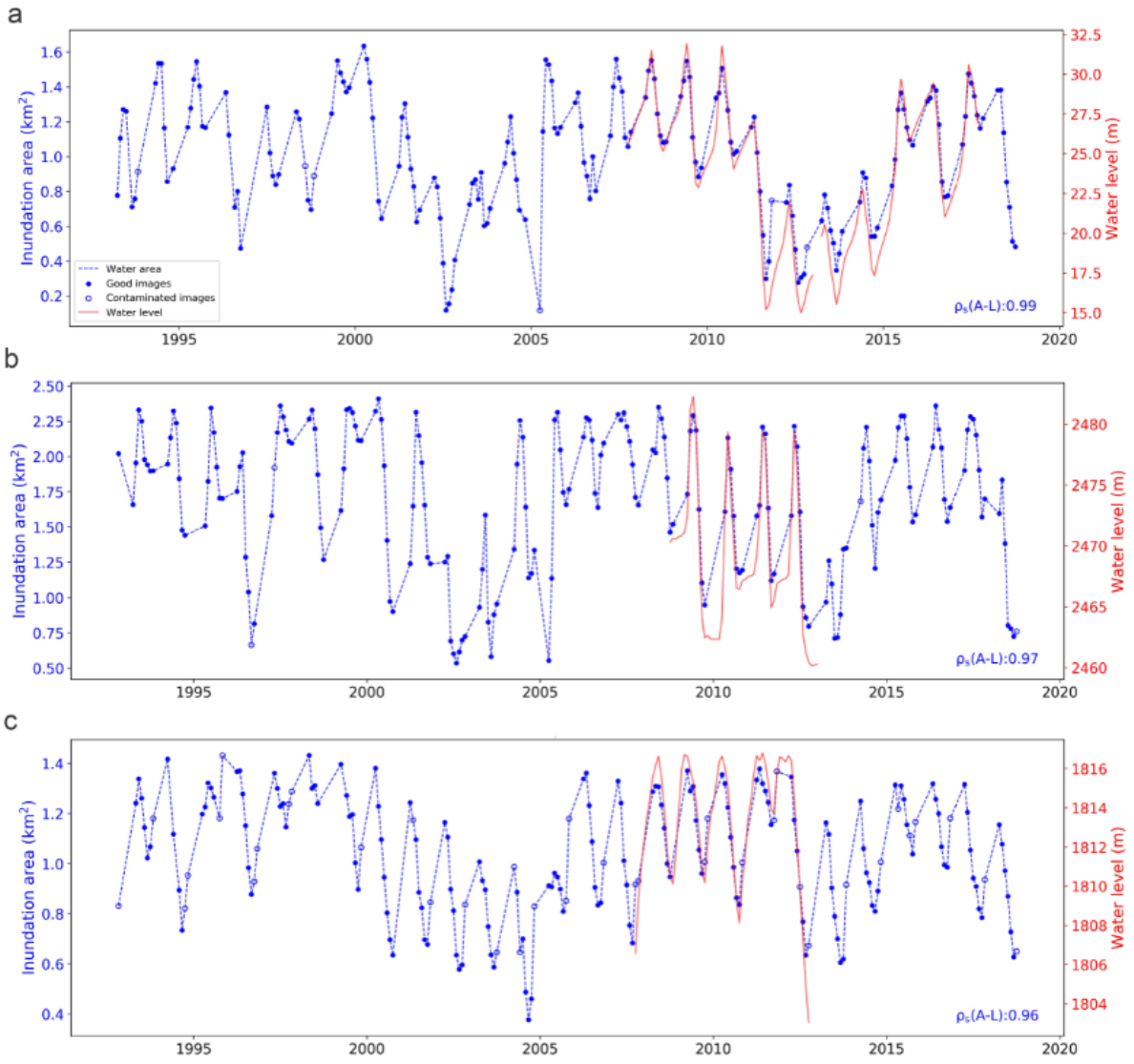

Figure 3.21 Produced area time series on three USGS-gauged small reservoirs (size about 1 km2). (a) Costilla reservoir (36.89°N, 105.27°W). (b) Lemon reservoir (37.40°N, 107.66°W). (c) Rifle Gap reservoir (39.63°N, 107.75°W). Solid and hollow blue dots illustrate water areas from good and contaminated images, respectively. Red lines show gauging water levels (accessed from https://waterdata.usgs.gov).

3.4.2 Potential applications to other satellite missions

Our proposed method is generic, given its applicability to both global lakes/reservoirs (as validated in Section 3.3) and some other existing/future sensors. For example, the European Space Agency's Sentinel-2 mission (1A launched in 2015 and 1B in 2017) may benefit from this approach in assessing intra-annual lake/reservoir dynamics using its high-resolution (10-m) optical imagery. Preliminary test seems promising given the example of Sobradinho Reservoir (41.65°W, 9.69°S) in Brazil (Figure 3.22). Inundation area in this tropical reservoir was monitored during 28 out of the 31 months after the launch of Sentinel-2, owing to the inclusion of recovered areas under contaminations. Visual examination of the produced area time series indicates that water areas recovered from contaminated images match those from good images in magnitude and variation pattern, with a temporal improvement ratio of 40% (Figure 3.22). With such improvements, our method demonstrates a potential to assist similar multi-spectral sensors in improving the temporal continuity of surface water monitoring.

Additionally, our proposed water area recovery method may also benefit the forthcoming SWOT mission (expected in 2022), a joint effort from NASA, the French National Centre for Space Studie (CNES), the Canadian Space Agency, and the UK Space Agency. One primary objective of the SWOT mission is to measure water extents and levels of all lakes and reservoirs larger than 250×250 m at a 21-day temporal frequency (Biancamaria et al. 2016). However, due to topographic layovers, dark radar returns, and the 20-km nadir gap, SWOT's InSAR instrument will sometimes only observe part of a large water body (Rodríguez 2015). Although tested on Landsat optical imagery, the conceptual design of our proposed water area recovery allows for the estimation of full lake/reservoir areas from partial observations, regardless of whether extent observations are acquired from optical or SAR images. Especially, surface measurements from

the SWOT's InSAR instrument will not be severely affected by clouds, which simplifies the disturbing scenarios in water area recovery. The high recovery accuracies for the simulated contaminations from good images (refer back to Figure 3.6) further indicate a promising potential to recover lake/reservoir areas from SWOT's partial observations, and thus to help maintain the mission goal of continuous lake extent and volume monitoring.

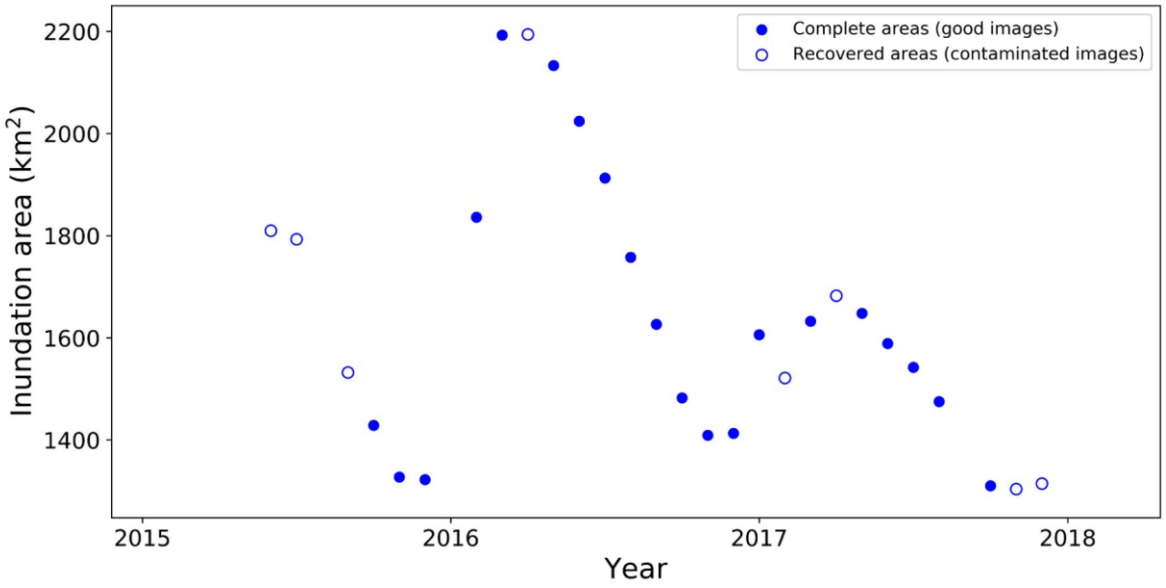

Figure 3.22 Area time series for Sobradinho Reservoir (9.69°S, 41.65°W) in Brazil, produced by the proposed method from 10-m resolution Sentinel-2 optical imagery. Solid and hollow blue dots illustrate water areas from good and contaminated images, respectively.

3.4.3 Limitations

We acknowledge several limitations in our method. As our method aims to strike a balance between mapping accuracy and improved temporal frequency, we constrained the use of bad images to those with cloud and other contaminations lower than 50% within each lake/reservoir ROI. Such a stringent quality requirement limited our improvement of temporal coverage. As we previously discussed, more severely contaminated images can be included at

users' discretion, but probably with a cost in mapping accuracy. As a result, temporal frequencies of our produced area time series are monthly at best and bi-monthly on average. These frequencies substantially facilitate the monitoring of surface water dynamics using Landsat images, although they may not suffice the detection of transient changes in some large fluvial lakes (such as on a daily basis) as offered by MODIS observations. For the sake of computational efficiency, our recovery emphasizes the values of lake/reservoir areas, rather than detailed inundation boundaries. Exact inundation boundaries are often unnecessary for understanding lake/reservoir budget changes, given that volumetric variation can be deduced by level or area values through calibrated hypsometry (area-level relations). However, the delineation of inundation boundaries is feasible by spatially interpolating our mapped isobaths. Additionally, similar to existing methods, our area recovery requires that at least part of the lake/reservoir shoreline under which the full water area is to be recovered must be clearly exposed in the contaminated image. In other words, a poor shoreline exposure is expected to increase the uncertainty of the recovered water area. The errors would also likely increase when severe hysteresis occurs in the water body and thus a singular hypsometric relation was weakened. However, most of the studied 428 lakes/reservoirs exhibit strong area-level correlations (with a medium of 0.8), which were not significantly reduced by our area recovery.

3.5 Conclusions

The novel mapping method proposed in this study contributes to improving the temporal frequency for Landsat-based water extent monitoring by accurately recovering inundation areas from contaminated images. Evaluated on 428 lakes and reservoirs worldwide with satellite radar altimetry levels, the recovered water areas by this method achieved a mean relative error of only

2.2%. The combined water area time series from both good and contaminated images show strong correlations with altimetry water levels, with Spearman's rho (rank correlation coefficient) greater than ~0.8 for most lakes/reservoirs. The combined area time series increased the monthly coverage using good images alone by an average of 43%, achieving a bi-monthly frequency for open surface water mapping. Inclusion of recovered water areas also extended the observable ranges of lake/reservoir hypsometric relations, thus improving the potential to deriving volumetric changes. Compared with the GSW-based estimate using good-quality imagery only (Busker et al. 2019), our monitoring frequency for the tested 428 lakes/reservoirs increased by an average of 78% during the overlapping period (October 1992 to October 2015), and the area-level correlations improved by 0.12. Besides a global validation, the proposed method is overall robust under five challenging regional scenarios, including lakes in fluvial floodplains, reservoirs with complex geometric boundaries, water bodies in mountain regions, saline lakes with high mineral concentrations, and high-latitude lakes under frequent ice/snow covers.

We developed this mapping method using archival Landsat images, considering that they allow for a retroactive production of a double-decadal area record for global lakes and reservoirs. However, the procedure of our recovery method is generic to image types. As we further tested on the high-resolution Sentinel-2 images, our method appears promising for revealing improved intra-annual details in lake/reservoir areas during the latest 4 years. This potential may be enhanced if spectral images from existing and future sensors are synergized. Additionally, as our recovery method is source-independent and flexible in time, it is potentially applicable to the forthcoming SWOT mission for recovering lake/reservoir areas from partial observation due to topographic layovers and inter-track gaps. Given such merits, we foresee extended applications

of our proposed method to monitoring open water body dynamics by multiple sensors. The produced global lake/reservoir area time series (GLATS) will be available on the website https://lakewatch.users.earthengine.app/view/glats.

3.6 References

Alexander, L.V., Allen, S.K., Bindoff, N.L., Breon, F.-M., Church, J.A., Cubasch, U., Emori, S., Forster, P., Friedlingstein, P., & Gillett, N. (2013). Summary for policymakers.

Allen, G.H., & Pavelsky, T.M. (2018). Global extent of rivers and streams. Science, 361, 585-588, https://doi.org/10.1126/science.aat0636.

Alsdorf, D.E., Rodriguez, E., & Lettenmaier, D.P. (2007). Measuring surface water from space. Reviews of Geophysics, 45, RG2002, https://doi.org/10.1029/2006RG000197.

Bergé-Nguyen, M., & Crétaux, J.-F. (2015). Inundations in the inner Niger delta: monitoring and analysis using MODIS and global precipitation datasets. Remote Sensing, 7, 2127-2151, https://doi.org/10.3390/rs70202127.

Biancamaria, S., Lettenmaier, D.P., & Pavelsky, T.M. (2016). The SWOT mission and its capabilities for land hydrology. Surveys in Geophysics, 37, 307-337, https://doi.org/10.1007/s10712-015-9346-y.

Birkett, C., Reynolds, C., Beckley, B., & Doorn, B. (2011). From research to operations: the USDA global reservoir and lake monitor. Coastal altimetry (pp. 19-50): Springer.

Busker, T., Roo, A.d., Gelati, E., Schwatke, C., Adamovic, M., Bisselink, B., Pekel, J.-F., & Cottam, A. (2019). A global lake and reservoir volume analysis using a surface water dataset and satellite altimetry. Hydrology and Earth System Sciences, 23, 669-690, https://doi.org/10.5194/hess-23-669-2019.

Cohen, A.S. (2003). Paleolimnology: the history and evolution of lake systems. Oxford University Press.

Cooley, S.W., Smith, L.C., Stepan, L., & Mascaro, J. (2017). Tracking Dynamic Northern Surface Water Changes with High-Frequency Planet CubeSat Imagery. Remote Sensing, 9, 1306, https://doi.org/10.3390/rs9121306.

Crétaux, J.-F., Abarca-del-Río, R., Berge-Nguyen, M., Arsen, A., Drolon, V., Clos, G., & Maisongrande, P. (2016). Lake volume monitoring from space. Surveys in Geophysics, 37, 269-305, https://doi.org/10.1007/s10712-016-9362-6.

Crétaux, J.-F., Biancamaria, S., Arsen, A., Bergé-Nguyen, M., & Becker, M. (2015). Global surveys of reservoirs and lakes from satellites and regional application to the Syrdarya river basin. Environmental Research Letters, 10, 015002, https://doi.org/10.1088/1748-9326/10/1/015002.

Crétaux, J.-F., Jelinski, W., Calmant, S., Kouraev, A., Vuglinski, V., Bergé-Nguyen, M., Gennero, M.-C., Nino, F., Del Rio, R.A., & Cazenave, A. (2011). SOLS: A lake database to monitor in the Near Real Time water level and storage variations from remote sensing data. Advances in space research, 47, 1497-1507, https://doi.org/10.1016/j.asr.2011.01.004.

Donchyts, G., Baart, F., Winsemius, H., Gorelick, N., Kwadijk, J., & van de Giesen, N. (2016). Earth's surface water change over the past 30 years. Nature Climate Change, 6, 810-813, https://doi.org/10.1038/nclimate3111.

Du, Z., Li, W., Zhou, D., Tian, L., Ling, F., Wang, H., Gui, Y., & Sun, B. (2014). Analysis of Landsat-8 OLI imagery for land surface water mapping. Remote sensing letters, 5, 672-681, https://doi.org/10.1080/2150704X.2014.960606.

Farr, T.G., Rosen, P.A., Caro, E., Crippen, R., Duren, R., Hensley, S., Kobrick, M., Paller, M., Rodriguez, E., & Roth, L. (2007). The shuttle radar topography mission. Reviews of Geophysics, 45, RG2004, http://doi.org/10.1029/2005RG000183.

Feng, M., Sexton, J.O., Channan, S., & Townshend, J.R. (2016). A global, high-resolution (30-m) inland water body dataset for 2000: First results of a topographic–spectral classification algorithm. International Journal of Digital Earth, 9, 113-133, https://doi.org/10.1080/17538947.2015.1026420.

Feyisa, G.L., Meilby, H., Fensholt, R., & Proud, S.R. (2014). Automated Water Extraction Index: A new technique for surface water mapping using Landsat imagery. Remote Sensing of Environment, 140, 23-35, https://doi.org/10.1016/j.rse.2013.08.029.

Fisher, A. (2014). Cloud and cloud-shadow detection in SPOT5 HRG imagery with automated morphological feature extraction. Remote Sensing, 6, 776-800, https://doi.org/10.3390/rs6010776.

Fisher, A., Flood, N., & Danaher, T. (2016). Comparing Landsat water index methods for automated water classification in eastern Australia. Remote Sensing of Environment, 175, 167-182, https://doi.org/10.1016/j.rse.2015.12.055.

Gao, H., Birkett, C., & Lettenmaier, D.P. (2012). Global monitoring of large reservoir storage from satellite remote sensing. Water Resources Research, 48, W09504, https://doi.org/10.1029/2012WR012063.

Gleick, P.H. (2010). Roadmap for sustainable water resources in southwestern North America. Proceedings of the National Academy of Sciences, 107, 21300-21305, https://doi.org/10.1073/pnas.1005473107.

Gorelick, N., Hancher, M., Dixon, M., Ilyushchenko, S., Thau, D., & Moore, R. (2017). Google Earth Engine: Planetary-scale geospatial analysis for everyone. Remote Sensing of Environment, 202, 18-27, https://doi.org/10.1016/j.rse.2017.06.031.

Grill, G., Lehner, B., Thieme, M., Geenen, B., Tickner, D., Antonelli, F., Babu, S., Borrelli, P., Cheng, L., & Crochetiere, H. (2019). Mapping the world's free-flowing rivers. Nature, 569, 215, https://doi.org/10.1038/s41586-019-1111-9.

Haas, E.M., Bartholomé, E., & Combal, B. (2009). Time series analysis of optical remote sensing data for the mapping of temporary surface water bodies in sub-Saharan western Africa. Journal of Hydrology, 370, 52-63, https://doi.org/10.1016/j.jhydrol.2009.02.052.

Haddeland, I., Heinke, J., Biemans, H., Eisner, S., Flörke, M., Hanasaki, N., Konzmann, M., Ludwig, F., Masaki, Y., & Schewe, J. (2014). Global water resources affected by human interventions and climate change. Proceedings of the National Academy of Sciences, 111, 3251-3256, https://doi.org/10.1073/pnas.1222475110.

Hinkel, K.M., Lenters, J.D., Sheng, Y., Lyons, E.A., Beck, R.A., Eisner, W.R., Maurer, E.F., Wang, J., & Potter, B.L. (2012). Thermokarst lakes on the Arctic Coastal Plain of Alaska: Spatial and temporal variability in summer water temperature. Permafrost and Periglacial Processes, 23, 207-217, https://doi.org/10.1002/ppp.1743.

Huang, C., Chen, Y., Zhang, S., & Wu, J. (2018). Detecting, Extracting, and Monitoring Surface Water From Space Using Optical Sensors: A Review. Reviews of Geophysics, 56, 333-360, https://doi.org/10.1029/2018RG000598.

Hui, F., Xu, B., Huang, H., Yu, Q., & Gong, P. (2008). Modelling spatial‐temporal change of Poyang Lake using multitemporal Landsat imagery. International Journal of remote sensing, 29, 5767-5784, https://doi.org/10.1080/01431160802060912.

Jiang, H., Feng, M., Zhu, Y., Lu, N., Huang, J., & Xiao, T. (2014). An automated method for extracting rivers and lakes from Landsat imagery. Remote Sensing, 6, 5067-5089, https://doi.org/10.3390/rs6065067.

Khandelwal, A., Karpatne, A., Marlier, M.E., Kim, J., Lettenmaier, D.P., & Kumar, V. (2017). An approach for global monitoring of surface water extent variations in reservoirs using MODIS data. Remote Sensing of Environment, 202, 113-128, https://doi.org/10.1016/j.rse.2017.05.039.

Klein, I., Gessner, U., Dietz, A.J., & Kuenzer, C. (2017). Global WaterPack–A 250m resolution dataset revealing the daily dynamics of global inland water bodies. Remote Sensing of Environment, 198, 345-362, https://doi.org/10.1016/j.rse.2017.06.045.

Lehner, B., & Döll, P. (2004). Development and validation of a global database of lakes, reservoirs and wetlands. Journal of Hydrology, 296, 1-22, https://doi.org/10.1016/j.jhydrol.2004.03.028.

Lehner, B., Liermann, C.R., Revenga, C., Vörösmarty, C., Fekete, B., Crouzet, P., Döll, P., Endejan, M., Frenken, K., & Magome, J. (2011). High‐resolution mapping of the world's reservoirs and dams for sustainable river‐flow management. Frontiers in Ecology and the Environment, 9, 494-502, https://doi.org/10.1890/100125.

Li, J., & Sheng, Y. (2012). An automated scheme for glacial lake dynamics mapping using Landsat imagery and digital elevation models: A case study in the Himalayas. International Journal of remote sensing, 33, 5194-5213, https://doi.org/10.1080/01431161.2012.657370.

Lyerly, S.B., The average Spearman rank correlation coefficient, Psychometrika, 17, 1952, 421-428, https://doi.org/10.1007/BF02288917.

McFeeters, S.K. (1996). The use of the Normalized Difference Water Index (NDWI) in the delineation of open water features. International Journal of remote sensing, 17, 1425-1432, https://doi.org/10.1080/01431169608948714.

Mekonnen, M.M., & Hoekstra, A.Y. (2016). Four billion people facing severe water scarcity. Science advances, 2, e1500323, https://doi.org/10.1126/sciadv.1500323.

Messager, M.L., Lehner, B., Grill, G., Nedeva, I., & Schmitt, O. (2016). Estimating the volume and age of water stored in global lakes using a geo-statistical approach. Nature Communications, 7, 13603, https://doi.org/10.1038/ncomms13603.

Murray, N.J., Phinn, S.R., DeWitt, M., Ferrari, R., Johnston, R., Lyons, M.B., Clinton, N., Thau, D., & Fuller, R.A. (2019). The global distribution and trajectory of tidal flats. Nature, 565, 222, https://doi.org/10.1038/s41586-018-0805-8.

Nie, Y., Liu, Q., Wang, J., Zhang, Y., Sheng, Y., & Liu, S. (2018). An inventory of historical glacial lake outburst floods in the Himalayas based on remote sensing observations and geomorphological analysis. Geomorphology, 308, 91-106, https://doi.org/10.1016/j.geomorph.2018.02.002.

Oki, T., & Kanae, S. (2006). Global hydrological cycles and world water resources. Science, 313, 1068-1072, https://doi.org/10.1126/science.1128845.

Otsu, N. (1979). A threshold selection method from gray-level histograms. IEEE transactions on systems, man, and cybernetics, 9, 62-66, https://doi.org/10.1109/TSMC.1979.4310076.

Pekel, J.-F., Cottam, A., Gorelick, N., & Belward, A.S. (2016). High-resolution mapping of global surface water and its long-term changes. Nature, 540(7633), 418, https://doi.org/10.1038/nature20584.

Pekel, J.-F., Vancutsem, C., Bastin, L., Clerici, M., Vanbogaert, E., Bartholomé, E., & Defourny, P. (2014). A near real-time water surface detection method based on HSV transformation of MODIS multi-spectral time series data. Remote Sensing of Environment, 140, 704-716, https://doi.org/10.1016/j.rse.2013.10.008.

Pokhrel, Y.N., Hanasaki, N., Yeh, P.J., Yamada, T.J., Kanae, S., & Oki, T. (2012). Model estimates of sea-level change due to anthropogenic impacts on terrestrial water storage. Nature Geoscience, 5, 389-392, https://doi.org/10.1038/ngeo1476.

Rodríguez, E. (2015). Surface Water and Ocean Topography mission (SWOT), Science Requirements Document. JPL document D-61923.

Rossow, W.B., & Schiffer, R.A. (1999). Advances in understanding clouds from ISCCP. Bulletin of the American Meteorological Society, 80, 2261-2287, https://doi.org/10.1175/1520-0477(1999)080<2261:AIUCFI>2.0.CO;2.

Schwatke, C., Dettmering, D., Bosch, W., & Seitz, F. (2015). DAHITI–an innovative approach for estimating water level time series over inland waters using multi-mission satellite altimetry. Hydrology and Earth System Sciences, 19, 4345-4364, https://doi.org/10.5194/hess-19-4345-2015.

Schwatke, C., Scherer, D., & Dettmering, D. (2019). Automated Extraction of Consistent Time-Variable Water Surfaces of Lakes and Reservoirs Based on Landsat and Sentinel-2. Remote Sensing, 11, 1010, https://doi.org/10.3390/rs11091010.

Sheng, Y., Song, C., Wang, J., Lyons, E.A., Knox, B.R., Cox, J.S., & Gao, F. (2016). Representative lake water extent mapping at continental scales using multi-temporal Landsat-8 imagery. Remote Sensing of Environment, 185, 129-141, doi:10.1016/j.rse.2015.12.041.

Smith, L.C., Sheng, Y., MacDonald, G., & Hinzman, L. (2005). Disappearing arctic lakes. Science, 308, 1429-1429, https://doi.org/10.1126/science.1108142.

Song, C., Sheng, Y., Wang, J., Ke, L., Madson, A., & Nie, Y. (2017). Heterogeneous glacial lake changes and links of lake expansions to the rapid thinning of adjacent glacier termini in the Himalayas. Geomorphology, 280, 30-38, https://doi.org/10.1016/j.geomorph.2016.12.002.

Sun, D., Yu, Y., & Goldberg, M.D. (2011). Deriving water fraction and flood maps from MODIS images using a decision tree approach. IEEE Journal of Selected Topics in Applied Earth Observations and Remote Sensing, 4, 814-825, https://doi.org/10.1109/JSTARS.2011.2125778.

Tao, S., Fang, J., Zhao, X., Zhao, S., Shen, H., Hu, H., Tang, Z., Wang, Z., & Guo, Q. (2015). Rapid loss of lakes on the Mongolian Plateau. Proceedings of the National Academy of Sciences, 112, 2281-2286, https://doi.org/10.1073/pnas.1411748112.

Van Beek, L., Wada, Y., & Bierkens, M.F. (2011). Global monthly water stress: 1. Water balance and water availability. Water Resources Research, 47, 1–17, https://doi.org/10.1029/2010WR009791.

Verpoorter, C., Kutser, T., Seekell, D.A., & Tranvik, L.J. (2014). A global inventory of lakes based on high‐resolution satellite imagery. Geophysical research letters, 41, 6396-6402, https://doi.org/10.1002/2014GL060641.

Vincent, W.F., & Laybourn-Parry, J. (2008). Polar lakes and rivers: limnology of Arctic and Antarctic aquatic ecosystems. Oxford university press. https://doi.org/10.1093/acprof:oso/9780199213887.001.0001.

Wang, C., Yu, M., & Gao, Q. (2017a). Continued Reforestation and Urban Expansion in the New Century of a Tropical Island in the Caribbean. Remote Sensing, 9, 731, https://doi.org/10.3390/rs9070731.

Wang, J., Sheng, Y., Hinkel, K.M., & Lyons, E.A. (2012). Drained thaw lake basin recovery on the western Arctic Coastal Plain of Alaska using high-resolution digital elevation models and remote sensing imagery. Remote Sensing of Environment, 119, 325-336, https://doi.org/10.1016/j.rse.2011.10.027.

Wang, J., Sheng, Y., & Tong, T.S.D. (2014). Monitoring decadal lake dynamics across the Yangtze Basin downstream of Three Gorges Dam. Remote Sensing of Environment, 152, 251-269, https://doi.org/10.1016/j.rse.2014.06.004.

Wang, J., Sheng, Y., & Wada, Y. (2017b). Little impact of the Three Gorges Dam on recent decadal lake decline across China's Yangtze Plain. Water Resources Research, 53, 3854–3877, https://doi.org/10.1002/2016WR019817.

Wang, J., Song, C., Reager, J.T., Yao, F., Famiglietti, J.S., Sheng, Y., MacDonald, G.M., Brun, F., Schmied, H.M., Marston, R.A., & Wada, Y. (2018). Recent global decline in endorheic basin water storages. Nature Geoscience, 11, 926-932, https://doi.org/10.1038/s41561-018-0265-7.

Wayand, N.E., Marsh, C.B., Shea, J.M., & Pomeroy, J.W. (2018). Globally scalable alpine snow metrics. Remote Sensing of Environment, 213, 61-72, https://doi.org/10.1016/j.rse.2018.05.012.

WMO (2016). The Global Observing System for Climate: Implementation Needs., 200, 325

Wurtsbaugh, W.A., Miller, C., Null, S.E., DeRose, R.J., Wilcock, P., Hahnenberger, M., Howe, F., & Moore, J. (2017). Decline of the world's saline lakes. Nature Geoscience, 10, 816–821, https://doi.org/10.1038/ngeo3052.

Xu, H. (2006). Modification of normalised difference water index (NDWI) to enhance open water features in remotely sensed imagery. International Journal of remote sensing, 27, 3025-3033, https://doi.org/10.1080/01431160600589179.

Yamazaki, D., Trigg, M.A., & Ikeshima, D. (2015). Development of a global~ 90 m water body map using multi-temporal Landsat images. Remote Sensing of Environment, 171, 337-351, https://doi.org/10.1016/j.rse.2015.10.014.

Yang, K., Yao, F., Wang, J., Luo, J., Shen, Z., Wang, C., & Song, C. (2017). Recent dynamics of alpine lakes on the endorheic Changtang Plateau from multi-mission satellite data. Journal of Hydrology, 552, 633-645, https://doi.org/10.1016/j.jhydrol.2017.07.024.

Yao, F., Wang, C., Dong, D., Luo, J., Shen, Z., & Yang, K. (2015). High-resolution mapping of urban surface water using ZY-3 multi-spectral imagery. Remote Sensing, 7, 12336-12355, https://doi.org/10.3390/rs70912336.

Yao, F., Wang, J., Yang, K., Wang, C., Walter, B.A., & Crétaux, J.-F. (2018). Lake storage variation on the endorheic Tibetan Plateau and its attribution to climate change since the new millennium. Environmental Research Letters, 13, 064011, https://doi.org/10.1088/1748-9326/aab5d3.

Zhan, S., Song, C., Wang, J., Sheng, Y., & Quan, J. (2019). A global assessment of terrestrial evapotranspiration increase due to surface water area change. Earth's Future, 7, .https://doi.org/10.1029/2018EF001066.

Zhang, G., Yao, T., Shum, C., Yi, S., Yang, K., Xie, H., Feng, W., Bolch, T., Wang, L., & Behrangi, A. (2017). Lake volume and groundwater storage variations in Tibetan Plateau's endorheic basin. Geophysical research letters, 44, 5550-5560, https://doi.org/10.1002/2017GL073773.

Zhang, S., Gao, H., & Naz, B.S. (2014). Monitoring reservoir storage in South Asia from multisatellite remote sensing. Water Resources Research, 50, 8927-8943, https://doi.org/10.1002/2014WR015829.

Zhao, G., & Gao, H. (2018). Automatic correction of contaminated images for assessment of reservoir surface area dynamics. Geophysical research letters, 45, 6092-6099, https://doi.org/10.1029/2018GL078343.

Chapter 4 - Recent storage changes in global lakes and reservoirs revealed from satellite imagery and altimetry

4.1 Introduction

Covering ~3% of Earth's continental area (Feng et al. 2016; Messager et al. 2016; Sheng et al. 2016; Verpoorter et al. 2014), surface water in lakes and reservoirs is a crucial component of the global hydrological and biogeochemical cycles (Bastviken et al. 2011; Müller Schmied et al. 2014; Oki and Kanae 2006). There are at least 1.4 million lakes greater than 10 ha (Meng 2019, Messager et al. 2016; Sheng et al. 2016). They store the largest proportion of liquid water on the land surface with a total volume of ~188 thousand km^3 (Messager et al. 2016), which is equivalent to four times of the mean annual runoff in global rivers (Oki and Kanae 2006). Due to their abundance and easy (open surface) accessibility, lakes and reservoirs serve as important water supplies for agricultural, industrial, and domestic water uses worldwide (Alsdorf et al. 2007). Spatial and temporal variations of lake/reservoir water storage are affected by climate change and anthropogenic activities (Haddeland et al. 2014). As the climate becomes warmer, the global hydrological cycle has been intensified with more frequent extreme weather (e.g., droughts and floods) (Allen and Ingram 2002), which directly influences the distribution of surface water availability. Additionally, intensified human water management is expected under a growing population, which further impacts the surface water storage through water withdrawal and damming (Wada et al. 2011; Wada et al. 2014). Previous studies have already shown that changes in lake and reservoir storage could be dramatic, as indicated by massive water impoundment in reservoirs and the desiccation of many large saline lakes (Chao et al. 2008; Gao et al. 2011; Pekel et al. 2016; Pokhrel et al. 2012; Wang et al. 2018; Wurtsbaugh et al. 2017).

The dynamics of lake and reservoir storage not only affect local water supply, energy generation, human and ecosystem health, but also have implications for the global sea level budget (Anderson et al. 2007; Conway et al. 2017; Griffin and Kellogg 2004; Wada et al. 2016). Wang et al. (2018) showed that within the global endorheic basins (about one-fifth of the total land area), open-surface water bodies may contribute 1.5 mm to the sea level rise during 2002 to 2016, which is comparable to that of groundwater (1.6 mm). Despite its importance, water storage in lakes and reservoirs is poorly monitored on the global scale, which is partially because the number of global in-situ hydrologic stations is in decline (Schwatke et al. 2015). Fortunately, storage changes in lakes can be deduced from satellite observations through a synergy of water level measurements by altimetry and water area measurements by imagery. This approach has been successfully applied to monitoring some of the largest lakes and reservoirs worldwide (Busker et al. 2019; Crétaux et al. 2016; Gao et al. 2012; Schwatke et al. 2019; Wang et al. 2018). However, existing global studies on lake storage dynamics are limited by the number of studied lakes (100 or so), low temporal resolution, or short time period (e.g., after the 2000s). Thus, the global patterns of long-term lake water storage changes remain unclear.

Existing assessments on recent lake area changes show notable patterns (Donchyts et al. 2016; Pekel et al. 2016; Zou et al. 2018). At the contiguous United States, humid regions (e.g., the Southeast and the North Great Plains) show increasing trends in surface water areas whereas arid/semiarid regions (e.g., the West and the southern Pacific region) experienced a decline in inundation areas during the past three decades (Zou et al. 2018). Globally, water area losses are more concentrated than area gains, and are mainly located in the world's arid and semiarid regions (Donchyts et al. 2016; Pekel et al. 2016). The contrasting patterns in surface water areas

indicate a possible divergence in surface water storage trends between arid and humid regions, which, however, has not been examined on the global scale.

This chapter aims to 1) test the hypothesized divergence in open-surface water storage between endorheic (arid) and exorheic (humid) regions (Objective 3); and 2) to reveal implications of open-surface water storage changes for the global water cycle and water resource management (Objective 4). To assess recent storage changes in global lakes and reservoirs, monthly storage time series were constructed for 1,196 major water bodies from 1992 to 2018 (i.e., the existing satellite altimetry era) using a synergy of multi-mission satellites. Storage uncertainty in smaller lakes and reservoirs was estimated using empirical geo-statistical approaches. The quantified lake storage changes were then applied to test whether there are divergent trends in open surface water storage between endorheic (arid) basins and exorheic (humid) basins. To reveal the implication of open-surface water storage changes for water resource management, storage trends were partitioned into artificial reservoirs, saline lakes, and natural freshwater lakes. Although this chapter does not aim at an explicit decoupling of human-climate impacts on lake storage dynamics, the water storage changes in recently filled reservoirs were isolated to facilitate the discussion of possible impacts of human water impoundments on surface water abundance. Finally, owing to this comprehensive monitoring of global lake/reservoir storage dynamics, the impact of open-surface water bodies on the recent sea level change was examined.

4.2 Datasets

4.2.1 Satellite imagery

I considered the entire Landsat archive, including Landsat 5 Thematic Mapper (TM), Landsat 7 Enhanced Thematic Mapper Plus (ETM+) and Landsat 8 Operational Land Imager (OLI), for mapping long-term water areas of lakes and reservoirs from 1992 to 2018. This period spans through the entire satellite altimetry era thus far. I used the top-of-atmosphere (TOA) reflectance products from these sensors, which is in line with some global studies on surface water extents (Allen and Pavelsky 2018; Donchyts et al. 2016; Pekel et al. 2016; Sheng et al. 2016). The considered images include not only cloud-free ones, but also those with reasonable contaminations of clouds and other data voids/gaps (for the detailed data selection criteria, refer to Section 3.1.1 in Chapter 3).

4.2.2 Satellite altimetry

Because access to in-situ water level measures is internationally restricted, this study used water levels that were observed by multi-mission satellite altimeters (e.g., TOPEX/Poseidon, Jason, SARAL/Altika, and Sentinel-3), as archived in three major databases: the Hydroweb (http://hydroweb.theia-land.fr) (Crétaux et al. 2011), the Database for Hydrological Time Series of Inland Waters (DAHITI: https://dahiti.dgfi.tum.de/en) (Schwatke et al. 2015), and the USDA Global Reservoir and Lake Monitor database (https://ipad.fas.usda.gov/cropexplorer/global_reservoir) (Birkett et al. 2011). Considering the accuracy and required temporal frequency (i.e., monthly), water levels in Hydroweb and DAHITI, which were derived from high-quality measurements, were prioritized. If a water body has water levels from Hydroweb and DAHITI, the one with longer record was used. The overall accuracy of altimetry-derived water levels for inland water bodies range from a few centimeters

for large water bodies to several decimeters for small or narrow water bodies (Crétaux et al. 2016).

4.2.3 Global dam and lake datasets

I used the recently developed global lake dataset HydroLAKES (Messager et al. 2016) to identify lakes and reservoirs across the entire terrestrial surface. HydroLAKES archives 1.4 million natural lakes and 6.7 thousand sizable reservoirs. However, the reservoirs in HydroLAKES are largely incomplete. Thus, a recently compiled global enhanced dam and reservoir inventory (GDRI) (Walter 2018; Walter et al. 2019) was used to supplement HydroLAKES for the inclusion of more complete reservoirs. Reservoirs archived in both HydroLAKES and GDRI have important attributes such as reservoir areas, dam heights, storage capacities, and completion years. This information provides critical parameters for inferring storage changes (see the Method in Section 4.3 for details).

4.2.4 Global drainage basins

The extents of global endorheic and exorheic basins were obtained from our recent study (Wang et al. 2018). These basin extents were determined with reference to two major global drainage databases. One is the 15-second HydroSHEDS drainage basin dataset (Lehner et al. 2008) and the other is the Global Drainage Basin Database (Masutomi et al. 2009). The delineated endorheic basins cover a total area of 31.9 million km^2, which is roughly one-fifth of global land area. Exorheic regions cover the rest four-fifths of global land mass. The extents of major river basins were acquired from the Global Runoff Data Center (http://grdc.bafg.de) (GRDC 2007). The GRDC was used to aggregate lake and reservoir storage trends in some major basins that represent various climatic and socioeconomic conditions.

4.3 Methods

4.3.1 Global water body type classification

We classified global water bodies into freshwater lakes, saline lakes, and artificial reservoirs by combining global lake/reservoir inventories with lake water classification methods. The applied lake/reservoir inventories include HydroLAKES and the global dam and reservoir inventory (GDRI) datasets (Messager et al. 2016; Walter 2018; Walter et al. 2019). Although HydroLAKES inventories 1.4 million natural lakes, it includes only 6.7 thousand artificial reservoirs that are originally documented in the Global Reservoir and Dam (GRanD) database (version 1.0) (Lehner et al. 2011). The number of these reservoirs is largely incomplete according to the World Register of Dams in the International Commission of Large Dams (ICOLD; www.icold-cigb.org). Thus, I here applied GDRI, an outcome of our group effort that inventories 82 thousand reservoirs, in order to incorporate smaller and recently impounded reservoirs. The GDRI dataset was also used to correct the misclassification of natural lakes as reservoirs in HydroLAKES, using spatial relationship analysis in ArcGIS. For the remaining natural lakes, each of them was further classified into a freshwater or saline lake using the classification methods as per Meng (2019) and Wang et al. (2015). In brief, the classification for many large lakes was referred to the documented salinity and/or water types in the existing literature. For the water bodies without documentations, a lake was classified to be saline based on hydrologic and spectral evidence, such as being located on a drainage sink/terminal and showing salt deposition near the lake shore in spectral images (refer to Meng (2019) for details). The overall accuracy for the water type classification is about 90% (Meng, 2019).

4.3.2 Calculating water storage variations in major lakes and reservoirs

Storage changes were estimated for 1,187 large water bodies with 229 natural freshwater lakes, 80 saline lakes, and 878 artificial reservoirs. The studied water bodies account for ~70%, 90%, and 75% of the total freshwater lake volume, saline lake volume, and impounded reservoir capacity, respectively (Figure 4.1 & Table 4.1).

Table 4.1 Number and total volume of studied water bodies.

Lake Type	Number of studied lakes	Total volume studied (10^3 Gt)	Relative total volume studied (%)
Saline lakes	80	82	98.6
Natural freshwater lakes	229	100	90.0
Reservoirs	878	6	73.3

For each studied water body, its monthly lake area time series was constructed during the period of 1992 to 2018 using a novel water mapping algorithm that was developed from the complete Landsat image archive. This algorithm is able to recover water areas from cloudy images and increase the temporal frequency to bi-monthly on average (Yao et al. 2019). The key rationale is that lakes are lentic water bodies where shorelines can be treated as topographic isolines (contours). Thus, a smaller extent with a lower isobath should be completely contained by a larger extent with a higher isobath. Even though a cloudy image may observe only part of the lake extent, the corresponding complete extent should be located between a lower and a higher isobaths that can be obtained from cloud-free images. If these two complete isobaths are close to each other, their water extents can be used to "gauge" the complete area associated with the partial extent through interpolation.

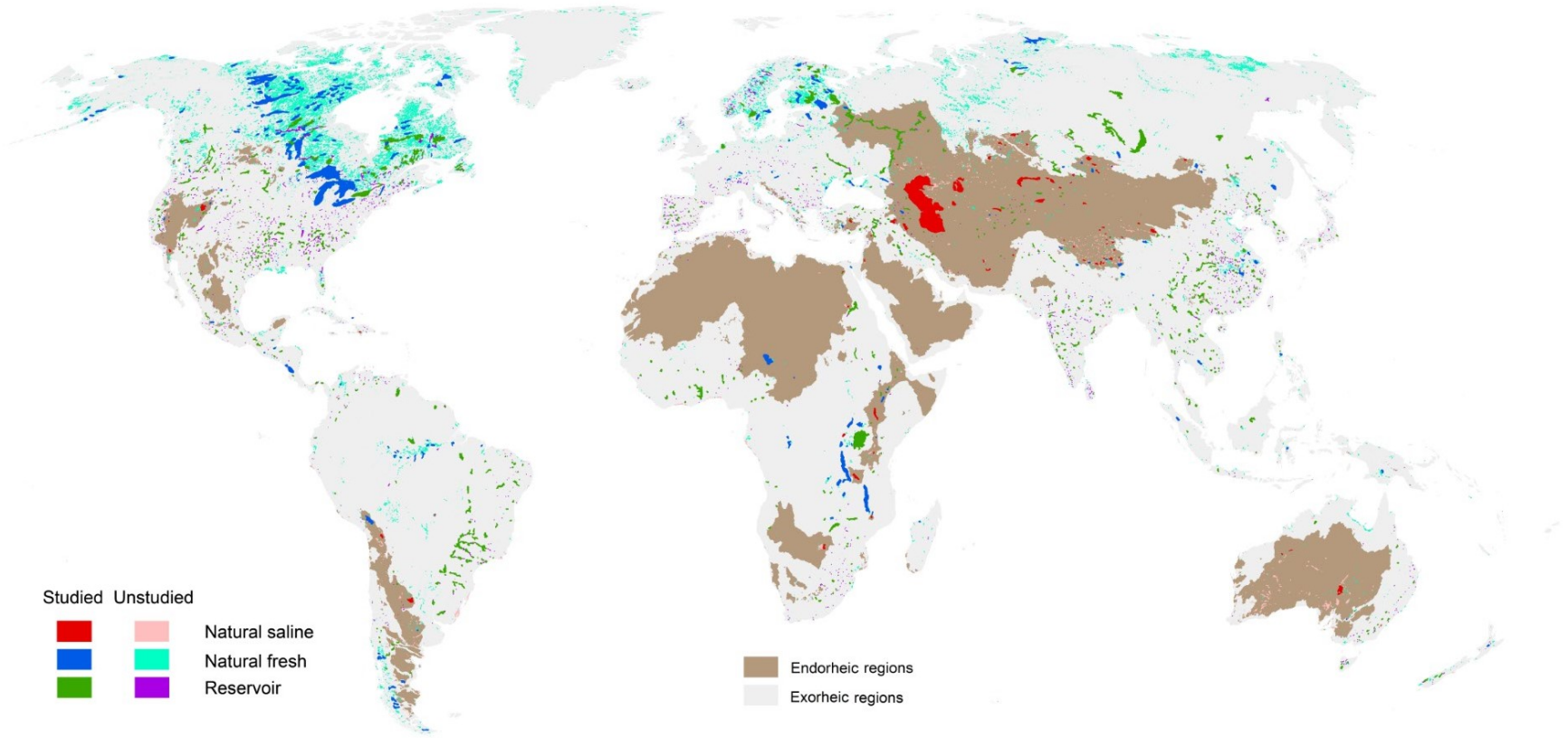

Figure 4.1 Distributions of studied and unstudied water bodies. Geometries of the lake polygons are based on HydroLAKES (Messager et al. 2016) and GRDI (Walter 2018) datasets.

Detailed technical procedures of this mapping method are given in Chapter 3 and Yao et al. (2019). In brief, the procedure starts with compositing all Landsat images that overlap each studied lake/reservoir region into monthly image series. Cloud and terrain shadow contaminations were masked using the image quality information, solar angles, and digital elevation models. Performing this monthly image composition maximized the portion of available high-quality observations. Multiple water indices were next compared on the basis of each lake/reservoir, in order to achieve the best accuracy of the initial water mapping. The remnant mapping errors from both cloud-free and contaminated images were further reduced using a refining process. The complete water area associated with each partial observation due to contamination was then recovered by a linear interpolation using a pair of lower and higher isolines delineated from cloud-free images. To reduce the recovery uncertainty, the pair of lower and higher isolines that are closest to the partial water extent was selected. Finally, the complete lake/reservoir areas, both directly mapped from cloud-free images and recovered from contaminated images, were combined to produce the water area time series.

To construct the hypsometry (e.g., relationship between lake areas and water levels), satellite-derived level time series were acquired from major global water level databases including the Hydroweb (Crétaux et al. 2011), G-REALM (Birkett et al. 2011), and DAHITI (Schwatke et al. 2015). For each of the 603 studied water bodies with available level data, the hypsometric curve $H(A, L)$ was calibrated as a polynomial function up to degree 3, using the monthly pairs of water area (A) and level (L). For the remaining 584 large reservoirs without level data, their hypsometric curves were approximated as empirical functions $H(h, s, c)$ of their dam heights (h), reservoir areas (s), and maximum capacities (c), assuming an exponential

relationship between reservoir areas and water levels. These parameters were collected from the global lake datasets mentioned above. These empirical hypsometries have been tested to be overall reliable, by referring to the water storage trends in a total of 92 reservoirs derived from calibrated hypsometries (i.e., based on water areas from Landsat and levels from radar altimetry) (Figure 4.2). For each lake or reservoir, monthly storage anomalies were calculated as the integrals of the hypsometric curve through monthly water areas:

$$\Delta V_i = \int_{A_{i-1}}^{A_i} H dA$$

where A_i and A_{i-1} are lake areas in two consecutive months, ΔV_i represents volume changes, and H represents the hypsometric function.

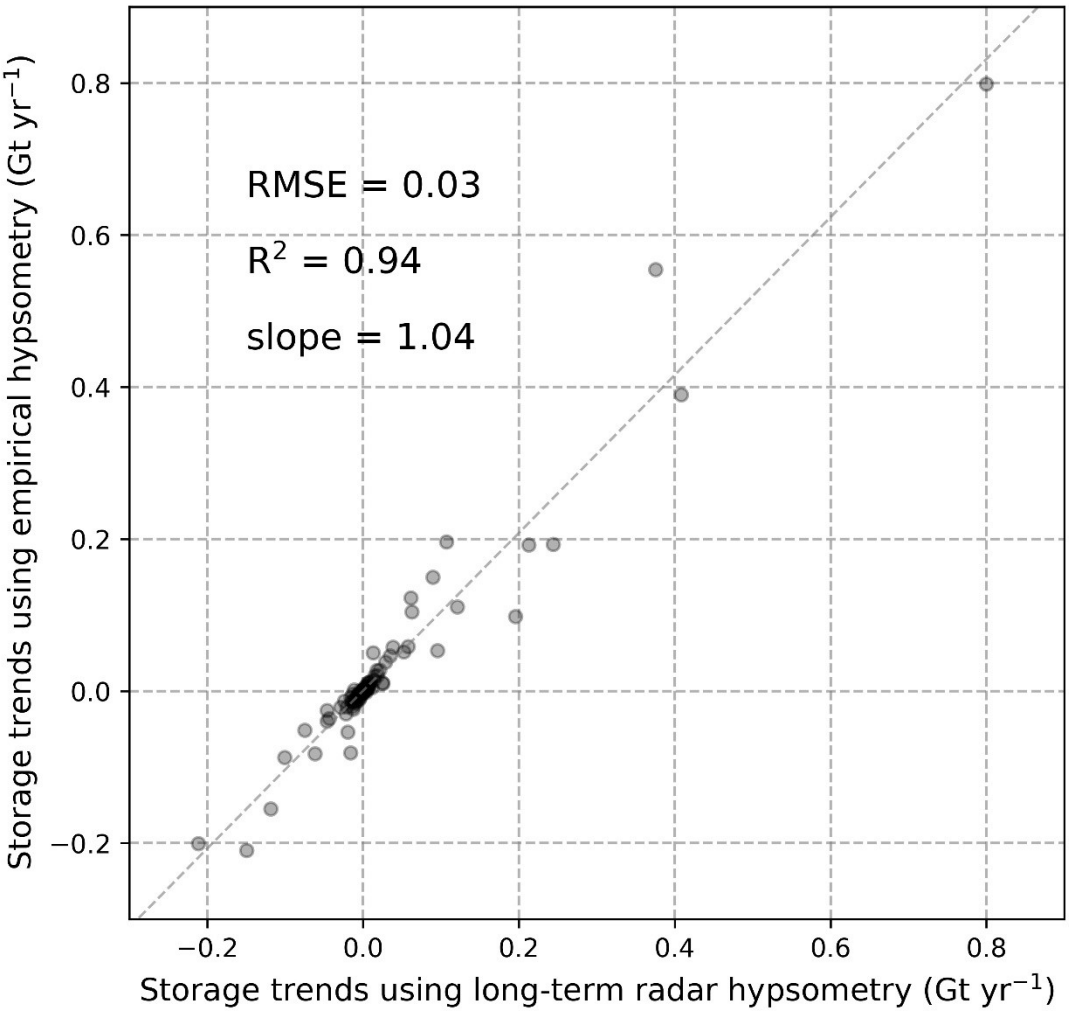

Figure 4.2 Accuracy assessment of reservoir water storage trends estimated from empirical hypsometries. Reservoir water storage trends estimated using empirical hypsometries were validated against the trends calculated using long-term radar altimetry and Landsat imagery for 92 reservoirs. These 92 reservoirs were selected based on the availability of radar altimetry levels and the confidence of referenced hypsometric curves (i.e., with R^2 values of the area-level fitting larger than 0.9).

The calculated time series storage anomalies were then deseasonalized by subtracting the climatology (the long-term monthly means) during the study period. The best-fit linear regression was applied on the deseasonalized time series to calculate the water storage trends.

Following error propagation rules, uncertainties of the estimated lake storage trends were integrated from several sources. For each of the water bodies with calibrated hypsometries, the uncertainty sources include: 1) the uncertainty in mapped water areas using Landsat, calculated using the reported median error of 3.6% (refer back to Chapter 3); 2) the water level uncertainty as provided by the altimetric database; and 3) uncertainty in the hypsometric curve, calculated as the root-mean square error (RMSE) of the polynomial fitting. For the reservoirs with empirical hypsometries, the uncertainty sources include those in the mapped water areas (source 1), level measurements (source 2), and empirical hypsometries. The uncertainty in empirical hypsometries was inferred by a comparison between the storage trends calculated using the available calibrated hypsometries and the storage trends using the empirical hypsometries. Only reservoirs with relatively low calibration errors, i.e., R^2 values of hypsometric curve fitting larger than 0.9, were used in the comparison. This selection was applied given a reasonable tradeoff between the number and the confidence of referenced hypsometries.

4.3.3 Inferring storage change uncertainty for small lakes and reservoirs

Considering that the global reservoir storage trends may be dominated by those of newly impounded reservoirs (Chao et al. 2008; Wada et al. 2016), the storage uncertainty in unsampled small reservoirs was inferred using the documented reservoir storage capacities and initial operation years as similar to Chao et al. (2008). For each new reservoir, its annual storage was assigned to zero before the reservoir's initial impoundment and to 85% of the maximum storage capacity after the initial impoundment (Chao et al. 2008).

To infer the uncertainty of storage changes in unsampled small natural lakes, historical water areas were combined with a geo-statistical approach to deduce storage changes. Annual water areas for each natural lake were calculated from the Joint Research Centre Global Surface

Water (GSW) dataset. According to Cael et al. (2017), lake area (A) and total volume (V) follow an overall power-law relationship ($V = 0.24\ A^{1.2\pm0.05}$). Assuming this scaling relationship as a proxy of hypsometric curves, volume changes (ΔV) for a given year could be calculated as $0.24({A_{given}}^{1.2} - {A_{prev}}^{1.2})$, where A_{given} is the water area for that given year and A_{prev} is the water area for the previous year. The best-fit linear regression was applied to calculate the trends in annual volume time series. It is important to note that the scaling volume-area relationship is only suitable for estimating the collective uncertainty of all unsampled lakes rather than any single lake. Thus, only aggregated trends over large geographic regions were used for uncertainty analysis.

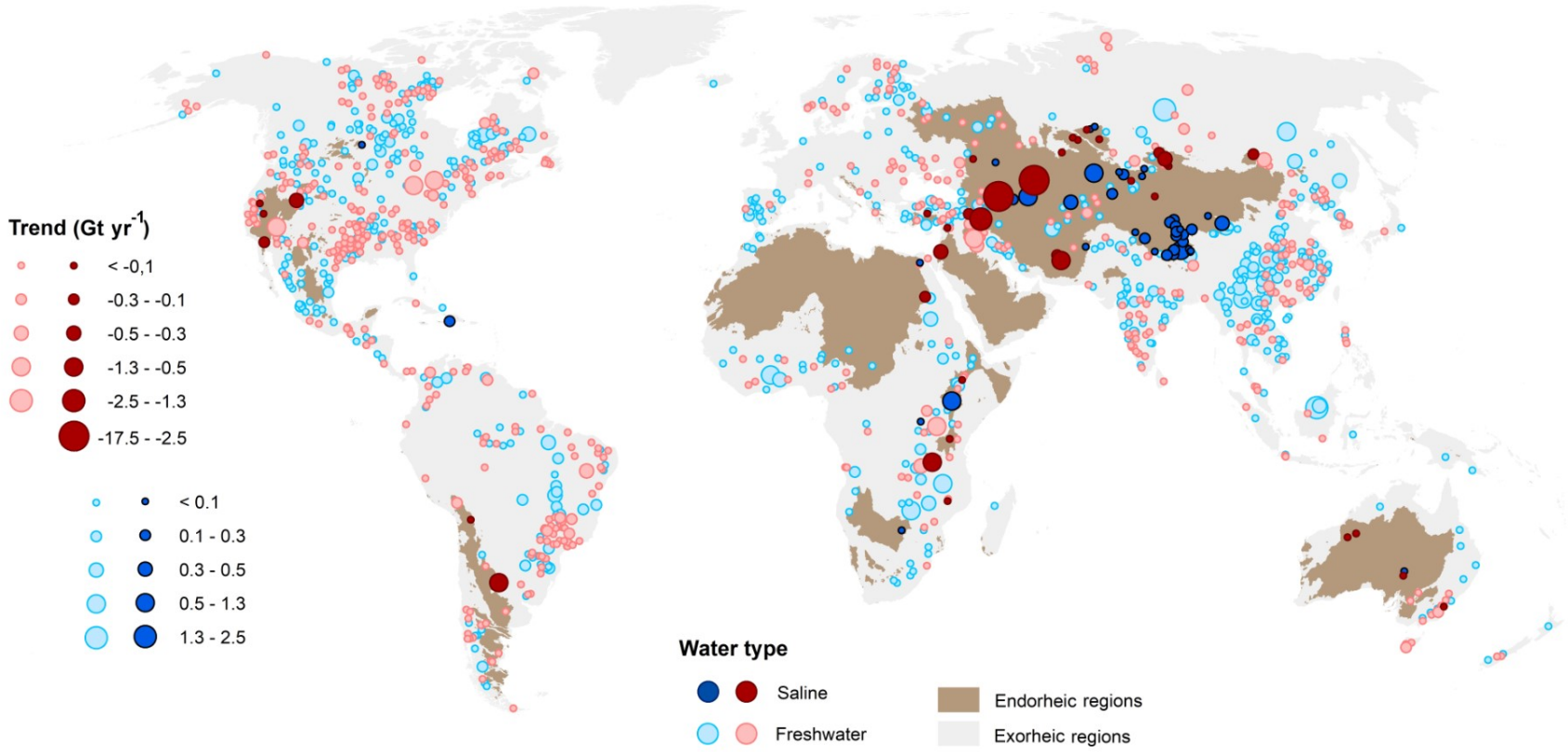

Figure 4.3 Trends in water storage for major lakes and reservoirs worldwide from 1992 to 2018.

4.4 Results and discussion

4.4.1 Global patterns of open-surface water storage changes

There are notable patterns in lake water storage changes during the past 26 years (Figure 4.3). Increased water storage is found in about 48% (or 600 in number) of the studied large water bodies. A total amount of 1,170 ± 24 Gt (or 45.03 ± 0.94 Gt yr^{-1}) of water was gained in these water bodies. Over 70% of these lakes show a significant (linear regression $p<0.05$) increasing trend in storage, accounting for 97% of the total increased storage. However, the increasing storage was offset by the water loss (-47.32 ± 2.61 Gt yr^{-1}) in the remaining 52% of studied large water bodies. Over 96% of the total water loss comes from significant decreasing trends ($p<0.05$).

The global map in Figure 4.3 reveals several hotspots that experienced evident lake water storage changes. To facilitate discussion, I aggregated lake water storage (LWS) trends to major river basins. Figure 4.4 shows some of the important river basins with significant LWS trends. As shown, large increasing trends are mostly found in humid basins, such as the Yangtze (4.18 ± 0.26 Gt yr^{-1}), the Zambezi (1.77 ± 0.15 Gt yr^{-1}), the Mekong (1.91 ± 0.16 Gt yr^{-1}), and the Nelson (1.07 ± 0.08 Gt yr^{-1}). In contrast, large decreasing trends largely stem from arid and semiarid basins, such as the Aral Sea (-7.25 ± 0.83 Gt yr^{-1}), Lake Chiquita (-0.84 ± 0.12 Gt yr^{-1}), the Colorado (-0.77 ± 0.11 Gt yr^{-1}), and the Euphrates (-0.76 ± 0.18 Gt yr^{-1}). This contrast suggests an increased inequality between open-surface water storages in wet and dry regions.

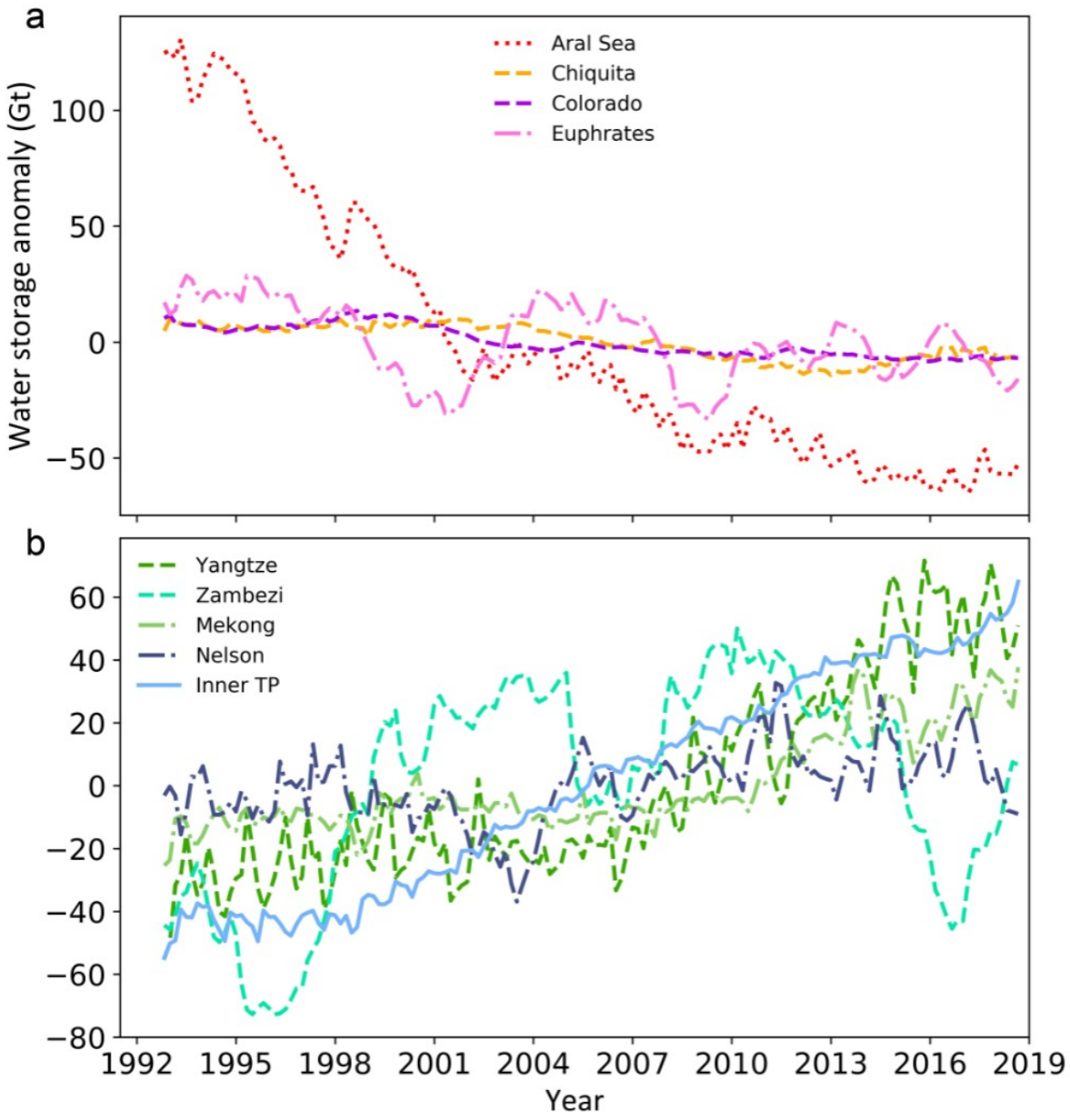

Figure 4.4 Major lake water storage trends in important hydrologic basins (or regions). (a) Basins with decreasing trends. (b) Basins with increasing trends.

4.4.2 Divergent trends in endorheic (arid) and exorheic (humid) regions

Figure 4.5 reveals a strong global divergence in LWS trends between endorheic and exorheic regions. The net lake water storage in endorheic regions significantly decreased at a rate of -20.61 ± 2.68 Gt yr^{-1} ($p<0.05$) whereas that in exorheic regions increased at a rate of 27.31 ± 1.59 Gt yr^{-1} ($p<0.05$). This divergence confirms Hypothesis 3 that the arid endorheic regions were losing surface water while the humid exorheic regions were accumulating surface water. Most of the water loss in global endorheic regions comes from the Caspian Sea Basin (-16.81 ± 2.45 Gt yr^{-1}). However, even though the Caspian Sea is excluded, LWS in the endorheic regions still exhibits a persistent decreasing trend (R^2 value of the linear fitting 0.7) albeit a much slower rate (-3.14 ± 1.11 Gt yr^{-1}). The second largest water loss (-7.25 ± 0.83 Gt yr^{-1}) in endorheic regions is found in the Aral Sea Basin (Figure 4.4). The water storage decline in the Aral Sea Basin is, however, largely balanced out by the lake storage increase (6.26 ± 0.32 Gt yr^{-1}) in the inner Tibetan Plateau which recently received increasing water supply from precipitation and to a lesser extent, melting runoff from the glacier (Wang et al. 2018; Yao et al. 2018; Zhang et al. 2017). Significant LWS declines are also found in most of the other major endorheic zones, such as Dry Andes and Patagonia (-1.27 ± 0.14 Gt yr^{-1}), Sahara and Arabia (-0.93 ± 0.29 Gt yr^{-1}), and Australia (-0.09 ± 0.09 Gt yr^{-1}). Western North America, the Great Rift Valley, and Southern Africa likely experienced water storage increase at a rate of 0.19 ± 0.20 Gt yr^{-1} and 0.01 ± 0.18 Gt yr^{-1}, respectively. However, LWS gains in these regions have large uncertainties. Lake storage increase in exorheic regions appears to be more spatially dispersed (Figure 4.3), given that no major river basin dominates the net increasing trend in exorheic basins. The largest LWS increase is found in the Yangtze Basin with a rate of 4.18 ± 0.26 Gt yr^{-1}, which only accounts for 15% of the net increase in exorheic regions.

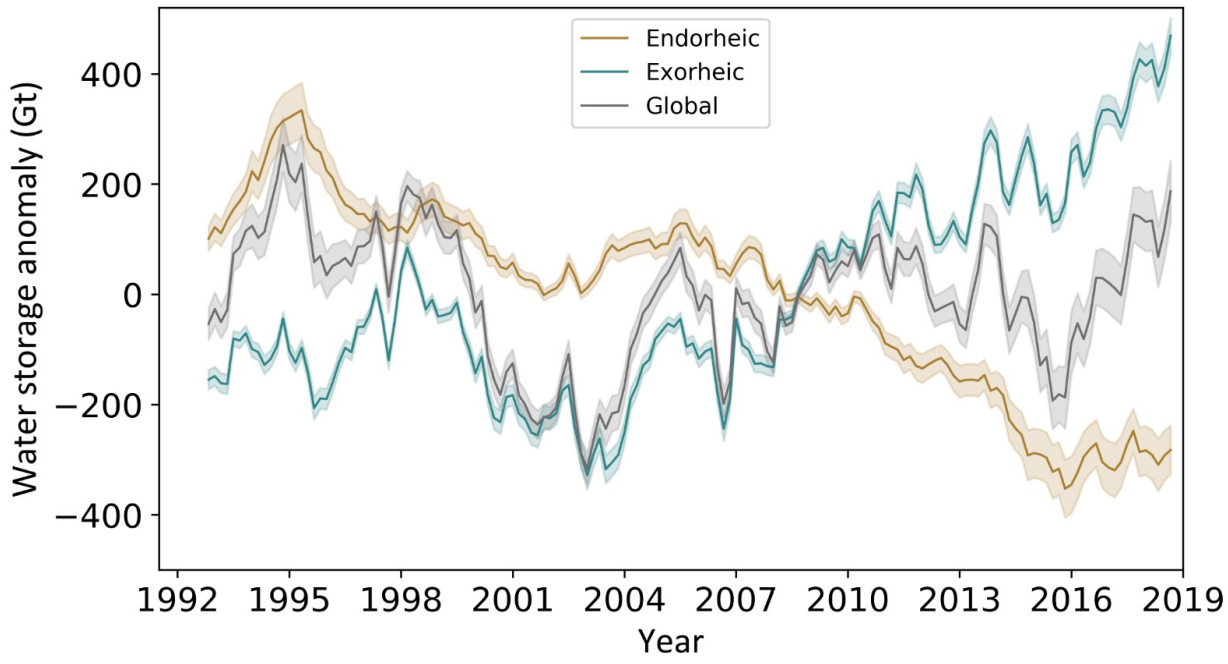

Figure 4.5 Global lake water storage time series with partitioning into endorheic and exorheic basins. Transparent shades illustrate 95% confidence intervals.

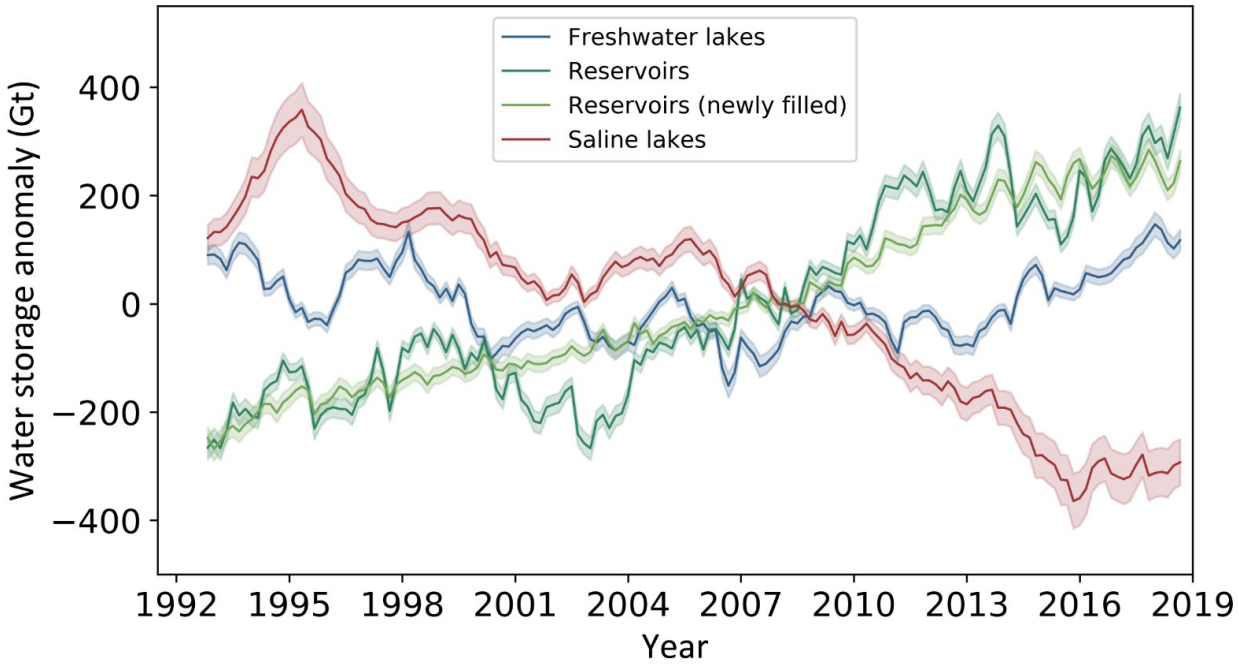

Figure 4.6 Water storage anomaly time series for different types of water bodies, including saline lakes, natural freshwater lakes, and artificial reservoirs. Transparent shades illustrate 95% confidence intervals.

4.4.3. Amplified contrast between fresh and saline water abundance

There is a remarkable contrast in the recent storage changes between saline lakes and freshwater lakes/reservoirs (Figure 4.6). Over the past 26 years, the freshwater lake volume increased by 767.0 Gt, whereas saline lake volume decreased by 595.4 Gt. The amplified difference between surface fresh and saline water abundance is about 1% of global lake volume (Messager et al. 2016), which is equivalent to 38 Lake Meads (the largest reservoir in the U.S.) at full capacity.

The net global decline in saline lake volume, previously suggested by regional evidence (Wurtsbaugh et al. 2017), is now confirmed by this study. The net storage in global saline lakes declined at a rate of 22.84 ± 2.68 Gt yr^{-1} over the studied 26 years. Nearly all continents experienced saline lake storage loss (Figure 4.7). The largest decline occurred in Asia, accounting for ~90% of the net global decline. Asia's saline water loss was largely driven by the desiccation of some of its largest water bodies, such as the Caspian Sea (-17.48 ± 2.07 Gt yr^{-1}), the Aral Sea (-7.36 ± 0.82 Gt yr^{-1}), Lake Urmia (-1.29 ± 0.18 Gt yr^{-1}), Goud-e-Zareh (-0.65 ± 0.09 Gt yr^{-1}), the Dead Sea (-0.40 ± 0.06 Gt yr^{-1}), and Lake Khyargas (-0.33 ± 0.05 Gt yr^{-1}) (Figure 4.3). Most of these saline lakes have been designated as the Ramsar sites of International Importance (Okuno et al. 2017; Wurtsbaugh et al. 2017). The desiccating saline water bodies not only reduced waterbird habitats, but also elevated their salinity level that could be too high for native species to survive (Micklin 2007). Additionally, the exposed saline lakebeds could increase sources for salt dust storms that threaten human health and nearby agriculture (Micklin 2007; Skiles et al. 2018). At a much less extent, saline water increased in some remote regions (e.g., inner Tibet and Lake Balkhash Basin) which experienced increasing precipitation and runoff from melting glaciers (Brun et al. 2017; Immerzeel et al. 2010; Wang et al. 2018; Yao et

al. 2018; Zhang et al. 2017). In addition to Asia's water loss, the remaining saline water loss (2.3 Gt yr^{-1}) can be partitioned to 43% in South America, 30% in Africa, 17% in North America, and 9% in Oceania.

In contrast to saline water loss, there is a widespread increase in reservoir storage during the study period (Figure 4.7). Over 70% of the increased reservoir storage is found in Asia which hosts the majority of global population (60%) and crop land (66%) (Bruinsma 2009), followed by Africa (accounting for 10%), North America (9%), South America (7%), and Europe (3%). Oceania is the only continent that experienced a decline in reservoir storage, which was likely induced by the decreasing reservoir inflow during the Millennium Drought (2001-2009). However, the magnitude of the water loss (0.2 Gt yr^{-1}) is much smaller than water gain in any other continents. Interestingly, the trends in reservoir storage dominate those in natural freshwater lakes for each of the six continents with different shares of natural freshwater lake abundance (Figure 4.7). This indicates that human water management has been intensified worldwide over the recent decades (see Section 4.4 for more discussions).

Different from reservoirs and saline lakes, large natural freshwater lakes generally exhibit no evident trends in water storage due to interannual fluctuations. Over 85% of them have a changing rate less than 0.1 Gt per year (Figure 4-1). At the continental level, freshwater storage in natural lakes increased in North America (1.8 Gt yr^{-1}), Africa (0.9 Gt yr^{-1}), Asia (0.8 Gt yr^{-1}), and Europe (0.7 Gt yr^{-1}), but decreased marginally at a rate 0.1 Gt yr^{-1} in both South America and Oceania which recently experienced severe droughts (Erfanian et al. 2017; Van Dijk et al. 2013).

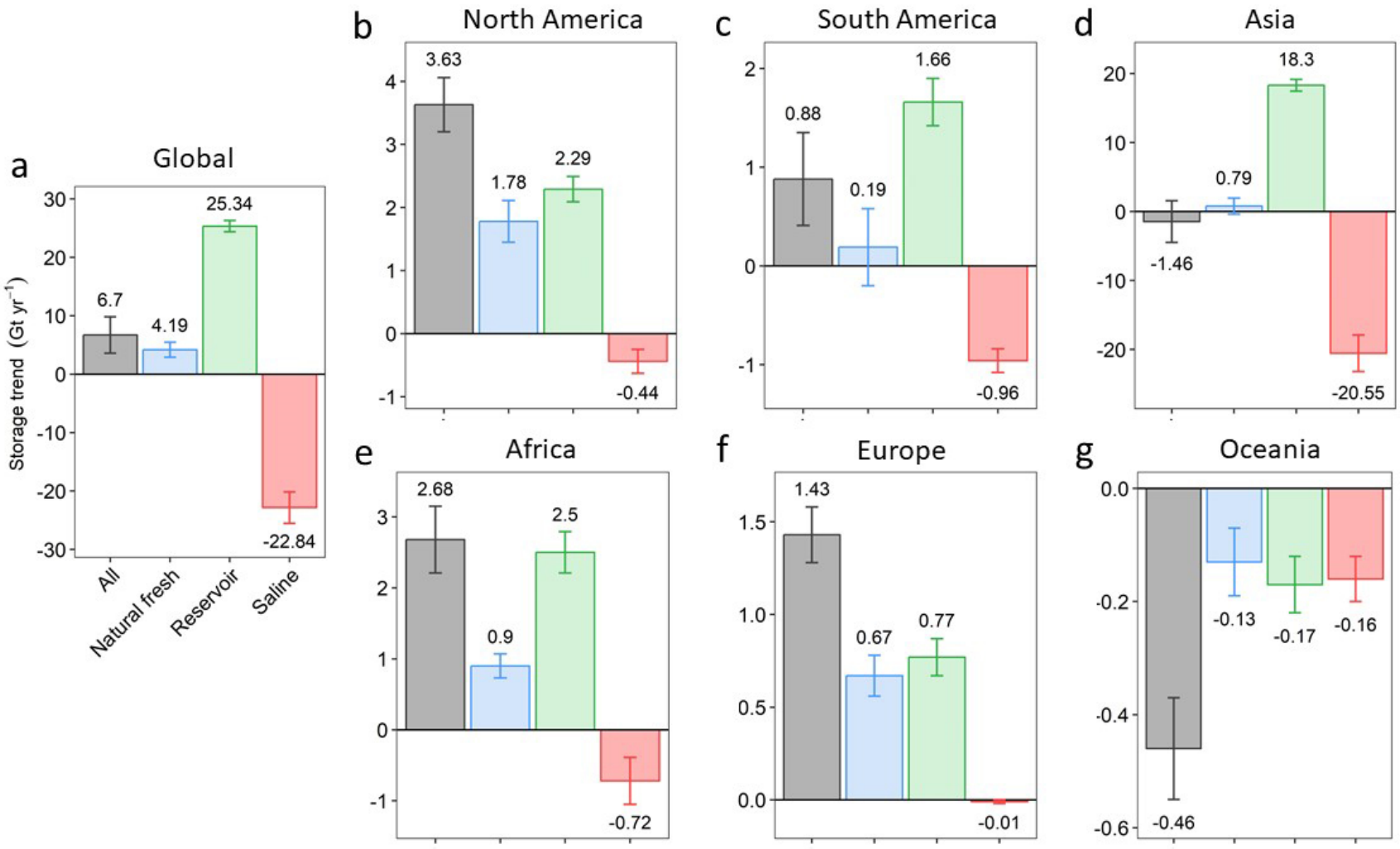

Figure 4.7 Partitioning global lake water storage changes by continents and water types. (a) Global total. (b) North America. (c) South America. (d) Asia. (e) Africa. (f) Europe. (g) Oceania. Error bars show 95% confidence intervals.

4.4.4. Elevated human water impoundment behind dams

The net increasing trend in freshwater storage could be largely attributed to the storage increase in new reservoirs (commissioned after the beginning of the study period) (Figure 4.6). This suggests that the global trend in open-surface freshwater storage was largely driven by human water management through continued dam building and reservoir impoundment. More than 95% of the net increase in global reservoir storage comes from new reservoirs in exorheic (humid) regions where surface runoff is abundant. New reservoirs are widespread in humid basins of the developing world, such as the Yangtze, the Mekong, the Nelson, the Rajang, the Yenisei and the Tocantins Basins (Figure 4.3). The best-known Three Gorges Dam in China was completed in 2003 and then filled to its maximum capacity (36 Gt, roughly equivalent to the full capacity of the largest U.S. reservoir Lake Mead) in 2010. The Three Gorges Dam along with many other dam projects have substantially elevated the local terrestrial water storage in the upstream Yangtze River Basin in southwestern China (Rodell et al. 2018). The Rajang Basin in Indonesia has the largest increase (2.64 ± 0.62 Gt yr^{-1}) in new reservoir storage, followed by the Yangtze (2.34 ± 0.19 Gt yr^{-1}), the Yenisei (1.94 ± 0.27 Gt yr^{-1}) and the Mekong (1.72 ± 0.14 Gt yr^{-1}). To a much lesser extent, a total amount of 1.11 ± 0.14 Gt of water was gained in the new reservoirs constructed within endorheic basins where surface flow is limited. The water storage impounded in new reservoirs explains over 80% of the net storage increase (1.38 ± 0.17 Gt yr^{-1}) in all reservoirs across the global endorheic basins. Since many reservoirs in arid regions function as water supplies, the increasing reservoir storage in global endorheic basins signifies an important source of streamflow reduction, which probably contributed to the desiccation of terminal/saline lakes downstream (Case 2013; Hassanzadeh et al. 2012; Wurtsbaugh et al. 2017).

4.4.5. Implications for the global hydrologic cycle

To investigate the contribution of open-surface water bodies to terrestrial water storage (TWS) changes, I further compared the storage trends in lakes and reservoirs with the TWS trends observed by the Gravity Recovery and Climate Experiment (GRACE) satellites during the GRACE era (from 2002 to 2016). During the past 14 years, global TWS declined at a rate of 164.76 Gt yr^{-1} with two-thirds of water loss coming from water-limited endorheic basins. By contrast, the net global lake/reservoirs water storage (LWS) increased at a rate of 6.70 Gt yr^{-1}, which only offset 4% of the TWS decrease. However, it is important to note that TWS has decreased in both exorheic basins and endorheic basins, whereas LWS shows divergent trends between them. As a result, lakes and reservoirs on a global scale do not substantially affect the net TWS trend during 2002-2016. This marginal global net LWS trend also masks the fact that LWS in endorheic regions actually accounts for 28% of the global TWS decline, which is in line with a recent estimate (Wang et al. 2018). Interestingly, despite a decreasing TWS in exorheic regions, LWS in exorheic regions increased at a rate of 38.42 Gt yr^{-1}, which matches two-third of the global TWS declining rate in magnitude (-58.44 Gt yr^{-1}). As the increasing LWS is mainly attributed to the construction of new reservoirs, this contrast indicates that direct human activities have substantially counteracted the climate-driven land water storage loss in humid regions.

During the studied 26 years (1992-2018), global lakes and reservoirs, with an increasing storage trend of 6.70 ± 3.12 Gt yr^{-1} (equivalent to a sea level of 0.02 mm yr^{-1}), potentially counteracted the observed sea level rise (3.4 mm yr^{-1}) by about 1%. This minor impact, again, integrates the divergent contributions from saline lakes (0.06 ± 0.01 mm yr^{-1}) and reservoirs (-0.07 ± 0.01 mm yr^{-1}).

4.5 Conclusions

This study provides a comprehensive estimate of storage variations in ~1,200 major lakes and reservoirs worldwide from 1992 to 2018, by synergizing multi-mission satellites. It substantially extends the number of studied water bodies in the existing global studies by a factor of 9-30. Additionally, it increases the temporal frequency of long-term water storage time series, owing to the use of a novel water mapping method that can accurately recover water areas from contaminated images (refer back to Chapter 3). The presented study here also reduces the biases in hypsometric calibration compared with those in a recent global LWS change analysis (Busker et al. 2019). Given such improvements in both spatiotemporal coverage and estimation bias, this chapter advances the understanding of recent storage dynamics in global lakes and reservoirs.

Globally, lake and reservoir storage slightly increased at a rate of 6.70 ± 3.12 Gt yr^{-1}. However, this masks a remarkable divergence between endorheic (arid) and exorheic (humid) basins. In endorheic basins, the net LWS decreased at a significant rate of -20.61 ± 2.68 Gt yr^{-1}, whereas exorheic basins experienced an increasing LWS trend at a rate of 27.31 ± 1.59 Gt yr^{-1} (p of both rates <0.05). The net LWS decrease in arid (endorheic) regions was dominated by water loss in saline lakes. The storage increase in humid (exorheic) regions was mainly attributed to the increasing freshwater storage. Consequently, the contrast between fresh and saline water abundance was amplified by ~1,400 Gt, which is equivalent to 38 Lake Meads (the largest reservoir in the US) at the full capacity.

This study confirmed the net storage decline (22.84 ± 2.68 Gt yr^{-1}) in global saline lakes as previously suggested by regional evidence (Chen et al. 2017; Hassanzadeh et al. 2012; Wurtsbaugh et al. 2017). All continents that host major saline lakes experienced saline water storage loss. The net global decline in saline lake storage is mainly contributed by Asia (90%),

followed by South America (4%), Africa (3%), North America (2%) and Oceania (1%). The desiccation of saline lakes was likely driven by long-term human water consumption and climate change (such as rising temperature that enhanced potential evapotranspiration) (Hassanzadeh et al. 2012; Wang et al. 2018; Wurtsbaugh et al. 2017). In contrast, water storage in freshwater lakes and reservoirs increased at 29.53 ± 2.58 Gt yr^{-1}. The increased freshwater storage is found in all continents except Oceania which was strongly influenced by the Millennium Drought during 2001-2009. The net global increase in freshwater storage was dominated by the filling of new reservoirs that were commissioned after the beginning of the study period. This suggests that the amplified contrast between saline and freshwater abundance was partially induced by human water impoundments.

Owing to the divergent trends, lakes and reservoirs on a global scale only exert a minor influence on the observed sea level change during the past 26 years. The positive contribution (0.06 ± 0.01 mm yr^{-1}) from saline lakes is completely offset by the negative contribution from artificial reservoirs (-0.07 ± 0.01 mm yr^{-1}). Consequently, the studied global lakes and reservoirs slowed down sea level rise by 0.02 ± 0.01 mm yr^{-1}, which counteracts ~1% of the observed rate of 3.4 mm yr^{-1} around the same period.

4.6 References

Alborzi, A., Mirchi, A., Moftakhari, H., Mallakpour, I., Alian, S., Nazemi, A., Hassanzadeh, E., Mazdiyasni, O., Ashraf, S., & Madani, K. (2018). Climate-informed environmental inflows to revive a drying lake facing meteorological and anthropogenic droughts. *Environmental Research Letters, 13*, 084010, doi:10.1088/1748-9326/aad246.

Allen, G.H., & Pavelsky, T.M. (2018). Global extent of rivers and streams. *Science*, 361, 585-588, doi:10.1126/science.aat0636.

Allen, M.R., & Ingram, W.J. (2002). Constraints on future changes in climate and the hydrologic cycle. *Nature, 419*, 224, doi:10.1038/nature01092.

Alsdorf, D.E., Rodriguez, E., & Lettenmaier, D.P. (2007). Measuring surface water from space. *Reviews of Geophysics,* 45, RG2002, doi:10.1029/2006RG000197.

Anderson, T.W., Tiffany, M.A., & Hurlbert, S.H. (2007). Stratification, sulfide, worms, and decline of the Eared Grebe (Podiceps nigricollis) at the Salton Sea, California. *Lake and Reservoir Management, 23*, 500-517, doi:10.1080/07438140709354034.

Bastviken, D., Tranvik, L.J., Downing, J.A., Crill, P.M., & Enrich-Prast, A. (2011). Freshwater methane emissions offset the continental carbon sink. *science, 331*, 50-50, doi:10.1126/science.1196808.

Birkett, C., Reynolds, C., Beckley, B., & Doorn, B. (2011). From research to operations: the USDA global reservoir and lake monitor. *Coastal altimetry* (pp. 19-50): Springer

Bruinsma, J. (2009). The resource outlook to 2050: by how much do land, water and crop yields need to increase by 2050. In, *Expert meeting on how to feed the world in* (pp. 24-26)

Brun, F., Berthier, E., Wagnon, P., Kääb, A., & Treichler, D. (2017). A spatially resolved estimate of High Mountain Asia glacier mass balances from 2000 to 2016. *Nature Geoscience, 10*, 668-673, doi:10.1038/ngeo2999.

Busker, T., Roo, A.d., Gelati, E., Schwatke, C., Adamovic, M., Bisselink, B., Pekel, J.-F., & Cottam, A. (2019). A global lake and reservoir volume analysis using a surface water dataset and

satellite altimetry. *Hydrology and Earth System Sciences*, 23, 669-690, doi:10.5194/hess-23-669-2019.

Case, H. (2013). *Salton Sea ecosystem monitoring and assessment plan*. US Department of the Interior, US Geological Survey

Chao, B.F., Wu, Y., & Li, Y. (2008). Impact of artificial reservoir water impoundment on global sea level. *Science, 320*, 212-214, doi:10.1126/science.1154580.

Chen, J., Pekker, T., Wilson, C., Tapley, B., Kostianoy, A., Cretaux, J.F., & Safarov, E. (2017). Long‐term Caspian Sea level change. *Geophysical research letters, 44*, 6993-7001, doi:10.1002/2017GL073958.

Conway, D., Dalin, C., Landman, W.A., & Osborn, T.J. (2017). Hydropower plans in eastern and southern Africa increase risk of concurrent climate-related electricity supply disruption. *Nature Energy, 2*, 946-953, doi:10.1038/s41560-017-0037-4.

Crétaux, J.-F., Abarca-del-Río, R., Berge-Nguyen, M., Arsen, A., Drolon, V., Clos, G., & Maisongrande, P. (2016). Lake volume monitoring from space. *Surveys in Geophysics*, 37, 269-305, doi:10.1007/s10712-016-9362-6.

Crétaux, J.-F., Jelinski, W., Calmant, S., Kouraev, A., Vuglinski, V., Bergé-Nguyen, M., Gennero, M.-C., Nino, F., Del Rio, R.A., & Cazenave, A. (2011). SOLS: A lake database to monitor in the Near Real Time water level and storage variations from remote sensing data. *Advances in space research*, 47, 1497-1507, doi:10.1016/j.asr.2011.01.004.

Donchyts, G., Baart, F., Winsemius, H., Gorelick, N., Kwadijk, J., & van de Giesen, N. (2016). Earth's surface water change over the past 30 years. *Nature Climate Change*, 6, 810-813, doi:10.1038/nclimate3111.

Erfanian, A., Wang, G., & Fomenko, L. (2017). Unprecedented drought over tropical South America in 2016: significantly under-predicted by tropical SST. *Scientific reports, 7*, 1-11, doi:10.1038/s41598-017-05373-2.

Feng, M., Sexton, J.O., Channan, S., & Townshend, J.R. (2016). A global, high-resolution (30-m) inland water body dataset for 2000: First results of a topographic–spectral classification

algorithm. *International Journal of Digital Earth, 9*, 113-133, doi:10.1080/17538947.2015.1026420.

Gao, H., Birkett, C., & Lettenmaier, D.P. (2012). Global monitoring of large reservoir storage from satellite remote sensing. *Water Resources Research*, 48, W09504, doi:10.1029/2012WR012063.

Gao, H., Bohn, T., Podest, E., McDonald, K., & Lettenmaier, D. (2011). On the causes of the shrinking of Lake Chad. *Environmental Research Letters, 6*, 034021, doi:10.1088/1748-9326/6/3/034021.

Global Runoff Data Centre (2007): Major river basins. GRDC in the Bundesanstalt fuer Gewasserkunde, 56068 Koblenz, Germany, http://grdc.bafg.de.

Griffin, D.W., & Kellogg, C.A. (2004). Dust storms and their impact on ocean and human health: dust in Earth's atmosphere. *EcoHealth, 1*, 284-295, doi:10.1007/s10393-004-0120-8.

Haddeland, I., Heinke, J., Biemans, H., Eisner, S., Flörke, M., Hanasaki, N., Konzmann, M., Ludwig, F., Masaki, Y., & Schewe, J. (2014). Global water resources affected by human interventions and climate change. *Proceedings of the National Academy of Sciences, 111*, 3251-3256, doi:10.1073/pnas.1222475110.

Hassanzadeh, E., Zarghami, M., & Hassanzadeh, Y. (2012). Determining the main factors in declining the Urmia Lake level by using system dynamics modeling. *Water Resources Management, 26*, 129-145, doi:10.1007/s11269-011-9909-8.

Immerzeel, W.W., Van Beek, L.P., & Bierkens, M.F. (2010). Climate change will affect the Asian water towers. *Science, 328*, 1382-1385, doi:10.1126/science.1183188.

Lehner, B., Liermann, C.R., Revenga, C., Vörösmarty, C., Fekete, B., Crouzet, P., Döll, P., Endejan, M., Frenken, K., & Magome, J. (2011). High‐resolution mapping of the world's reservoirs and dams for sustainable river‐flow management. *Frontiers in Ecology and the Environment,* 9, 494-502, doi:10.1890/100125.

Lehner, B., Verdin, K., & Jarvis, A. (2008). New global hydrography derived from spaceborne elevation data. *Eos, Transactions American Geophysical Union, 89*, 93-94, doi:10.1029/2008EO100001.

Masutomi, Y., Inui, Y., Takahashi, K., & Matsuoka, Y. (2009). Development of highly accurate global polygonal drainage basin data. *Hydrological Processes: An International Journal, 23*, 572-584, doi:10.1002/hyp.7186.

Meng, D. (2019). An improved geography of surface water abundance in lakes and reservoirs.

Messager, M.L., Lehner, B., Grill, G., Nedeva, I., & Schmitt, O. (2016). Estimating the volume and age of water stored in global lakes using a geo-statistical approach. *Nature Communications*, 7, 13603, doi:10.1038/ncomms13603.

Micklin, P. (2007). The Aral sea disaster. *Annu. Rev. Earth Planet. Sci., 35*, 47-72, doi:10.1146/annurev.earth.35.031306.140120.

Micklin, P.P. (1988). Desiccation of the Aral Sea: a water management disaster in the Soviet Union. *science, 241*, 1170, doi:10.1126/science.241.4870.1170.

Müller Schmied, H., Eisner, S., Franz, D., Wattenbach, M., Portmann, F.T., Flörke, M., & Döll, P. (2014). Sensitivity of simulated global-scale freshwater fluxes and storages to input data, hydrological model structure, human water use and calibration. *Hydrology & Earth System Sciences Discussions, 11*, doi:10.5194/hessd-11-1583-2014.

Oki, T., & Kanae, S. (2006). Global hydrological cycles and world water resources. *Science*, 313, 1068-1072, doi:10.1126/science.1128845.

Okuno, E., Gardner, R.C., Archabal, M., Murphy, K., & Willis, J. (2017). Bibliography of 2016 Scientific Publications on the Ramsar Convention or Ramsar Sites. *Available at SSRN 3063547*

Pekel, J.-F., Cottam, A., Gorelick, N., & Belward, A.S. (2016). High-resolution mapping of global surface water and its long-term changes. *Nature*, 540(7633), 418, doi:10.1038/nature20584.

Pokhrel, Y.N., Hanasaki, N., Yeh, P.J., Yamada, T.J., Kanae, S., & Oki, T. (2012). Model estimates of sea-level change due to anthropogenic impacts on terrestrial water storage. *Nature Geoscience*, 5, 389-392, doi:10.1038/ngeo1476.

Reager, J.T., Thomas, A.C., Sproles, E.A., Rodell, M., Beaudoing, H.K., Li, B., & Famiglietti, J.S. (2015). Assimilation of GRACE terrestrial water storage observations into a land surface model for the assessment of regional flood potential. *Remote Sensing, 7*, 14663-14679, doi:10.3390/rs71114663.

Rodell, M., Famiglietti, J.S., Wiese, D.N., Reager, J.T., Beaudoing, H.K., Landerer, F.W., & Lo, M.H. (2018). Emerging trends in global freshwater availability. *Nature, 557*, 651-659, doi:10.1038/s41586-018-0123-1.

Schwatke, C., Dettmering, D., Bosch, W., & Seitz, F. (2015). DAHITI–an innovative approach for estimating water level time series over inland waters using multi-mission satellite altimetry. *Hydrology and Earth System Sciences*, 19, 4345-4364, doi:10.5194/hess-19-4345-2015.

Schwatke, C., Scherer, D., & Dettmering, D. (2019). Automated Extraction of Consistent Time-Variable Water Surfaces of Lakes and Reservoirs Based on Landsat and Sentinel-2. *Remote Sensing, 11*, 1010, doi:10.3390/rs11091010.

Sheng, Y., Song, C., Wang, J., Lyons, E.A., Knox, B.R., Cox, J.S., & Gao, F. (2016). Representative lake water extent mapping at continental scales using multi-temporal Landsat-8 imagery. *Remote Sensing of Environment*, 185, 129-141, doi:10.1016/j.rse.2015.12.041.

Skiles, S.M., Mallia, D.V., Hallar, A.G., Lin, J.C., Lambert, A., Petersen, R., & Clark, S. (2018). Implications of a shrinking Great Salt Lake for dust on snow deposition in the Wasatch Mountains, UT, as informed by a source to sink case study from the 13–14 April 2017 dust event. *Environmental Research Letters, 13*, 124031, doi:10.1088/1748-9326/aaefd8.

Tong, X., Pan, H., Xie, H., Xu, X., Li, F., Chen, L., Luo, X., Liu, S., Chen, P., & Jin, Y. (2016). Estimating water volume variations in Lake Victoria over the past 22years using multi-mission altimetry and remotely sensed images. *Remote Sensing of Environment, 187*, 400-413, doi:10.1016/j.rse.2016.10.012.

Van Dijk, A.I., Beck, H.E., Crosbie, R.S., de Jeu, R.A., Liu, Y.Y., Podger, G.M., Timbal, B., & Viney, N.R. (2013). The Millennium Drought in southeast Australia (2001–2009): Natural and

human causes and implications for water resources, ecosystems, economy, and society. *Water Resources Research, 49*, 1040-1057, doi:10.1002/wrcr.20123.

Verpoorter, C., Kutser, T., Seekell, D.A., & Tranvik, L.J. (2014). A global inventory of lakes based on high‐resolution satellite imagery. *Geophysical research letters*, 41, 6396-6402, doi:10.1002/2014GL060641.

Wada, Y., Reager, J.T., Chao, B.F., Wang, J., Lo, M.-H., Song, C., Li, Y., & Gardner, A.S. (2016). Recent Changes in Land Water Storage and its Contribution to Sea Level Variations. *Surveys in Geophysics*, 1-22, doi:10.1007/s10712-016-9399-6.

Wada, Y., Van Beek, L., & Bierkens, M.F. (2011). Modelling global water stress of the recent past: on the relative importance of trends in water demand and climate variability. *Hydrology and Earth System Sciences, 15*, 3785-3805, doi:10.5194/hess-15-3785-2011.

Wada, Y., Wisser, D., & Bierkens, M.F. (2014). Global modeling of withdrawal, allocation and consumptive use of surface water and groundwater resources. *Earth System Dynamics Discussions, 5*, 15-40, doi:10.5194/esd-5-15-2014.

Walter, B. (2018). An Enhanced Inventory of Global Dams and Reservoirs and Their Contribution to Sea Level.

Walter, B., Wang, J., & Yao, F. (2019). An Enhanced Inventory of Global Dams and Reservoirs and Their Contribution to Sea Level. NASA Water Resources Science Team Meeting. Portland, Oregon, July 16-19, 2019.

Wang, J., Sheng, Y., Song, C., Urano, T., Satori, P., & Ford, S. (2015). A high-resolution global lake inventory with classified freshwater and saline types. American Geophysical Union: San Francesco, California, December 14–18, 2015.

Wang, J., Song, C., Reager, J.T., Yao, F., Famiglietti, J.S., Sheng, Y., MacDonald, G.M., Brun, F., Schmied, H.M., Marston, R.A., & Wada, Y. (2018). Recent global decline in endorheic basin water storages. *Nature Geoscience, 11*, 926-932, doi:10.1038/s41561-018-0265-7.

Winemiller, K.O., McIntyre, P.B., Castello, L., Fluet-Chouinard, E., Giarrizzo, T., Nam, S., Baird, I., Darwall, W., Lujan, N., & Harrison, I. (2016). Balancing hydropower and biodiversity in the Amazon, Congo, and Mekong. *Science, 351*, 128-129, doi:10.1126/science.aac7082.

Wurtsbaugh, W.A., Miller, C., Null, S.E., DeRose, R.J., Wilcock, P., Hahnenberger, M., Howe, F., & Moore, J. (2017). Decline of the world's saline lakes. *Nature Geoscience*, 10, 816–821, doi:10.1038/ngeo3052.

Yao, F., Wang, J., Wang, C., & Crétaux, J.-F. (2019). Constructing long-term high-frequency time series of global lake and reservoir areas using Landsat imagery. *Remote Sensing of Environment, 232*, 111210, doi:10.1016/j.rse.2019.111210.

Yao, F., Wang, J., Yang, K., Wang, C., Walter, B.A., & Crétaux, J.-F. (2018). Lake storage variation on the endorheic Tibetan Plateau and its attribution to climate change since the new millennium. *Environmental Research Letters, 13*, 064011, doi:10.1088/1748-9326/aab5d3.

Zhang, G., Yao, T., Shum, C., Yi, S., Yang, K., Xie, H., Feng, W., Bolch, T., Wang, L., & Behrangi, A. (2017). Lake volume and groundwater storage variations in Tibetan Plateau's endorheic basin. *Geophysical research letters*, 44, 5550-5560, doi:10.1002/2017GL073773.

Zou, Z., Xiao, X., Dong, J., Qin, Y., Doughty, R.B., Menarguez, M.A., Zhang, G., & Wang, J. (2018). Divergent trends doi:United States from 1984 to 2016. *Proceedings of the National Academy of Sciences*, 201719275, doi:10.1073/pnas.1719275115.

Chapter 5 - Summary and concluding remarks

5.1 Summary

This dissertation is motivated by an improved global understanding of water storage dynamics in lakes and reservoirs, which is vitally important for regional food security, ecosystem health, and energy generation (Bruinsma 2009; Conway et al. 2017; Jia et al. 2018). Despite manifold importance, water storage in lakes and reservoirs was poorly monitored at large geographic scales prior to this dissertation. Satellite remote sensing provides unique opportunities for measuring lake water storage, but leveraging different satellite missions is a challenging task (Crétaux et al. 2016). This dissertation overcame some of the most grant challenges in monitoring inland water body storage dynamics from optical and altimetric satellites. The methodological breakthroughs were then utilized to understand the recent lake and reservoir water budget across the climate-sensitive inner Tibetan Plateau and the entire global land surface. Specifically, this dissertation has addressed three major science questions:

Science question 1: how has the lake water storage across the inner Tibetan Plateau changed over the recent decades and what was the dominant driver (e.g., warming or wetting) (Chapter 2)?

Science question 2: how can we improve the methodology of water area time series mapping using existing remote sensing images, in order to better enable a temporarily consistent monitoring of water storage dynamics in the world (Chapter 3)?

Science question 3: did the recent global open-surface water storage changes exhibit a divergence between endorheic (arid) and exorheic (humid) regions, and if so, what does this divergence indicate for the global water cycle and water resource management (Chapter 4)?

5.2 Main conclusions

5.2.1 Recent Tibetan lake water storage changes predominated by net precipitation

Using a synergy of satellite imagery and freely-available DEMs, the net LWS across the inner Tibetan Plateau increased at an average rate of 7.34 ± 0.62 Gt yr^{-1} from 2002 to 2015, manifested as a dramatic monotonic increase of 9.05 ± 0.65 Gt yr^{-1} before 2012, a deceleration and pause in 2013–2014, and then an intriguing decline after 2014. By further incorporating satellite gravity observations to a water balance model, the net precipitation could explain 70% of the monotonic LWS increase before 2012. Despite a smaller total influence, warming-induced increasing runoff from glacier retreat, likely compensated for the LWS reduction caused by the initial net precipitation decrease in 2013–2014, which is manifested by a 2-year time lag between net precipitation and LWS declines. However, the impact of warming-induced glacial runoff was insufficient to offset the effect of net precipitation, leading to an evident LWS decrease in 2015. Therefore, net precipitation was found to be the first-order contributor to the recent LWS changes across the inner Tibetan Plateau.

5.2.2 Temporal consistency of lake area mapping improved by the leverage of contaminated imagery

The novel water mapping method introduced in Chapter 3 can substantially improve the temporal coverage in lake/reservoir area mapping, by accurately recovering water areas from contaminated images. Evaluated on 428 lakes and reservoirs worldwide with satellite radar altimetry levels, the recovered water areas by this method achieved a mean relative error of only 2.2%. The combined water area time series from both good and contaminated images show strong correlations with altimetry water levels, with Spearman's rho (rank correlation coefficient) greater than ~0.8 for most lakes/reservoirs. The combined area time series increased

the monthly coverage using good images alone by an average of 43%, achieving a bi-monthly frequency for open surface water mapping during the satellite altimetry era thus far. The water mapping method is overall robust under five challenging regional scenarios. Given such performance and a generic nature, this method can be potentially applied to assist water area recovery for other optical and SAR sensors (e.g., onboard Sentinel-2 and the Surface Water and Ocean Topography (SWOT)) and to estimate lake/reservoir storage dynamics in conjunction with altimetry sensors.

5.2.3 A strong divergence in open water storage trends between arid and humid regions

Chapter 4 provides a comprehensive examination of the spatiotemporal dynamics of global lake and reservoir storage over the past nearly three decades, by synergizing satellite imagery and a constellation of satellite altimeters. This chapter substantially extends the number of studied water bodies in the existing global studies by a factor of 9-30. Additionally, it increases the temporal frequency of long-term water storage time series, owing to the use of a novel water mapping method that can accurately recover water areas from contaminated images. Globally, lake and reservoir storage slightly increased at a rate of 6.70 ± 3.12 Gt yr^{-1}. However, this masks a remarkable divergence between endorheic (arid) and exorheic (humid) basins. The net LWS in endorheic basins significantly decreased at a rate of -20.61 ± 2.68 Gt yr^{-1} ($p<0.05$), whereas exorheic basins experienced an increasing LWS trend at a rate of 27.31 ± 1.59 Gt yr^{-1} ($p<0.05$). The net LWS decrease in arid (endorheic) regions was dominated by water loss in saline lakes. The storage increase in humid (exorheic) regions was mainly attributed to the increasing freshwater storage. Consequently, the contrast between fresh and saline water abundance was amplified by ~1,400 Gt, which is equivalent to 38 Lake Meads (the largest

reservoir in the U.S.) at the full capacity. This amplified contrast was partially induced by the increasing water impoundment behind dams. Due to the divergence, global lakes and reservoirs counteracted the observed sea level rise by only ~1% during the past nearly three decades.

5.3 Contributions and broader impacts

With the overarching goal to understand recent storage dynamics in lakes and reservoirs, this dissertation research has resulted in several important contributions. First, it advances the understanding of climate impacts on alpine lake dynamics across the inner Tibetan Plateau. Through a synergy of satellite imagery and freely-available digital elevation models, it provides an unprecedentedly detailed quantification of lake storage changes across the inner Tibetan Plateau over the past decade. By further incorporating satellite gravity observations to a water balance model, the dominant driver of this regional lake storage variation was attributed to net precipitation, rather than glacial melting. This finding is important for understanding hydrological processes on the climate-sensitive Tibetan Plateau. The produced lake area and storage change data set was released to the scientific data repository PANGAEA (doi:10.1594/PANGAEA.888706) in order to better facilitate other relevant research. Second, this dissertation brings a major methodological advance in leveraging multi-mission satellites for temporally consecutive monitoring of water body storage changes, which has important ramifications for the forthcoming SWOT satellite mission. SWOT's major science goal is to monitor open surface water storage and flux changes using synchronous measurements of water areas and levels. This synergy has been well explored in this dissertation, which can guide new algorithm developments for storage monitoring using SWOT. Additionally, the produced retrospective monthly storage time series in ~1,200 major lakes and reservoirs worldwide, which

will be available on the GEE website https://lakewatch.users.earthengine.app/view/glats, can be combined with SWOT's future measurements to enable a continuous assessment of lake/reservoir water storage during a longer-term period (e.g., since ~1990s). Finally, the scientific findings of this dissertation contribute to the field of hydrology. How surface fluxes and stocks have changed over time is a fundamental question in hydrology (Alsdorf et al. 2007). Existing estimates of storage changes are mostly limited by the number of studied lakes and the low temporal frequency. This dissertation substantially extends the number of studied water bodies in the existing global studies by a factor of 9-30. Additionally, it increases the temporal frequency of long-term water storage time series, owing to the use of a novel water mapping method that can accurately recover water areas from contaminated images. This improved global assessment confirms a multi-decadal divergence in global open-surface water storage between endorheic (arid/semiarid) and exorheic (more humid) regions, which has important implications for understanding climate impacts on surface water quantity.

The dissertation research has several broad impacts on water resource management, hydrological modeling, and political geography. First, its produced long-term open surface water storage can be used to improve the understanding of water availability and water stress. Existing global water stress assessments are mostly based on water fluxes (streamflow) alone without the consideration of lake and reservoir storage due to modeling and observational challenges. Ignoring open surface water storage may prevent accurate accounting of water stress, especially in arid regions where lakes and reservoirs often provide a major water supply. Combining changing storage in lakes and reservoirs provided by this dissertation with existing water flux estimates will provide an improved and more complete understanding of recent global water stress, which is essential for effective water resource management. Second, the hypsometric

curves of lakes and reservoirs constructed in this dissertation have the potential to improve surface hydrological modeling. The current DEM products do not provide accurate elevations of inundated regions (e.g., lakes and reservoirs). Due to a lack of bathymetric information, modeled outflows from lakes and reservoirs are often over-simplified. This dissertation provides calibrated hypsometric curves for about six hundred major lakes and reservoirs worldwide, which can be used to improve the model parameterization for surface flow estimation. Third, the dissertation also demonstrates some significance to political geography. Transboundary river basins cover about 40-50% of land areas and affect 145 countries (Cretaux et al. 2011). Due to ever-growing water demands, most of the transboundary rivers have been substantially regulated by dams. However, reservoir storage records are largely unavailable primarily due to political reasons. Growing competitions over limited water resources are expected in the near future. One important outcome of this dissertation will be a multi-decadal storage record of ~900 major reservoirs worldwide. This data will provide a scientific monitoring basis for political dialogues and approaching sustainable water management plans under a growing population and a warming climate.

5.4 References

Alsdorf, D.E., Rodriguez, E., & Lettenmaier, D.P. (2007). Measuring surface water from space. *Reviews of Geophysics*, 45, RG2002, doi:10.1029/2006RG000197.

Bruinsma, J. (2009). The resource outlook to 2050: by how much do land, water and crop yields need to increase by 2050. In, *Expert meeting on how to feed the world in* (pp. 24-26)

Busker, T., Roo, A.d., Gelati, E., Schwatke, C., Adamovic, M., Bisselink, B., Pekel, J.-F., & Cottam, A. (2019). A global lake and reservoir volume analysis using a surface water dataset and satellite altimetry. *Hydrology and Earth System Sciences*, 23, 669-690, doi:10.5194/hess-23-669-2019.

Conway, D., Dalin, C., Landman, W.A., & Osborn, T.J. (2017). Hydropower plans in eastern and southern Africa increase risk of concurrent climate-related electricity supply disruption. *Nature Energy, 2*, 946-953, doi:10.1038/s41560-017-0037-4.

Crétaux, J.-F., Abarca-del-Río, R., Berge-Nguyen, M., Arsen, A., Drolon, V., Clos, G., & Maisongrande, P. (2016). Lake volume monitoring from space. *Surveys in Geophysics*, 37, 269-305, doi:10.1007/s10712-016-9362-6.

Hassanzadeh, E., Zarghami, M., & Hassanzadeh, Y. (2012). Determining the main factors in declining the Urmia Lake level by using system dynamics modeling. *Water Resources Management, 26*, 129-145, doi:10.1007/s11269-011-9909-8.

Jia, Q., Wang, X., Zhang, Y., Cao, L., & Fox, A.D. (2018). Drivers of waterbird communities and their declines on Yangtze River floodplain lakes. *Biological Conservation, 218*, 240-246, doi:10.1016/j.biocon.2017.12.029.

Wang, J., Song, C., Reager, J.T., Yao, F., Famiglietti, J.S., Sheng, Y., MacDonald, G.M., Brun, F., Schmied, H.M., Marston, R.A., & Wada, Y. (2018). Recent global decline in endorheic basin water storages. Nature Geoscience, 11, 926-932, doi:10.1038/s41561-018-0265-7.

Wurtsbaugh, W.A., Miller, C., Null, S.E., DeRose, R.J., Wilcock, P., Hahnenberger, M., Howe, F., & Moore, J. (2017). Decline of the world's saline lakes. Nature Geoscience, 10, 816–821, doi:10.1038/ngeo3052.